



**HAL**  
open science

# Multi-scale rheology of pathological pulmonary mucus

Lydia Esteban Enjuto

► **To cite this version:**

Lydia Esteban Enjuto. Multi-scale rheology of pathological pulmonary mucus. *Biological Physics* [physics.bio-ph]. Université Grenoble Alpes [2020-..], 2023. English. NNT: 2023GRALI032. tel-04166944

**HAL Id: tel-04166944**

**<https://theses.hal.science/tel-04166944v1>**

Submitted on 20 Jul 2023

**HAL** is a multi-disciplinary open access archive for the deposit and dissemination of scientific research documents, whether they are published or not. The documents may come from teaching and research institutions in France or abroad, or from public or private research centers.

L'archive ouverte pluridisciplinaire **HAL**, est destinée au dépôt et à la diffusion de documents scientifiques de niveau recherche, publiés ou non, émanant des établissements d'enseignement et de recherche français ou étrangers, des laboratoires publics ou privés.

## THÈSE

Pour obtenir le grade de

### DOCTEUR DE L'UNIVERSITÉ GRENOBLE ALPES

École doctorale : I-MEP2 - Ingénierie - Matériaux, Mécanique, Environnement, Energétique, Procédés, Production

Spécialité : 2MGE : Matériaux, Mécanique, Génie civil, Electrochimie

Unité de recherche : Laboratoire Rhéologie et Procédés

## Rhéologie multi-échelle du mucus pulmonaire pathologique

### Multi-scale rheology of pathological pulmonary mucus

Présentée par :

**Lydia ESTEBAN**

#### Direction de thèse :

**Hugues BODIGUEL**

PROFESSEUR DES UNIVERSITES, Université Grenoble Alpes

Directeur de thèse

**Max MAURIN**

PROFESSEUR DES UNIVERSITES - PRATICIEN HOSPITALIER,  
Université Grenoble Alpes

Co-encadrant de thèse

**Clément DE LOUBENS**

CHARGE DE RECHERCHE, CNRS

Co-encadrant de thèse

**Matthieu Robert de Saint Vincent**

Rheonova

Co-encadrant de thèse

#### Rapporteurs :

**Annie VIALLAT**

DIRECTEUR DE RECHERCHE, Centre Interdisciplinaire de Nanoscience de Marseille (CINaM)

**Thierry AUBRY**

PROFESSEUR DES UNIVERSITES, Université de Bretagne Occidentale

#### Thèse soutenue publiquement le **23 juin 2023**, devant le jury composé de :

**Hugues BODIGUEL**

PROFESSEUR DES UNIVERSITES, Université Grenoble Alpes

Directeur de thèse

**JEAN-FRANÇOIS BERRET**

DIRECTEUR DE RECHERCHE, CNRS

Président du jury

**Claude VERDIER**

DIRECTEUR DE RECHERCHE, CNRS

Examineur

**Arnaud BOURDIN**

PROFESSEUR DES UNIVERSITES - PRATICIEN HOSPITALIER,  
HÔPITAL ARNAUD DE VILLENEUVE

Examineur

**Annie VIALLAT**

DIRECTEUR DE RECHERCHE, Centre Interdisciplinaire de  
Nanoscience de Marseille (CINaM)

Rapporteuse

**Thierry AUBRY**

PROFESSEUR DES UNIVERSITES, Université de Bretagne  
Occidentale

Rapporteur

**Grégory CHAGNON**

PROFESSEUR DES UNIVERSITES, Université Grenoble Alpes

Examineur

#### Invités :

**Max MAURIN**

PROFESSEUR DES UNIVERSITES - PRATICIEN HOSPITALIER, Université Grenoble Alpes





# Acknowledgements

First of all, I want to thank the members of the jury for their interest in this project and their acceptance to evaluate my PhD project. I am also grateful to the Comité de Suivi Individuel (CSI) *Bruno Degano* and *Claude Verdier* for their guidance and encouragement along these years.

I would like to thank *Hugues Bodiguel*, my thesis director for trusting in me to carry out with this project as well as for the independence that he has given me in my job. Thank you for all those instructive remarks to keep improving which always led to amazing ideas while keeping a smile and optimism. Thank you as well to *Matthieu Robert de Saint Vincent*, supervisor of my PhD, for all your advice along the project and your encouraging words. Thank you so much for always finding the time to give me advice about oral presentations, posters and pushing me to improve my writing skills. I will always remember my first abstract full of corrections and how the last poster of the thesis had none, a little victory for myself! Thank you to *Max Maurin* for sharing with me his bacteriology knowledge and for his PhD co-direction.

Thank you as well to all the team of Rheonova for their constant support and for making me feel one more since the first day. In particular, thanks *Christelle* and *Jeremy* for giving me the human support I needed in many moments.

I want to deeply thank the Centre de Ressource et de Compétence de Mucoviscidose (CRCM) in the CHU and specially their physiotherapists who have provided us with the samples for this project. I am deeply thankful to *Joane Quentin* for keeping me always in mind when patients came to the hospital, this PhD would not have been possible without her great work. From the CHU, thank you so much to the team in the Institut de Biologie et Pathologie (IBP) for welcoming me so well in your lab. In particular, thank you *Julien Peyroux* and *Camille Brunet* for those coffees but overall for all those lessons in bacteriology and how to work in a biological laboratory. Thank you too to *Léa Ponderand* and *Yvan Caspar* for your constant help.

I am so happy to thank all those in the Laboratoire Rhéologie et Procédés (LRP) who have made this project possible. First of all thank you all for your enormous patience with my french learning, it is an extra knowledge I take from this experience and without your kindness and help I would not have improved so much. Thank you *Didier Blésès*, *Mohamed Karrouch*, *Frédéric Hugenell* and *Eric Faivre* for your incredible patience and always helpful ideas. Thank you so much to *Louise Infuso*, *Sylvie Garofalo* and *François Bergerot* for being so helpful and kind. *Denis Roux*,

thank you for sharing with me your perspective of science and life. *Vincent Verdoot*, I take a friend with me here, thank you for all those psychology-climbing sessions which completely reloaded my energy!

Through these years many PhD students have come and gone from the lab and each of them has left a memory on me. First I would like to thank *Martial* for his patient explanations about mucus and biology. Continuing with the team, thank you *Mai* for bringing light into the biological matters which were completely obscure for me during this thesis. Thank you for sharing your love for gastronomy and for your craziness. Thank you *Revaz* and *Medhi* for guiding me through the lab when I just arrived and giving me so many ideas showing me how fun science could be. *Maxime* and *Valentin*, two really different but both caring humans which have always been available for a talk, a coffee or a beer. Thank you for all those dinners filled with music and political discussions. Et bien sûre, merci à ma belle *Madame Razafindramangafara*, merci for your love, merci for your dances and merci for sharing with me your incredible energy. *Khadija*, *Adja*, *Emilie*, thank you so much for so much fun wherever we were and for sharing with me your beautiful cultures. Muchísimas gracias a *Diego* for your optimism and affection, I admire so much your strength and positive attitude. Thank you as well to *Xavier*, *Julie* and *Faisal* for their support and conversations.

And well, the new wave of PhD and post-docs in the lab have also left a mark on me. Thank you *Lorenzo* and *Rohan* for your kindness and advice. And thank you *Dacil* and *Nissrine* for your strength and encouraging words when working until the lab's closing hour. A big thank you too to *Bryan*, *Paul* and *Nishan* as well as to *Ioan Petrescu* for his work done during his internship.

I want to strongly thank the family I have chosen, my friends from *Tres Cantos* who whatever issue I have just make me happy and forget about it. Thank you as well to my *Grenobloise family*, you make life fun, everyday is a day to discover something new with you!

And my family, thank you all for your support even if some of you did not understand why I was doing a PhD. Each of you has your own superpower, from getting a boat to go to the other side of the world to find a better life in a country where you could not even talk the language, to fighting for what you want to do even if work and health are not following. Thank you for sharing your love for life. I love you all and deeply miss you *Mangorrino*.

My last words go for my constant support, *Luis*, thank you for always being there with exactly what I need and for making me laugh everyday of my life for the last six years. I know with you I am a better person, thank you for teaching me to enjoy calm and patience.

# Abstract

Pulmonary mucus plays a crucial role in the respiratory system by protecting and maintaining the health of the airways and lungs. Mucus serves as a physical barrier that captures inhaled particles and pathogens preventing them from reaching the pulmonary tissues. The subsequent clearance of mucus along with the trapped particles and pathogens, occurs through the coordinated beating of hair-like structures known as cilia which are lining the airways. This mucociliary clearance avoids bacterial colonisation and infection. Mucus from muco-obstructive diseases such as cystic fibrosis (CF) and non-cystic fibrosis bronchiectasis (NCFB) is thick and sticky. The high viscoelasticity of pathological mucus affects its ability to be cleared out of the respiratory tract effectively. Therefore, mucus tends to stay blocked in the airway system promoting bacteria proliferation which can lead to chronic infections.

This thesis aims to understand the mechanisms involved in the rheological properties of pulmonary sputum. We have focused on understanding how the rheology of CF and NCFB expectorations correlates to their composition and structure.

To achieve this objective we have first developed and published a robust protocol to handle and store sputum samples before rheometry. Sputa has been found to be extremely sensitive to high temperatures and ageing effects. On the contrary, freezing and storing samples at  $-80\text{ }^{\circ}\text{C}$  presents no influence on the rheological properties of sputa. Moreover, vortexing reduces the heterogeneity of sputum, diminishing the variability between aliquots. We have therefore approved a simple reliable protocol in which samples can be frozen and stored at  $-80\text{ }^{\circ}\text{C}$  after removing the saliva and vortexing.

Then we have systematically measured sputum's macrorheology obtaining insights into the overall flow and deformation properties of sputum. We have identified distinct rheological characteristics between purulent and mucoid samples, motivating the development of a user-independent technique based on image processing to accurately quantify sputum purulence.

Firstly, solid concentration is correlated with sputum's purulence and rheology.  $G^*$  presents a drastic increase with organic content while the concentration of salt in sputum does not appear to have a significant impact on its mechanical properties.

Secondly, our observations reveal differences between purulent and mucoid samples regarding their response to neutrophil count. Purulent expectorations exhibit a significant increase in  $G^*$  with higher neutrophil counts. However, contra-intuitively, mucoid samples present a decrease in viscoelasticity in the presence of large number of neutrophils. Furthermore, we have found that the recruitment of neutrophils is not linked to the overall quantity of bacteria but rather specific bacterial colonies. Expectorations predominantly colonised by mucoid *p. aeruginosa* or containing *h. influenzae* exhibited a higher neutrophil count, resulting in purulent sputum with a

pronounced viscoelasticity. Additionally, we have observed that patients with severe lung conditions and a critical stress exceeding 20 Pa tend to have highly purulent samples. Consequently, these severe patients present dark purulent sputum characterised by low flowing capacity, which likely contributes to lung obstruction and the persistence of chronic infections.

Finally, we show the significant influence of purulence on the recovery capacity of sputum following large strain. Although all samples experienced a decrease in their flowing properties, the restoration of their viscoelastic behaviour in the linear range is incomplete. Purulent expectorations exhibited a reduction in their  $G^*$ , while mucoid sputum showed an increase. Furthermore, their temporal evolution differs notably, with purulent samples losing half of  $G^*$  within the first 6 hours, whereas mucoid expectorations remain unchanged over 24 hours.

# Resumé

Le mucus pulmonaire joue un rôle crucial dans le système respiratoire en protégeant la santé des voies respiratoires. Le mucus sert de barrière physique qui capture les particules inhalées et les agents pathogènes les empêchant d'atteindre les tissus pulmonaires. L'élimination ultérieure du mucus ainsi que des particules piégées et des agents pathogènes se produit par le battement de structures ressemblant à des cheveux appelées cils qui tapissent les voies respiratoires. Cette clairance mucociliaire évite la colonisation bactérienne et l'infection. Le mucus des maladies muco-obstructives telles que la mucoviscidose et la dilatation des bronches (DDB) est épais et collant. La haute viscoélasticité du mucus pathologique affecte sa capacité à être évacuée efficacement. Par conséquent, le mucus a tendance à rester bloqué dans les voies respiratoires, favorisant les infections chroniques.

Cette thèse vise à comprendre les mécanismes impliqués dans la rhéologie des expectorations des patients de mucoviscidose et DDB. Pour atteindre cet objectif, nous avons d'abord développé et publié un protocole robuste pour manipuler et stocker des échantillons d'expectorations avant la rhéométrie. Les expectorations se sont avérées extrêmement sensibles aux températures élevées et aux effets du vieillissement. Au contraire, la congélation et la conservation des échantillons à  $-80\text{ }^{\circ}\text{C}$  ne présentent aucune influence sur leur rhéologie. De plus, le vortex réduit l'hétérogénéité des expectorations, diminuant la variabilité entre les aliquotes. Nous avons donc approuvé un protocole simple et fiable dans lequel les échantillons peuvent être congelés et conservés à  $-80\text{ }^{\circ}\text{C}$  après élimination de la salive et vortex.

Ensuite, nous avons systématiquement mesuré la macrorhéologie des expectorations. Nous avons identifié des caractéristiques rhéologiques distinctes entre les échantillons purulents et mucoïdes, motivant le développement d'une technique indépendante de l'utilisateur basée sur le traitement d'image pour quantifier avec précision la purulence.

Premièrement, la concentration solide est corrélée à la purulence et à la rhéologie des expectorations.  $G^*$  présente une augmentation drastique avec le contenu organique alors que la concentration en sel ne semble pas avoir d'impact significatif sur ses propriétés mécaniques.

Deuxièmement, nos observations révèlent des différences entre les échantillons purulents et mucoïdes en ce qui concerne l'inflammation. Les expectorations purulentes présentent une augmentation significative de  $G^*$  avec un nombre de neutrophiles plus élevé. Cependant, contre-intuitivement, les échantillons mucoïdes présentent une diminution de la viscoélasticité en présence des neutrophiles. De plus, nous avons constaté que le recrutement des neutrophiles n'est pas lié à la quantité globale de bactéries mais plutôt à des colonies bactériennes spécifiques. Les expectorations majoritairement colonisées par les mucoïdes *p. aeruginosa* ou contenant *h. influenzae*

zae présentait un nombre de neutrophiles plus élevé, entraînant des expectorations purulentes avec une viscoélasticité prononcée. De plus, nous avons observé que les patients souffrant d'affections pulmonaires sévères et d'un stress critique supérieur à 20 Pa ont des échantillons très purulents.

Enfin, nous montrons l'influence significative de la purulence sur la capacité de récupération des crachats suite à un effort important. Bien que tous les échantillons aient connu une diminution de leurs propriétés d'écoulement, la restauration de  $G^*$  n'est pas complète. Les expectorations purulentes ont montré une réduction de leur  $G^*$ , tandis que les expectorations mucoïdes ont montré une augmentation. De plus, leur évolution temporelle diffère notablement, les échantillons purulents perdant la moitié de  $G^*$  dans les 6 premières heures, alors que les expectorations mucoïdes restent inchangées sur 24 heures.

# Contents

<b>Acknowledgements</b>	<b>2</b>
<b>Abstract</b>	<b>4</b>
<b>Resumé</b>	<b>6</b>
<b>1 Introduction</b>	<b>11</b>
1.1 Muco-obstructive diseases . . . . .	11
1.2 Mucus and sputum . . . . .	12
1.3 Sputum rheology . . . . .	13
1.3.1 Disease identification and treatment evaluation . . . . .	14
1.3.2 Rheology for patient follow-up . . . . .	15
1.4 Objectives of the thesis project . . . . .	17
<b>2 Materials and methods</b>	<b>18</b>
2.1 Rheology . . . . .	18
2.1.1 Rheometry tests . . . . .	19
2.1.2 Large Amplitude Oscillatory Shear rheology . . . . .	20
2.2 Statistical analysis . . . . .	24
2.2.1 Population distributions . . . . .	24
2.2.2 Mean and variance equality . . . . .	24
2.3 Sample collection . . . . .	25
2.4 Quantitative colour analysis . . . . .	26
2.5 Model fluid of bronchial expectorations . . . . .	28
<b>Sample management</b>	<b>28</b>
<b>3 Sputum handling for rheology</b>	<b>31</b>
<b>4 Vortex effect</b>	<b>49</b>
4.1 Heterogeneity of sputum . . . . .	50
4.2 Mixing procedures . . . . .	51
4.3 Vortex mixing efficiency . . . . .	53
4.4 Vortex effect on rheology . . . . .	55
4.5 Conclusions . . . . .	56

<b>5</b>	<b>Homogenisation of viscoelastic fluids</b>	<b>58</b>
5.1	Experimental set up . . . . .	59
5.1.1	Flow rate . . . . .	60
5.1.2	Relaxation time . . . . .	61
5.2	Results . . . . .	62
5.2.1	No viscoelastic contrast between matrix and inclusion . . . . .	62
5.2.2	Viscoelastic contrast between matrix and inclusion . . . . .	63
5.2.3	Size dependency . . . . .	64
5.3	Conclusions . . . . .	65
	<b>Sputum rheology and clinical findings</b>	<b>66</b>
<b>6</b>	<b>Solid concentration influence on rheology</b>	<b>69</b>
6.1	Sputum composition . . . . .	69
6.2	Sputum under large strain . . . . .	76
6.2.1	Recovery . . . . .	79
6.3	Conclusions . . . . .	84
<b>7</b>	<b>Infection</b>	<b>86</b>
7.1	Purulence . . . . .	86
7.2	Infection effects on sputum properties . . . . .	89
7.3	Bacteria . . . . .	90
7.4	Neutrophils . . . . .	95
7.5	Conclusions . . . . .	98
<b>8</b>	<b>Conclusions and perspectives</b>	<b>99</b>
8.1	Sputum handling prior to rheometry . . . . .	99
8.1.1	Vortex effect on sputum . . . . .	99
8.2	Solid content of sputum . . . . .	100
8.3	Purulence . . . . .	102
8.3.1	Image treatment method . . . . .	102
8.3.2	Purulence and organic concentration . . . . .	102
8.3.3	Purulence and patient's severity . . . . .	103
8.3.4	Purulence and mechanical behaviour of sputum . . . . .	103
	<b>Bibliography</b>	<b>103</b>
<b>A</b>	<b>Mucins identification and quantification</b>	<b>110</b>

# Chapter 1

## Introduction

### 1.1 Muco-obstructive diseases

Muco-obstructive diseases are a group of chronic respiratory diseases characterised by the production of thick, sticky mucus in the airways leading to anomalous mucus clearance favouring bacterial growth and causing airway obstruction and impaired lung function. These diseases can cause chronic respiratory symptoms such as cough, shortness of breath, and sputum overproduction [1], which can significantly diminish quality of life. In addition, muco-obstructive diseases are associated with a high risk of respiratory infections and exacerbations, which can result in hospitalisation and increased mortality [2, 3].

The most common muco-obstructive diseases are chronic obstructive pulmonary disease (COPD), cystic fibrosis (CF), primary ciliary dyskinesia (PCD) and non cystic fibrosis bronchiectasis (NCFB) [1]. Along this project we have worked with sputum samples collected from CF and NCFB and COPD patients.

#### **Cystic Fibrosis**

Cystic fibrosis is a rare disease that primarily affects people of European descent and is estimated to affect close to 90,000 people worldwide [2]. CF is caused by mutations in the CFTR (cystic fibrosis transmembrane conductance regulator) gene, which is responsible for the regulation of sodium, chloride and bicarbonate in the epithelium. In CF, the CFTR protein is dysfunctional, resulting in the production of anomalous mucus that clogs the airways and other organs [4, 1].

#### **Non-Cystic Fibrosis Bronchiectasis**

NCFB is characterised by permanent dilation and thickening of the bronchial walls [5, 6]. NCFB can occur due to severe respiratory infections or as a secondary condition associated with other underlying lung diseases such as COPD, asthma, or immunodeficiency disorders [7].

#### **Chronic Obstructive Pulmonary Disease**

According to the World Health Organization (WHO), it is the third leading cause of death worldwide, with 3.23 million deaths in 2019. Smoking is the primary cause of

COPD, but exposure to air pollution, chemical fumes, and dust can also contribute to the development of the disease. Symptoms of COPD include coughing, wheezing, shortness of breath, and chest tightness. There is no cure for COPD, but treatment can help manage symptoms and slow the progression of the disease.

## 1.2 Mucus and sputum

Mucus helps to protect the lungs and airways from harmful substances such as bacteria, viruses, and pollutants. It is produced by specialised cells called goblet cells that are found in the lining of the respiratory tract.

In healthy individuals, mucus is a thin and watery substance [8] that is cleared through the beating of hair-like structures called cilia move the mucus and the trapped particles up and out of the lungs, where they can be expelled through the mouth as sputum. Sputum is therefore a mixture of mucus and other substances such as saliva, airway lining fluid, and cellular debris that can be produced by the lungs and airways. In healthy individuals, sputum production is usually minimal and is typically cleared by the respiratory system without issue. In individuals with respiratory diseases, mucus and sputum production can become excessive and difficult to clear, leading to a range of symptoms such as coughing, wheezing, and shortness of breath. Moreover, if mucus is not cleared from the respiratory tract, pathogens will stay trapped in the mucus network proliferating and leading to chronic infections.

Mucus is composed mainly of water, mucins, trapped pathogens and particles and in case of infection inflammatory cells.

### Water

Water is an essential component of mucus, typically making up the majority of its volume. In healthy individuals, mucus is about 97.5% water. However, in mucobstructive diseases, the water content of mucus can become lower than normal, resulting in thicker, stickier mucus that is more difficult to clear from the airways. This can lead to increased risk of respiratory infections and other complications.

### Mucins

Mucins are large, glycosylated proteins that give mucus its viscous and adhesive properties. There are mainly two types in pulmonary mucus: MUC5B which is mostly in charge of cleaning the respiratory tract and MUC5AC which is produced as a defence against pathogens [9, 10].

### Pathogens

Pathogens, such as bacteria, viruses, and fungi, can be present in mucus. Mucus contains antibodies and other immune system molecules that help to neutralize and eliminate these pathogens. However, if the immune system is compromised or mucus stays blocked in the airway system, the pathogens may be able to multiply and cause illness.

## Inflammatory cells

Inflammatory cells can be found in mucus and sputum samples as they are recruited through the innate immune system due to infection. The most common inflammatory cells found in mucus and sputum are neutrophils, eosinophils, and macrophages.

Neutrophils are the first cells to be recruited to the site of infection or inflammation and are responsible for engulfing and destroying bacteria. Their presence in mucus and sputum is a common indicator of bacterial infections. Eosinophils, on the other hand, are involved in allergic reactions and parasitic infections. Their presence in mucus and sputum can indicate conditions such as asthma. Lastly, macrophages are responsible for clearing debris, dead cells, and foreign particles from the airways.

In Fig 1.1 the loop created during chronic infection is presented through a figure from Boucher et al. (2019) [1].<sup>2</sup>

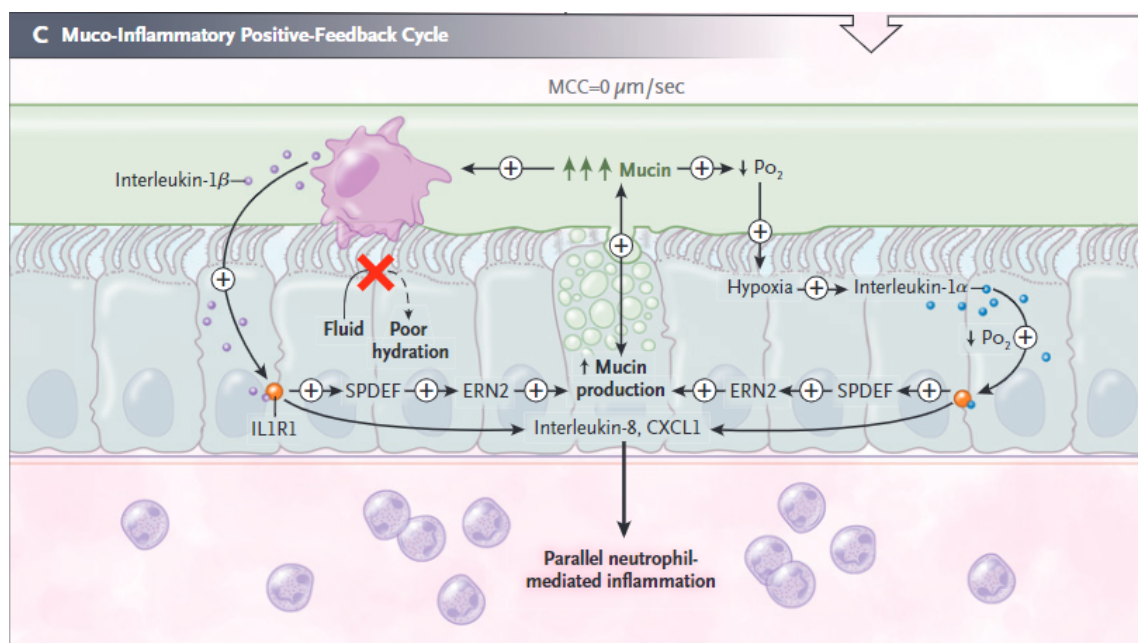


Figure 1.1: Generation of persistent inflammatory response. Figure from Boucher et al. [1]. Pathogens increase mucin secretion that with poor hydration, leads to abnormal mucus reducing the mucus clearance (MCC) as the cilia are crushed by the thick mucus layer. Hyperconcentrated mucus activates the macrophages which trigger the production of proinflammatory mediators (interleukin-1 $\alpha$  and -1 $\beta$ ) and cytokines (IL8 and CXCL1) leading to an increase in mucin production which positively feeds the whole loop. The secretion of proinflammatory mediators recruit neutrophil inflammation.

## 1.3 Sputum rheology

Rheology is the science which studies flow and deformation properties of complex fluids such as mucus. Rheology can be assessed at the micro- and macro- scales. Micro-rheology refers to the study of the dynamics and properties of the constituents of a complex fluid at the microscopic scale by tracking the motion of microscopic particles suspended within it. By analysing the motion of these particles, one can

infer information about the viscoelastic properties of the material. Macro-rheology, on the other hand, is a technique that measures the bulk mechanical properties of the material, such as its viscosity and elasticity. This is typically done by subjecting the material to a known deformation or stress, and then measuring the resulting response. Sputum exhibits both micro- and macro-rheological behaviour, and its rheological properties are determined by the interactions between its various components at different length scales.

Sputum is a complex and heterogeneous fluid and while microrheology may be more sensitive to local heterogeneities in the samples, macrorheology measures bulk properties, making it more representative of the overall behaviour. Furthermore, macrorheology is often more accessible and easier to perform than microrheology, which can require specialised equipment and expertise. Therefore, while microrheology can provide valuable information, we have focused our study on the macrorheological behaviour of sputum as it could be an easier method to rapidly obtain information about the bulk mechanical properties of sputum.

### 1.3.1 Disease identification and treatment evaluation

The study of sputum rheology has already been conducted with the aim of differentiating between healthy and diseased sputum, as well as distinguishing between various respiratory diseases. Still, contrasting results can be found in literature on the subject. For instance, while Serisier et al. [11] found no rheological differences between healthy and CF sputum, Patarin et al. [12] retrieved significant increases of viscoelasticity and the flow point in CF and COPD expectorations as shown in Fig 1.2.

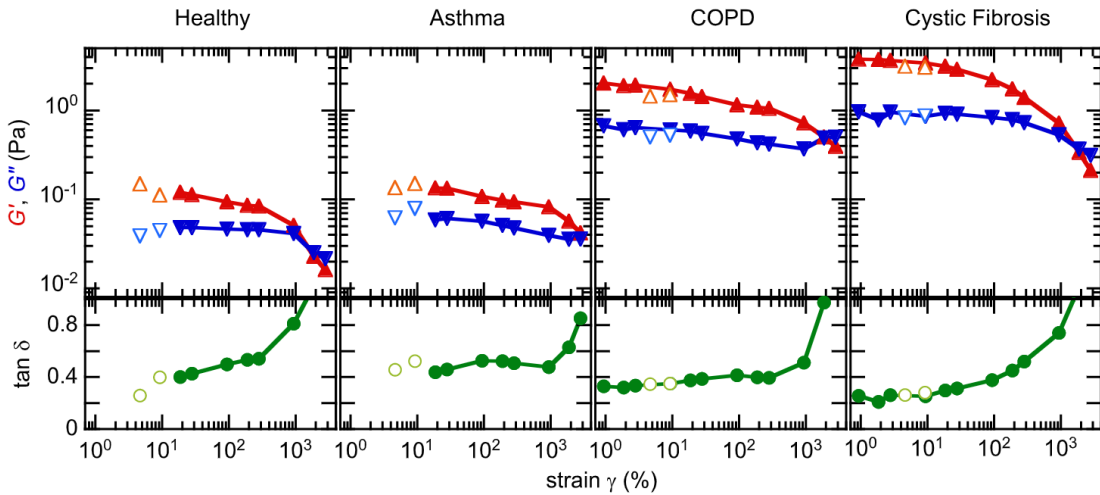


Figure 1.2: Figure from Patarin et al. [12] comparing the elastic and viscous modulus ( $G'$  and  $G''$ ) and the damping ratio ( $\tan \delta = G''/G'$ ) as a function of applied strain ( $\gamma$ ) measured in sputum from healthy subjects and patients of asthma, COPD and CF.

In addition, other research groups have focused on developing treatments that can improve the clearance of mucus from the airways. For example, inhaled hypertonic saline, which increases the water content of mucus, can improve sputum clearance in patients with CF. Other treatments such as mucolytic agents [13, 14]

and airway clearance techniques aim to reduce the viscosity and elasticity of sputum, making it easier to clear from the airways.

### 1.3.2 Rheology for patient follow-up

However, still now a days the surveillance of these diseases is a major challenge, especially as the existing tests are essentially qualitative. The measurement of rheological properties could hence be a powerful diagnostic tool as it is quantitative, making it possible to characterise pulmonary diseases. Moreover, sputum rheology could be considered a direct biomarker of muco-obstructive disease as changes in sputum rheology could reflect changes in the underlying disease processes that affect mucus production, clearance, and viscosity.

#### Solid concentration

Changes in sputum rheology can reflect changes in mucus hydration, impacting on its elasticity, which can affect mucus clearance and therefore increase the risk of infection. In particular, Hill et al. [8] and Boucher et al. [1] have shown how the osmotic pressure raises with increasing solid matter. The increase of osmotic pressure leads to the crushing of the cilia enabling the mucociliary clearance as shown in Fig 1.1. Moreover, Hill et al. [15] had previously observed a change from a viscous-dominated solution to a gel-like fluid at a solid concentration of 4% in samples generated *in vitro*. The evolution into a highly elastic gel therefore difficulties the penetration of the cilia in the mucus layer and the diffusion of trapped particles.

#### Mucin concentration

When increasing the solid concentration, a higher amount of mucins is expected in the samples and indeed Horsley et al. [16] found how  $G'$  decreased its value with decreasing mucin content in 15 CF patients.

However, when investigating the techniques for mucin quantification, big differences are found in literature. Anderson et al. reported an increase of mucins in NCFB mucus collected by bronchoscopy [17] compared to healthy mucus. On the contrary, Rubin et al. [3] observed a decrease in mucin concentration of CF patients compared to healthy subjects. These are just some examples pointing out the difficulty of quantifying mucin concentration accurately as they are really long glycosilated proteins. In fact, Henderson et al. [18] showed how depending in the technique used, the conclusions were completely opposed. While they observed and increase of MUC5B in CF through size exclusion chromatography and differential refractometry, they measure a decrease when working with agarose gel electrophoresis. Due to the complexity of mucin identification and quantification, we have focused our study on the effect of bacteria and the consequent recruitment of inflammatory cells on rheology.

#### Infection

One of the first indications of infection is the increase of purulence which is described as a change of colour of the expectorations with healthy sputum as a transparent gel, while infected samples become yellow and green. Serisier et al. [11] showed

how  $G'$  was significantly increased in purulent CF expectorations. However, as their study was done with a relatively low amount of samples (4 mucoid and 8 purulent expectorations) we will investigate this further with a larger group of expectorations. Moreover, we will also investigate the evolution of the rheological variables through a gradient of purulence.

The issue now is to properly comprehend the origin of sputum's purulence as contrasting information can be found. It seems it could be due to polymers secreted by bacteria which form biofilms as *pseudomonas aeruginosa* [19, 20] or it could come from the inflammatory cells such as eosinophils or neutrophils [21, 20].

For instance, Tomaiuolo et al. [22] found higher  $G'$  in CF sputum which was mainly colonised by *burkholderia cepacia* and *stentrophomonas maltophilia* (Fig 1.3). Still this dependence has not been confirmed by other groups and all the samples fall into a small range of viscoelasticity.

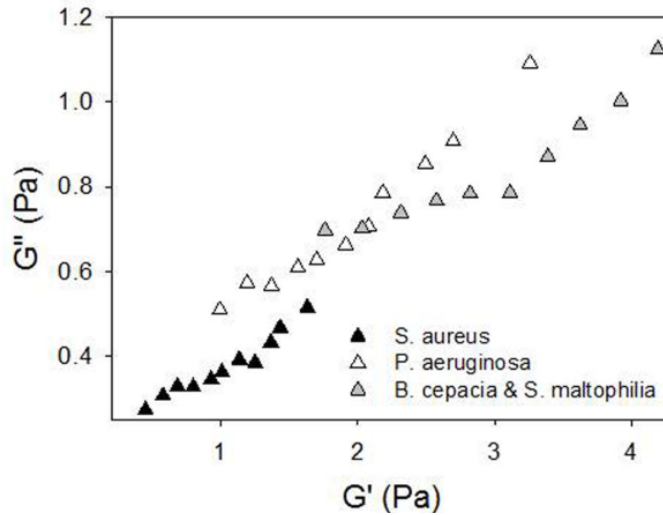


Figure 1.3:  $G'$  and  $G''$  evolution as a function of the main bacteria found in CF samples. The figure is from Tomaiuolo et al. [22].

Other studies have seen correlations between immune defence cells and sputum rheology. While Volpato et al. [23] found that the presence of eosinophils in asthma, COPD and NCFB samples was positively correlated with the sputum's critical stress ( $\sigma_c$ ), Serisier et al. [11] indirectly correlated  $G'$  to neutrophil elastase concentration in purulent CF samples. However, in this last study the rheometry was measured with a different group of samples than the neutrophil assessment which does not lead to a high reliability which is also observed in their big error bars.

Therefore, learning about the origin of the mechanical and rheological properties of airways mucus could help understanding the evolution of muco-obstructive diseases. Moreover, the identification of pathological biomarkers could help health professionals improve patient's follow-up and evaluate the effectiveness of interventions such as mucolytic agents, airway clearance techniques, and antibiotics by monitoring changes in sputum rheology over time.

## 1.4 Objectives of the thesis project

My thesis work aimed to:

- establish a protocol for the collection and storage of sputum samples prior to characterisation,
- characterise sputum rheology
- understand the correlations between sputum rheology and its composition, in particular bacterial impact.

This document presents the outcomes of the experiments conducted to achieve these objectives. We have divided this report into two parts.

The first one is focused on how to handle samples before rheology covering issues such as freezing, acceptable time between collection and analysis and influence of the vortex in chapter 3. Since homogenisation was observed to be the most delicate parameter, in chapter 4 we investigated how the mixing quality could be improved by altering the vortexing duration. In addition, we designed a passive homogenising system to reduce the impact of user variability. This device was found not to be suitable for sputum homogenisation due to practical concerns. However, in chapter 5 we present a study of the behaviour of viscoelastic fluids through a porous media.

In the second part we first characterised the rheology and solid composition of CF and NCFB expectorations (chapter 6) to then investigate the role of infection on sputum's mechanical properties in chapter 7.

# Chapter 2

## Materials and methods

### 2.1 Rheology

Rheology characterises the deformation of a body under the influence of stresses [24]. While ideal elastic solids store energy and are completely recovered when the stresses are removed, ideal Newtonian fluids dissipate the energy applied for the strain and flow deforming irreversibly. Sputum, as many soft materials is in between: it is able to store some of the applied energy while another part is lost and permanently deforms the system. In this section we define the parameters involved in rheometry which will be used in this thesis as well as the methodology to carry out the measurements.

When applying a tangential force to a solid it reacts deforming in the direction of the applied force. The shear stress,  $\sigma$  is defined as the ratio between the exerted force and the tangential surface. The material's strain or deformation,  $\gamma$  is calculated as  $\gamma = \Delta x/h$ , where  $\Delta x$  is the tangential displacement and  $h$  is the sample's thickness. On the one hand, ideal elastic systems show a linear relationship between stress and strain at low deformations  $\gamma = G\sigma$ .  $G$  is the shear modulus and is independent of strain and time for these ideal elastic materials. On the other hand, viscoelastic materials as sputum have a  $G$  which also considers its flowing capability, it is known as complex shear modulus,  $G^*$  and is composed by the elastic or storage modulus,  $G'$  and by the viscous or loss modulus,  $G''$ .

To address the viscoelastic behaviour of our samples we have carried out oscillatory rheometry. A sinusoidal shear strain is imposed  $\gamma = \gamma_0 \sin(\omega t)$  with a certain amplitude,  $\gamma_0$  and rotational speed,  $\omega = 2\pi f$  with  $f$  the frequency in Hz. The system will respond with a sinusoidal shear stress  $\sigma = \sigma_0 \sin(\omega t + \delta)$  and a phase shift  $\delta$ . An ideal elastic fluid reacts immediately to the exerted deformation ( $\delta = 0^\circ$ ) while an viscous fluid takes some time to react as the applied energy is transformed into heat and structure reorganisation. To address the material's capability to store and release this energy, the modulus of  $G^*$  is calculated by  $|G^*| = \sigma_0/\gamma_0$  and can be split into its real and imaginary parts  $G'$  and  $G''$ :  $G^*(\omega) = G'(\omega) + iG''(\omega)$ . Therefore the system's response can be rewritten as a function of  $G'$  and  $G''$  as follows  $\sigma(t) = \gamma_0[G'(\omega)\sin(\omega t) + G''(\omega)\cos(\omega t)]$ .

This analysis considers the sinusoidal response to be a perfect sinusoid which is true at low strains but, at high strains, the signal starts deforming. Through the Large Amplitude Oscillation Shear (LAOS) approach we can consider the multiple harmonics the deformed signal can be decomposed into while classical rheometry,

known as Small Amplitude Oscillation Shear (SAOS), only considers the first harmonic. In this section we will first describe the different rheometry tests we have applied along this report and we will then go into some details of the LAOS analysis which we have tested on a small number of sputum samples in chapter 6.

### 2.1.1 Rheometry tests

A rheometer is a device that measures the mechanical response of materials by applying a controlled deformation or stress to a material and measuring the resulting response, such as strain, stress, or viscosity. It is composed of a motor to apply a controlled deformation or stress to the sample, a force sensor to measure the resistance of the sample to the applied stress and a pair of measuring geometries which will be in contact with the sample and will ensure to have a well-defined simple shear. There are mainly two categories of rheometers: those that regulate an applied shear stress and measure the resulting strain rate, and those that regulate a strain rate and measure the resulting shear stress. We have used strain rate controlled rheometers such as Rheomuco (Rheonova) and ARES-G2 (TA Instruments) and stress controlled rheometers as ARG2 and DHR3 (TA Instruments). The geometries used were 25 mm diameter plate-plate rough geometries to minimise the effect of sputum's heterogeneity. All the measurements of sputum samples were performed at 37 °C and when the tests were long, an anti-evaporation trap was used with water droplets or a humid sponge surrounding the sample.

The following types of tests have been used:

#### Flow sweep

Flow sweeps are commonly used in rheology to study the flow behaviour of materials. It is a type of test in which a rheometer applies a range of increasing or decreasing shear rates ( $\dot{\gamma}$ ) to a sample and measures the resulting stress or viscosity ( $\eta$ ) through the Newtonian flow law  $\sigma = \eta\dot{\gamma}$ . Newtonian fluids have a constant viscosity which is independent to the strain rate and a shear stress which increases proportionally to  $\dot{\gamma}$ . In contrast,  $\eta$  and  $\sigma$  evolve with  $\dot{\gamma}$  in viscoelastic fluids.

We have typically applied shear rates from 0.01 to 1000 s<sup>-1</sup>.

#### Strain sweep

Strain sweeps, also called amplitude sweeps, are tests in which an increasing strain is exerted at a constant frequency to obtain the elastic and viscous modulus. At low strains,  $G'$  and  $G''$  for viscoelastic fluids are independent to the applied deformation and show a plateau which in sputum samples ends around 10%. We have applied increasing strains from 10<sup>-1</sup> to 10<sup>4</sup> % at 1 Hz to explore the behaviour of sputum in both the small and large deformation domains. We have then systematically taken the values of  $G'$  and  $G''$  at  $\gamma = 5\%$  which we call  $G'_{5\%}$  and  $G''_{5\%}$  in this document.

With a part of the collected expectorations we have also performed recovery tests to address the reversibility of sputum's structure. For these tests we have simply performed three consecutive strain sweeps.

## Frequency sweep

As explained before, viscoelastic materials have a time-dependent behaviour which can be assessed through frequency sweep tests. In this case a constant strain is imposed while the frequency changes. With sputum samples we have chosen a input strain of 5%, as with this value we are sure to stay in the lineal domain. We explored the frequency range between 0.01 and 10 Hz.

## Time Sweep

A time sweep tells us about the evolution of the sample in time. In a time sweep we set the strain value and the frequency of the oscillations. We have chosen to work at  $\gamma = 5\%$  and  $f = 1$  Hz. This way we stay at small deformations in order to study the sample "at rest".

### 2.1.2 Large Amplitude Oscillatory Shear rheology

Conventional rheometry brings light into the frequency dependent viscoelastic moduli  $G'$  and  $G''$  when solicited at small strain. Still, mucus is often under large strain both within the pulmonary tract when coughing or expectorating. The Large Amplitude Oscillatory Shear rheology of mucus is, to date, essentially unknown, and yet it could represent a more powerful indicator of obstructive pathology than the currently used linear viscoelasticity.

Viscoelastic materials can be characterised by imposing an oscillatory shear strain ( $\gamma$ ) and measuring the stress response ( $\sigma$ ). When the strain amplitude is small (SAOS), the response is linear, and the material's properties are described by the elastic and viscous modulus ( $G'$  and  $G''$ ). This first behaviour corresponds to section I in Fig 2.1 A. Then, the strain amplitude keeps increasing and the response becomes non-linear, the measured signal is no longer a single-harmonic sinusoidal (see graphs B of Fig 2.1) but a deformed sinusoidal. This first nonlinear region is known as MAOS (Medium Amplitude Oscillation Shear) and is indicated by II in Fig 2.1 A. In this region the material changes from an elastic deformation to a plastic deformation. If the amplitude of the strain is still increased, the material will reach a critical point known as crossover point were the loss modulus will overcome the storage modulus. This point marks the transition from a solid-like behaviour to a liquid-like behaviour, known as the LAOS domain. From this point, the material is able to flow.

## Lissajous curves

Graphically, we can observe the evolution of the measured stress with increasing deformation through the Lissajous curves. If we plot the stress response against the shear strain ( $\gamma$ ), we obtain the elastic Lissajous (Fig 2.1 C). When plotting the stress response as a function of the imposed strain rate,  $\dot{\gamma}(t) = \omega\gamma_0\cos(\omega t)$  we can observe the viscous response of the fluid (Fig 2.1, D). The study of the Lissajous curves, gives us information of the onset of the nonlinear regime as these curves lose their mirror planes. In the linear domain, the curve is an ellipse in which its axes are its mirror planes whereas curves in the nonlinear domain lose these symmetries (Fig 2.1 C and D). Moreover, these curves give visual information of the material's reaction

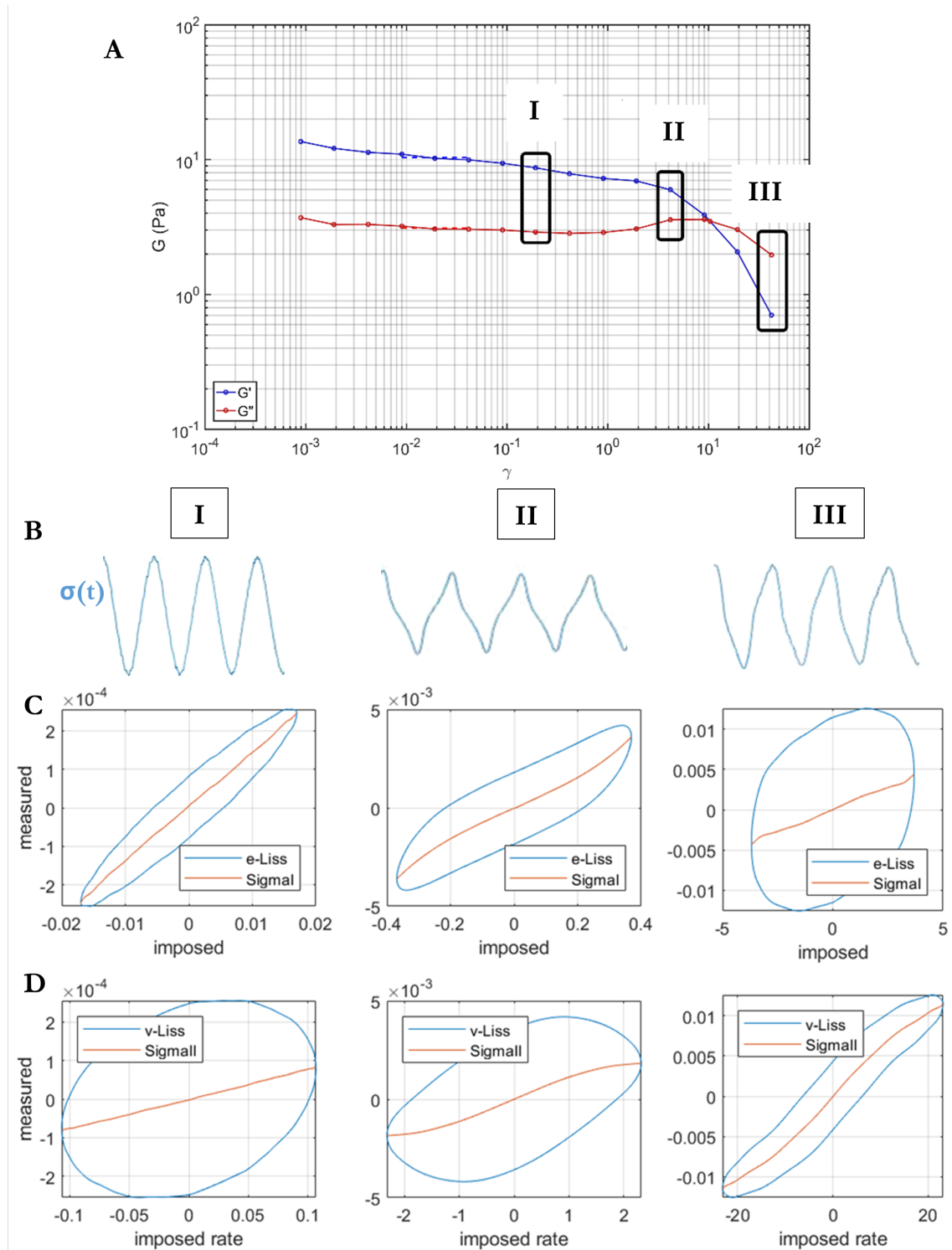


Figure 2.1: A: Strain sweep plot of a sputum sample from a patient with NCFB. I: Linear domain, II: nonlinear domain between the yield point and the crossover (MAOS) and III: nonlinear domain after the crossover (LAOS). B: signal captured by the rheometer when applying increasing strain. C and D: In blue, elastic and viscous Lissajous curves at different regimes from the strain sweep A. On the x-axis strain and on the y-axis the stress which are represented with arbitrary units. In red, the stress obtained by the Fourier decomposition of the signal.

to strain. In Fig 2.1 C we can see the sample is a strain stiffening material as the measured stress in the y-coordinate increases when increasing the applied strain. Furthermore, when increasing the strain rate (Fig 2.1 D), the measured stress is reduced, indicating it is a shear thinning material.

### Beginning of nonlinearities

However, even if with the Lissajous curves we are able to see the transition from linear to nonlinear domain, it is still interesting to arrive to these same conclusions through a quantitative value to automatically analyse large sets of data and facilitate the comparison between samples. First we need to decompose the measured stress signal into its harmonics to study the stress response in the MAOS and LAOS region. Stress can be expressed as a composition of both the elastic and viscous components as a Fourier series:

$$\sigma(t) = \gamma_0 \sum_{n \text{ odd}} [G'_n(\omega, \gamma_0) \sin(n\omega t) + G''_n(\omega, \gamma_0) \cos(n\omega t)]$$

where  $n$  is the order of the harmonics.

At low strains, the signal is sinusoidal (see blue signal in Fig 2.2) and its intensity is going to be described by the intensity of the first harmonic,  $I_1$ . When the signal loses its sinusoidal shape (black signal), the third harmonic is considered (orange sinusoidal). By decomposing the deformed signal into their harmonics, we can obtain the Fourier intensities of the  $n$ -th harmonic ( $I_n$ ). The Fourier intensities are proportional to the odd power of the strain amplitude ( $I_n \propto \gamma_0^n$ ,  $n = 1, 3, 5, \dots$ ) [25]. Therefore, the ratio of intensity from the third harmonic to the first  $I_3/I_1$  will increase when the nonlinearities start appearing.

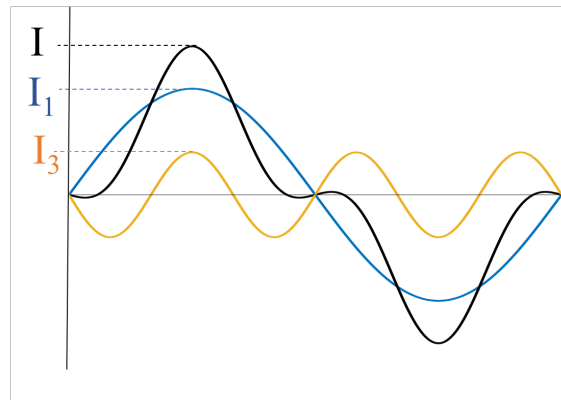


Figure 2.2: Decomposition of a deformed sinusoidal signal (black) into its first and third harmonics (blue and orange signals).  $I$ ,  $I_1$  and  $I_3$  are the signal intensities.

In many cases the signals we analyse have too much noise at low strains for proper quantification. For this reason, we compare  $I_3/I_1$  with its previous harmonic,  $I_2/I_1$ . When the normalised intensity of the second harmonic is lower than the third harmonic normalised intensity (see graph B in Fig 2.3) we assume the level of noise will be similar for  $I_2$  and  $I_3$ . Therefore, when  $I_3/I_1$  exceeds  $I_2/I_1$  we can be confident we are analysing the non-linear signal as the third harmonic is measured.

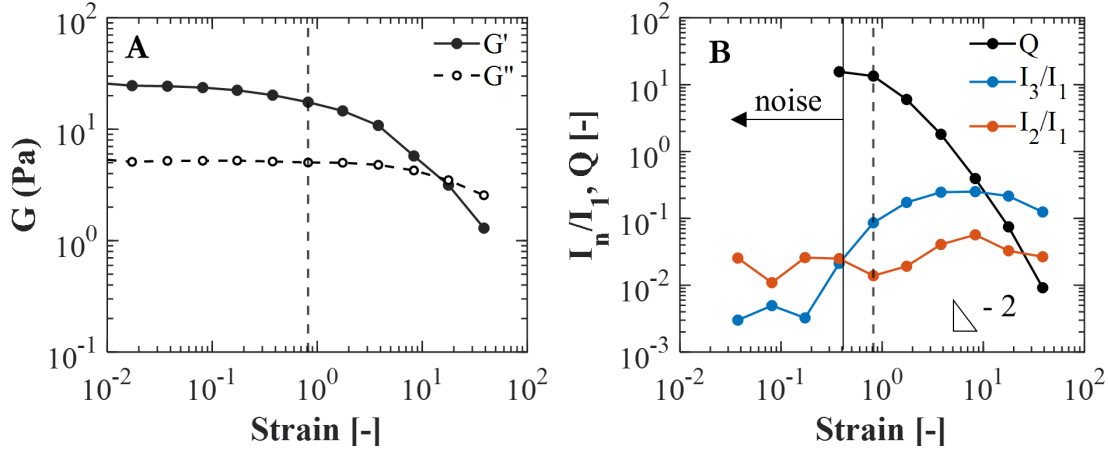


Figure 2.3: A:  $G'$  and  $G''$  of an exacerbated NCFB sample plotted against the imposed strain, only considering the first harmonic. B: Normalised intensities of the second and third harmonic in red and blue. The dashed line indicates the beginning of the nonlinear domain.

Hyun et al. [26] defined a nonlinear coefficient  $Q$  to locate the beginning of the nonlinear domain marked with a dashed line on Fig 2.3.  $Q$  is dependant on the strain amplitude ( $\gamma_0$ ) and the third and first harmonic intensity ratio ( $I_3/I_1$ ).

$$Q(\gamma_0) = \frac{I_3}{I_1} \frac{1}{\gamma_0}$$

Along the small deformations,  $Q$  shows a constant value, see Fig 2.3 C in which the first points are not plotted due to the large amount of noise. Once the MAOS domain starts,  $Q$  will evolve giving information about the sample's micro structure. Hyun et al. [26] observed that  $Q$  increased for entangled polymers and dropped for untangled polymers, still they do not explain the mechanism behind these observations. When increasing the strain the only way  $Q$  can increase is if  $I_3/I_1 > \gamma_0$ , this means the nonlinear stress measured by the captor is stronger than the applied strain. Therefore, entangled polymers would be storing the stress as the crosslinked connections are not able to break. In the case of sputum,  $I_3/I_1$  does not evolve much in the nonlinear domain (see Fig 2.3) and, following the equation defining  $Q$ , its value is reduced when the strain increases. Therefore, the material deforms.

### Material's reaction to large strain

Along the nonlinear regime, different materials will react differently to increasing strain as seen visually in the Lissajous curves. Here we describe a quantitative method to evaluate the intracycle alterations of the Lissajous curves.

The previous Fourier decomposition of the stress signal can be fitted through the Chebyshev polynomial ( $T_n$ ) of the 1<sup>st</sup> kind [27]:

$$\sigma'(x) = \gamma_0 \sum_{n:\text{odd}} e_n(w, \gamma_0) T_n(x)$$

$$\sigma''(y) = \gamma_0 \sum_{n:\text{odd}} v_n(w, \gamma_0) T_n(y)$$

where  $e_n$  and  $v_n$  are the elastic and viscous coefficients of the Chebyshev polynomial. Therefore, from the Fourier decomposition of the stress,  $e_n$  and  $v_n$  can be expressed as a function of the viscoelastic moduli as follows:

$$e_n = G'_n(-1)^{\frac{1-n}{2}}$$

$$v_n = \frac{G''_n}{\omega}$$

In the linear regime,  $e_3 \sim 0$  as the behaviour is dominated by the first harmonic. When we enter in the nonlinear domain, the third harmonic is larger than the first one and  $e_3 > 0$  will indicate strain stiffening and  $e_3 < 0$  strain softening. The same way,  $v_3 \sim 0$  for small deformations and at large deformations it will indicate shear thickening when  $v_3 > 0$  and shear thinning when  $v_3 < 0$ .

In chapter 6 we will test the LAOS analysis on sputum samples. We will investigate at which strain  $Q$  starts dropping to identify the beginning of the non-linear domain and we will see the evolution of this coefficient  $Q$ . Then, we will calculate the coefficients of the Chebyshev polynomial ( $e_3$  and  $v_3$ ) to evaluate the strain stiffening and shear-thinning behaviour of sputum.

## 2.2 Statistical analysis

We will be working with different data types and variables throughout this document and will want to compare within cohorts. Therefore, we first need to know which is the probability distribution describing our data to correctly choose the applicable statistical tests.

### 2.2.1 Population distributions

We have used Shapiro-Wilk tests and the graphical quantile-quantile (Q-Q) plots to test normality in our distributions.

Q-Q plots are probability plots in which we have compared the probability distribution of our measured variables with the standardised normal distribution  $N(0,1)$ . For each data point, the abscissa represents its position, in quantiles, within the distribution. The central point is the mean value, and a point at  $x = +1$  is 1 standard deviation above the mean, while  $x = +2$  corresponds to 2 standard deviations over the mean. The inverse interpretation is given to  $x = -1$  and  $x = -2$ , 1 and 2 standard deviations lower than the mean value. If the plotted distributions lie on a diagonal straight line it means our variables follow normal distributions.

As the rheological variables tested often follow log-normal distributions, the logarithmic values of these variables follow normal distributions. We will therefore often refer to the logarithmic values of the rheological variables defined as  $g^* = \log_{10}(G^*)$ ,  $g' = \log_{10}(G')$ ,  $g'' = \log_{10}(G'')$ ,  $s_c = \log_{10}(\sigma_c)$  and  $d_c = \log_{10}(\gamma_c)$ .

### 2.2.2 Mean and variance equality

When the logarithm of the variables follow normal distributions, we have been able to apply bilateral f-tests and t-student tests to analyse the variance and mean equality to the logarithmic values. This methodology is a common practice in literature [28,

29] as the standard arithmetic mean is not representative of log-normal distributions. Rheological properties can vary from one patient to another by up to two orders of magnitude. The arithmetic mean ( $M$ ) is therefore very sensitive to the highest values. In contrast, the geometric mean (which is simply the exponential of the arithmetic mean of the logarithmic data) is less influenced by high outliers and better represents the data distribution. Nevertheless, when performing mean equality tests on logarithmically transformed data, it is important to have in mind that the test is not for the equality of the mean of the raw data ( $M$ ), but rather for the equality of the mean of the log-transformed variable ( $\mu$ ). The two can differ significantly when the variances ( $\sigma^2$ ) of the two tested variables are not the same [30], since  $M = \exp(\mu + \sigma^2/2)$ .

## 2.3 Sample collection

Sputum samples in this document have been collected from the “Centre de Ressource et de Compétence de Mucoviscidose” at Grenoble Alpes University Hospital. All patients included gave their informed written consent and their clinical information were anonymised and kept confidential. The study was approved by the French research ethics committee (Comité de Protection des Personnes, number 20.09.08.61213). In addition, data collected from the Montpellier University Hospital has been used for the LAOS analysis.

Donors were adults suffering from one of the following two obstructive lung diseases: Cystic Fibrosis (CF) or Non Cystic Fibrosis Bronchiectasis (NCFB).

Two expectorations, one for rheometry and one for bacteriology, were obtained during their regular follow-ups with the help of a physiotherapist through autogenic drainage [31] in sterile flat bottom tubes. Autogenic drainage is an airway clearance technique based on the movement of sputum through controlled breathing moving mucus from the deeper lung towards the central airways.

Samples for rheology were subsequently kept less than one hour in the fridge at 4 °C and then saliva was removed with the help of the pipette prior to analysis. The obtained volume was highly variable ranging from 0.3 ml to 3 ml. A small amount of each sample (0.2ml) was used to test the presence of SARS-CoV-2 by reverse PCR. Only 3 expectorations were tested positive and were discarded from this study. Therefore, all the samples included in this document were tested negative for this virus.

The other sample was directly sent to the bacteriology department of the CHU Grenoble hospital where a purulence classification is given to the samples by visual inspection following a colour chart [21, 32] as the one shown in Fig 2.4. Samples are divided in three categories: purulent, semi-purulent and salivary.

Then, a small amount of the sample is spread on a microscope plate and, after gram staining, a count of neutrophils and epithelial cells is done with a x50 objective. The laboratory technicians counts the cells per frame in at least 10 microscope fields and, after averaging, they give one of the following classifications:

- **Absence:** < 2 cells/field
- **Rare:** from 2 to 5 cells/field
- **Some:** > 5 cells/field

Then, bacterial count is carried out after incubation of a small sputum volume on Trypticase Soy Agar (TSA) plates.



Figure 2.4: Colour scale to determine purulence of sputum (patent no. 00218892/1994). The image is from Allegra et al. [19].

## 2.4 Quantitative colour analysis

The methodology used in the hospital to assess purulence is qualitative and user-dependent following 2.4. For this reason we decided to obtain a quantitative procedure through image treatment.

Colours can be described through the HSV colour model by their tone (h), saturation (s) and value (v). The tone, also known as hue, is the pure colour pigment while the saturation depicts the amount of grey in a particular colour in which lower s values introduces more grey fading the colour. Lastly, the value describes the brightness of the colour, it is in some way a transparency measurement. Through image processing we can obtain these values for a given picture and compare them with other images.

Before rheometry, we pipetted 25  $\mu\text{l}$  of sample in a 1x1 cm square gene frame and covered it with a coverslip to avoid evaporation. Then we placed it on a microscope equipped with a colour camera and a x20 objective and took 5 pictures per sample at random places to use as replicas, see Fig 2.5 A, B and C for examples of the collected images. With the same setup we also took pictures of a gene frame filled with water to use as reference.

We imported the images to Matlab and first extracted the RGB (red, green and blue) values of each pixel and divided them by the RGB values of the water sample. Second, we calculated the average RGB values for all the pixels in the image and transformed them into HSV values. Third, we calculated the mean for the 5 replicas per sample. Lastly, in the cases with more than one aliquot per sample, the previous procedure was repeated and the sample's mean and standard deviation was obtained.

We quantified 33 CF and 16 NCFB samples and obtained the values in Fig 2.5 D and E. The colours of the markers are the calculated colour for each sample. We can observe the value h does not evolve keeps similar values around its mean, 0.108.

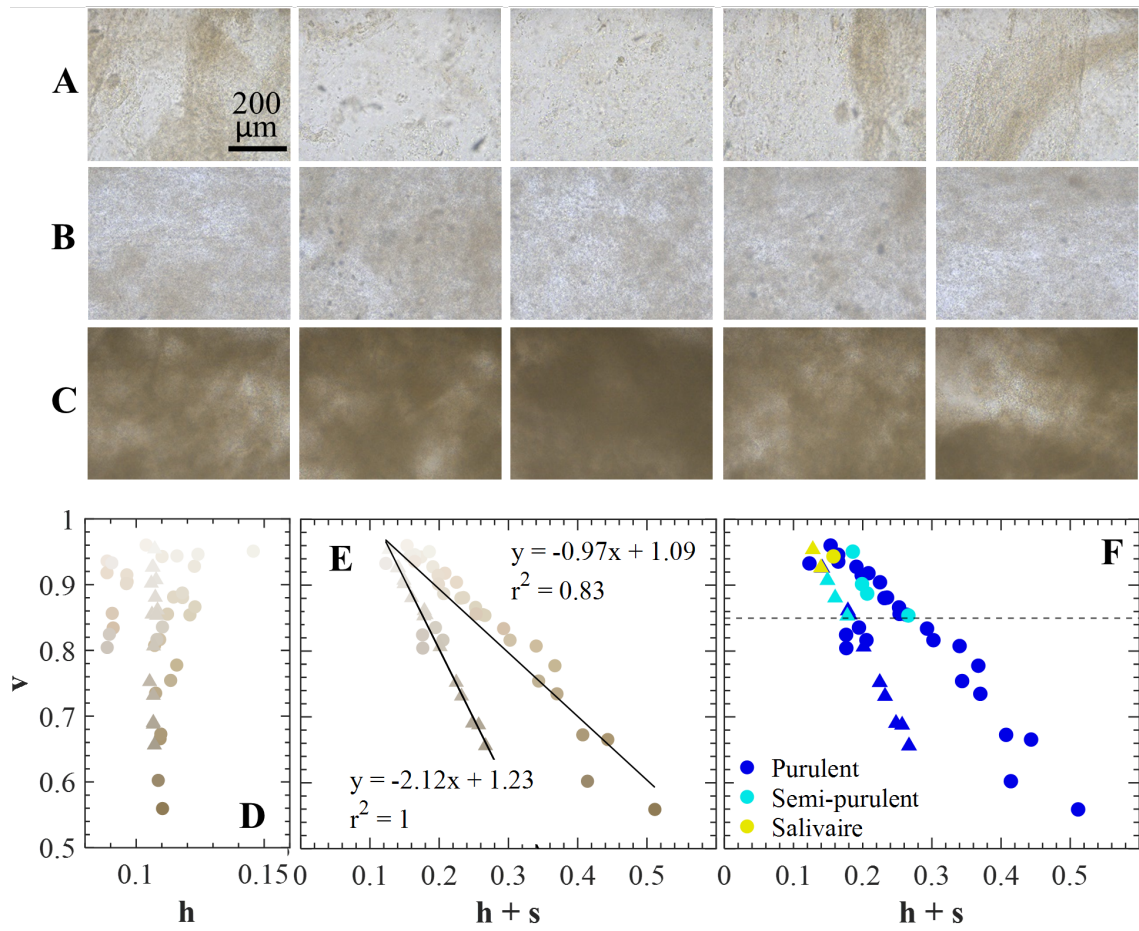


Figure 2.5: A,B and C: Images taken for three sputum samples. D, E: hsv values obtained for 33 CF (circles) and 16 NCFB (triangles) expectorations. The mean standard deviation of each measurement is 0.02. The colour of the markers are the calculated colour for each sample. F: Comparison between purulence classification through visual inspection (coloured markers) and the s and v calculated values. The dotted line marks a limit between purulent and semi-purulent classification.

Contrarily,  $v$  varies its values along a wider range. As  $h + s + v = 1$ , in Fig 2.5 E we have plotted the evolution of  $v$  as a function of  $h + s$  and see how the points follow a tendency: while the lighter samples have low saturation and tone ( $s + h$ ) and high value ( $v$ ), the dark samples show high  $s + h$  and low  $v$ . Therefore, the correlation between  $s + h$  and  $v$  is shown to be linear with the y-intercept  $\sim 1$ . Differences are observed between CF (circles) and NCFB (triangles) samples. NCFB sputa is greyer than CF and the slope of their linear correlation is double than for CF samples.

Fig 2.5 F shows the purulence classification given by the colour chart. We observe that from a certain  $s$  and  $v$  values, all the samples are considered purulent. However, the categorical classification starts having problems with the light expectorations: samples with similar  $s$ ,  $v$  and  $h$  values are categorised differently. Our methodology can be implemented to work with a gradient of purulent levels or by categorising the purulence level by setting a quantitative threshold.

## 2.5 Model fluid of bronchial expectorations

Certain aspects of this research, specifically the investigation of homogenisation (chapters 4 and 5), required the use of fluids that exhibit rheological properties similar to those of sputum. This approach allowed me to overcome the challenges of working with human samples, including their variability and limited availability.

Sputum is a shear thinning viscoelastic fluid characterised by its decrease of viscosity with increasing shear rate as shown in the flow sweeps in Figure 2.6 A. Moreover, sputum is highly elastic as the elastic modulus is higher than the viscous modulus in the amplitude sweeps plotted in Figure 2.6 B. At low strain,  $G'$  and  $G''$  are independent to the applied strain showing a plateau with  $G'$  values from 1 to 100 Pa. When increasing the applied strain, sputum's elasticity decreases reaching a crossover of  $G'$  with  $G''$  at around 1000% strain. Over this critical point the sample starts flowing and behaves as a fluid.

To reproduce this behaviour, we used Flopaam 6035, a high molecular weight synthetic polyacrylamide which reproduces the rheological behaviour of sputum. It is also a shear thinning fluid (see Figure 2.6 C). At low strains, it has a strong elastic response and reaches the crossover point at around 1000%, see Figure 2.6 D. Moreover, its elastic and viscous moduli can be tuned by varying the polyacrylamide concentration with plateau values of  $G'$  ranging from 0.5 to 100 Pa for concentrations from 0.05% to 1%. We have therefore used Flopaam 6035 as a model fluid during the homogenisation and vortex experiments as well as for the preparation of certain set ups.

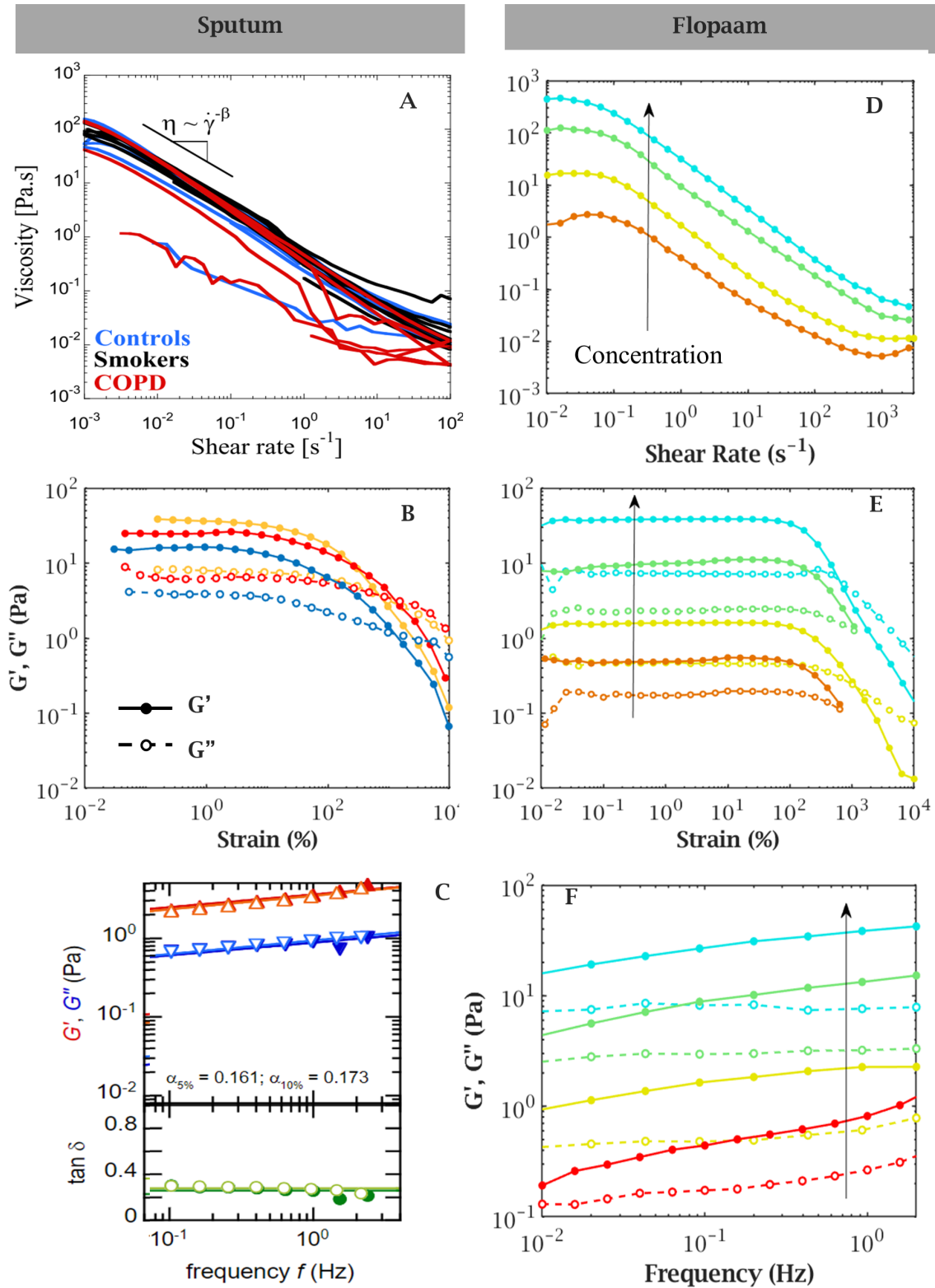


Figure 2.6: A: Flow sweeps of sputum samples of control subjects, smokers, and COPD patients from the PhD of Jory [33]. B: Characteristic amplitude sweeps of CF (orange and blue) and NCFB (red) sputum samples. C: Frequency sweep of a CF sputum sample, the figure is taken from the supplementary material of Patarin et al. [12]. D, E and F: Flow sweeps, strain sweeps and frequency sweeps for increasing concentrations of Flopaam 6035 from 0.05% (red) to 1% (blue).

# Sample management

## Chapter 3

# Sputum handling for rheology

The rheology of sputum has been the subject of study for several years for different research groups around the world as it seems it could be a powerful biophysical marker for monitoring muco-obstructive pulmonary diseases such as CF and NCFB. Yet, rheometry has not been implemented as a standard clinical practice as variable results can be found in literature. The lack of a standardised protocol for processing sputum samples from collection to analysis can result in highly variable and inconsistent results.

In this chapter, we aim to establish a standardised and robust protocol for handling sputum samples before rheological measurements. It is presented as article format as it has been published in Scientific Reports under the DOI 10.1038/s41598-023-34043-9.

We investigated the effect of heating sputa as it could be required to eliminate the activity of certain pathogens such as the COVID virus or the *Mycobacterium tuberculosis* and found heating is completely destructive. We then evaluated the evolution of rheology along time to find strong differences between purulent and semi-purulent samples. While purulent sputa reduced to half their  $G'$  and  $G''$  in the first 6h, semi-purulent kept their viscoelasticity constant within 24h. However, we have proven storing samples at  $-80^{\circ}\text{C}$  and thawing them at  $37^{\circ}\text{C}$  prior to measurement does not affect rheometry. Therefore we recommend samples should be frozen as soon as possible after collection and stored until the measurement. Lastly, we observed the variability of rheological measurements was largely due to the sample's macroscopic heterogeneity and can be significantly reduced by non-destructive vortex homogenisation. The vortexing protocol however did not seem to be enough for some samples which presented large differences within aliquots. The protocol followed in this chapter consisted on gradually increasing the vortex intensity until the sample formed a torus, after which the stirring was maintained for 30 seconds. We hypothesise increasing the vortex time could reduce the variability observed within aliquots and we test this hypothesis in chapter 4.

These findings define a robust and unified protocol for simple sputum handling in rheometry, recommending vortexing and snap freezing of sputum samples immediately after collection when direct testing is not feasible.

# Sputum handling for rheology

Lydia Esteban Enjuto<sup>1,2,\*</sup>, Matthieu Robert de Saint Vincent<sup>1,2</sup>, Max Maurin<sup>3</sup>, Bruno Degano<sup>4</sup>, and Hugues Bodiguel<sup>1</sup>

<sup>1</sup>Univ. Grenoble Alpes, CNRS, Grenoble-INP, LRP UMR5520, Grenoble France

<sup>2</sup>Rheonova. 1 Allée de Certèze, 38610 Gières, France

<sup>3</sup>Univ. Grenoble Alpes, CNRS, CHU Grenoble Alpes, TIMC, Grenoble, France

<sup>4</sup>Univ. Grenoble Alpes, INSERM U1030, CHU Grenoble Alpes, Grenoble, France

\*estebanl@univ-grenoble-alpes.com

## ABSTRACT

The rheology of sputum is viewed as a powerful emerging biophysical marker for monitoring muco-obstructive pulmonary diseases such as cystic fibrosis (CF) and non-CF bronchiectasis (NCFB). However, there is no unified practice to process sputa from collection to analysis, which can lead to highly variable, and sometimes inconsistent results. The main objective of this study is to bring light into the handling of sputum samples to establish a standardised and robust protocol before rheological measurements.

Sputum collected from 22 CF and 10 NCFB adults, was divided into control (vortexed and fresh: non-heated and non-frozen) and three treated conditions (either non-vortexed, heated or frozen). In addition, 6 CF expectorations were used to study the dynamics of ageing over 24 hours. Sputum's mechanical properties were measured with a rotational rheometer to obtain their properties at rest, elastic ( $G'$ ) and viscous moduli ( $G''$ ), and at the onset of flow, critical deformation ( $\gamma_c$ ) and critical stress ( $\sigma_c$ ). We demonstrate that heating sputum is completely destructive while freezing sputa at  $-80$  °C has no discernible effect on their rheology. We also show that the variability of rheological measurements largely resulted from the sample's macroscopic heterogeneity, and can be greatly reduced by non-destructive vortex homogenisation. Finally, we observed contrasted ageing effects as a function of purulence: while the viscoelasticity of purulent samples reduced by half within six hours after collection, semi-purulent samples did not evolve.

These results guide towards a robust unified protocol for simple sputum handling in rheometry. We therefore suggest to vortex and snap freeze sputum samples immediately after collection when direct testing is not possible.

## Background

Muco-obstructive lung diseases as defined by Boucher<sup>1</sup> clinically present “cough, sputum production, and episodic exacerbations” leading to the obstruction of the airways. These diseases include cystic fibrosis (CF), non cystic fibrosis bronchiectasis (NCFB), primary ciliary dyskinesia (PCD) and chronic obstructive pulmonary disease (COPD).

In these diseases, bronchial mucus is hyper-secreted and thickened, which results in anomalous mucus clearance, thereby favouring bacterial growth and subsequently infection<sup>2,3</sup>. Techniques to help patients drain the mucus out of their airway system involve chest physiotherapy<sup>4</sup>, and the use of mucolytic treatments which directly alter the mucus structure<sup>5,6</sup>. These methods consist in either altering the breathing airflow to improve mucus mobilisation, or reducing mucus viscoelasticity, two physical concepts which can be quantified through rheology. The elastic ( $G'$ ) and viscous moduli ( $G''$ ) assess the viscoelastic character of mucus at rest, and the critical stress ( $\sigma_c$ ) and deformation ( $\gamma_c$ ) determine its flowing ability.

The potential of sputum rheology as a direct biomarker of health status has been brought forward since the 1980s<sup>7-11</sup>. Measuring the rheological properties of sputum indeed presents two decisive advantages. First, mucus is readily available from obstructive pulmonary disease patients with airway obstruction in the form of sputum. Sputum is expelled through the mouth, during a physiotherapy session for instance, by NCFB or CF patients who have not been treated with a CFTR regulator. Second, rheology quantitatively characterises physical properties linked to mucus transport. Despite this interest, sputum rheology has not yet been adopted in routine as the quantitative link between rheology and bronchial obstruction still remains an open question<sup>12-14</sup>. One of the present limitations resides in the fact that there is no standardised protocol on the way samples should be treated prior to measurement. Moreover, the immediate access to a rheometer, as well as to an expert choice of measurement protocols, is not always possible for many clinical research teams. Having a consistent procedure to store samples with no effect on rheology would encourage multidisciplinary collaborations making rheology more accessible.

The development of sputum rheology also poses several practical questions. The first one relates to the rheological measurement itself, in terms of spatial as well as temporal scale to be investigated. Micrometre-scale rheology techniques, also referred to as microrheology<sup>15-17</sup>, are indeed relevant to probe the mucus environment as it would be perceived at the

scale of cilia, and thereby assess the effectiveness of mucociliary clearance<sup>14</sup>. Although these techniques do not require large volumes of sample, they imply seeding (sub-)micrometric probe particles therein, and often require specific instrumentation and competency. Macrorheology at the other end considers the mucus sample as a whole, which may be more representative of its global transport properties. Rheological measurements typically consist in exerting oscillatory strains (or stresses) and measuring the resulting stresses (or strains) through the sample. Oscillatory sets with gradually varying frequency probes the structure of the sample at different time scales. In bronchial mucus, the elastic and viscous moduli typically follow weak power laws with frequency in the range 0.1–10 Hz with  $G' > G''$ <sup>17–20</sup>, which illustrates a soft gel-dominated behaviour from the time scale of the ciliary beating motion to that of mucus drainage. Frequency tests do not give any information on the behaviour of mucus under large deformation. Conversely, increasing the amplitude of oscillations, at fixed frequency, allows to probe the mucus behaviour from quasi-rest up to flowing conditions<sup>18,20</sup>, and therefore simulate more representatively the wide range of strains that can be exerted through the various natural and assisted clearance mechanisms.

Due to its relative simplicity of operation, macrorheology is often preferred in preclinical studies. Visual inspection of CF sputa evidences that they are in general composed of two phases: a light and clear matrix, and thick, opaque mucous plugs dispersed therein. This heterogeneity is problematic in rheometry as the samples tested may over-represent one of these two rheologically distinct phases. A proposed solution consists in homogenising samples prior to measurements by vortexing, but it is still debated as potentially disruptive to the sample's structure<sup>9,10,21</sup>. Other groups prefer to isolate the plugs before analysis<sup>22</sup>, through a protocol that complicates the direct use of sputum rheology in the hospital's routine.

Another immediate question, particularly acute in the context of the Covid-19 pandemic, is linked to biosafety when manipulating potentially contaminated samples. In the field of tuberculosis, Friedrich *et al.*<sup>23</sup> had already proved the inactivation of *Mycobacterium tuberculosis* by heating sputum. This inactivation could eliminate the need for category 3 BSL (biosafety level). The same way, in the context of SARS-CoV-2, preventive heating of samples to inactivate the SARS-CoV-2 virus has been suggested<sup>24,25</sup>, allowing immediate analysis of sputum without waiting for its detection through q-PCR. The effect of heating on the structure of sputa is however unknown. Alternatively, delaying the measurement raises the question of sample long-term conservation. The freezing of sputa has been validated for cell count after storage at  $-20\text{ }^{\circ}\text{C}$  with the use of cryopreservants<sup>26</sup>, and for bacterial DNA detection at  $-80\text{ }^{\circ}\text{C}$ <sup>27</sup>. The few existing rheological tests on thawed sputa have been carried out after freezing at  $-20\text{ }^{\circ}\text{C}$  without additives<sup>28</sup>, or at  $-80\text{ }^{\circ}\text{C}$  mixing results of expectorations coming from different obstructive diseases<sup>29</sup>. Without freezing, samples can rapidly undergo alterations, including enzymatic degradation<sup>30</sup>, alteration of bacterial components<sup>28,31</sup> and oxidation of mucins<sup>32</sup>. Thus, the effect of ageing on rheology must also be addressed as samples cannot always be treated rapidly.

In the present paper, we address these questions from a practical standpoint, to progress towards a unified protocol for sputum rheology in CF and NCFB. Starting from fresh, vortex-homogenised samples as reference, we first quantify the factors of variability within the sputum sample population and within aliquots. We then systematically assess the effect of non-homogenisation, heating, direct freezing and snap freezing by cross-comparing 'treated' (prepared with the condition to be assessed) to 'control' (prepared with the reference protocol) aliquots of each sample. This direct cross-comparison helps us to overcome the limitation of sample variability. Finally, we address the effect of sample ageing through continuous rheological measurements under controlled atmosphere, evidencing a possible dichotomy according to the initial aspect of the samples. Our results provide guidelines towards protocol recommendations to perform sputum rheological measurements in routine.

## Methods

All experiments were carried out in accordance with relevant guidelines and regulations.

### Sputum processing

#### *Clinical protocol*

Sputum samples were obtained from the "Centre de Ressource et de Compétence de Mucoviscidose" at the Grenoble Alpes University Hospital. All patients included gave their written informed consent and their clinical information were anonymised and kept confidential. The study was approved by the French research ethics committee (Comité de Protection des Personnes, case number 20.09.08.61213).

#### *Sample collection*

Expectorations were induced by autogenic drainage<sup>33</sup> with the help of a physiotherapist and immediately transferred into sterile flat bottom tubes at  $4\text{ }^{\circ}\text{C}$ . Samples were macroscopically heterogeneous, composed of saliva, coloured bronchial mucus plugs and translucent mucus. The volume collected varied between patients and diseases. NCFB expectorations were larger than CF samples with volumes ranging from 0.55 ml to 7 ml while CF samples were between 0.4 ml and 5 ml. Purulence was determined by visual inspection following the colour classification proposed in ref.<sup>2</sup>. Expectorations colours ranged from clear to dark yellow/green. A small fraction (0.2 ml) was used to test the presence of SARS-CoV-2 by reverse-PCR. All

samples of the study tested negative for this virus. Then, within 1 hour after sample collection, saliva was removed and, unless otherwise stated, the expectoration was homogenised. The sample was vortexed, gently increasing the stirring intensity until the sample visually takes the shape of a torus and starts flowing (see Supplementary Figure S1 for specific details). This vortex intensity was then maintained during 30 s. Visually, all aliquots looked homogeneous after this procedure. We decided to use the vortexed samples as controls, since, as will be shown in the results, variability was greatly increased for the non-vortexed ones, in particular for the case of CF. When possible, samples were then divided into at least two aliquots. Each sample thus provided at least one aliquot for the studied condition, and at least one control, so that treated and control samples could be cross-compared. Whenever additional aliquots were obtained, they were used as replicates. The typical volume per aliquot was about 500  $\mu\text{l}$ , which allowed reliable rheological measurements (330  $\mu\text{l}$  required).

### **Treatments**

We investigated the effect of four different conditions by comparison with controls (fresh vortexed samples):

- Heating ( $N_{\text{CF}} = 3$ ) — fresh samples were homogenised and heated at 56 °C for 30 min<sup>24,25</sup>. The samples were then let 15 min to cool back to room temperature.
- Freezing ( $N_{\text{CF}} = 4$ ) — fresh samples were homogenised and brought into a –80 °C freezer. Prior to measurement, they were thawed quickly at 37 °C.
- Snap freezing ( $N_{\text{CF}} = 7$ ,  $N_{\text{NCFB}} = 4$ ) — fresh samples were homogenised and put into dry ice for rapid freezing before storage in the –80 °C freezer. Prior to measurements, they were thawed quickly at 37 °C.
- Not vortexing ( $N_{\text{CF}} = 8$ ,  $N_{\text{NCFB}} = 4$ ) — fresh samples were not homogenised prior to sample aliquoting. Visually, non-homogenised CF aliquots featured large (several mm) thick plugs within a slightly turbid liquid matrix; instead, non-homogenised NCFB samples looked monophasic.

In addition, we also assessed the ageing of  $N_{\text{CF}} = 6$  samples when kept at room temperature during 24 h.

### **Data Analysis**

Statistical analysis was performed with Matlab R2020b. We verified normality with the Shapiro-Wilk test and compared control from treated samples by bilateral t-tests.

## **Rheology**

### **Strain sweeps**

Rheological measurements were performed with a rotating rheometer, Rheomuco (Rheonova, France), operating in oscillation at 1 Hz and 37 °C, with rough, plane-plane geometries (25 mm diameter). The gap between the plates was dependent of the volume of the aliquot and ranged from 0.5 to 1 mm. Samples were submitted to strain steps of increasing amplitude between 0.1 % and 10,000 %; due to low signal-to-noise ratio the measurements obtained below 1 % strain were systematically ignored. The values of the elastic and viscous moduli were automatically extracted at 5 % strain ( $G'_{5\%}$  and  $G''_{5\%}$ ), as well as the critical strain  $\gamma_c$  (where  $G' = G'' = G'_c$ ) and the corresponding critical stress  $\sigma_c = \sqrt{2}G'_c\gamma_c$ . As these rheological quantities follow log-normal distributions<sup>20</sup>, we define  $g' = \log_{10} G'$ ,  $g'' = \log_{10} G''$ ,  $d_c = \log_{10} \gamma_c$ , and  $s_c = \log_{10} \sigma_c$ , with  $G'$ ,  $G''$  and  $\sigma_c$  expressed in Pascals, and  $\gamma_c$  unit less.

### **Ageing of sputum**

Ageing experiments consisted in continuously exerting a low-amplitude (5 %) oscillating strain during 24 h with an ARG2 rheometer (TA Instruments). The sample was kept at room temperature (25 °C) within an isolation chamber, under a constant flow of water-saturated air to preserve it from drying.

## **Results**

In this study 26 expectorations were collected from 22 stable CF patients, 13 men and 9 women with ages from 19 to 53 years ( $33.3 \pm 9.6$ ), and 10 expectorations from NCFB patients, all women between 19 and 45 years ( $31.4 \pm 8.2$ ). Demographic and other relevant patients data are summarised in the Supplementary Table S1.

### **Rheological parameters**

#### **CF and NCFB sputa are rheologically similar**

Rheologically, sputum behaves like a soft gel with very high stretching ability, partly returning to its original state when released and thereby showing a predominant elastic response. Under strong efforts, beyond a critical deformation  $\gamma_c$  or stress  $\sigma_c$ , some bonds in the network break. The gel then loses most of its elastic character and flows. Figure 1 illustrates this general

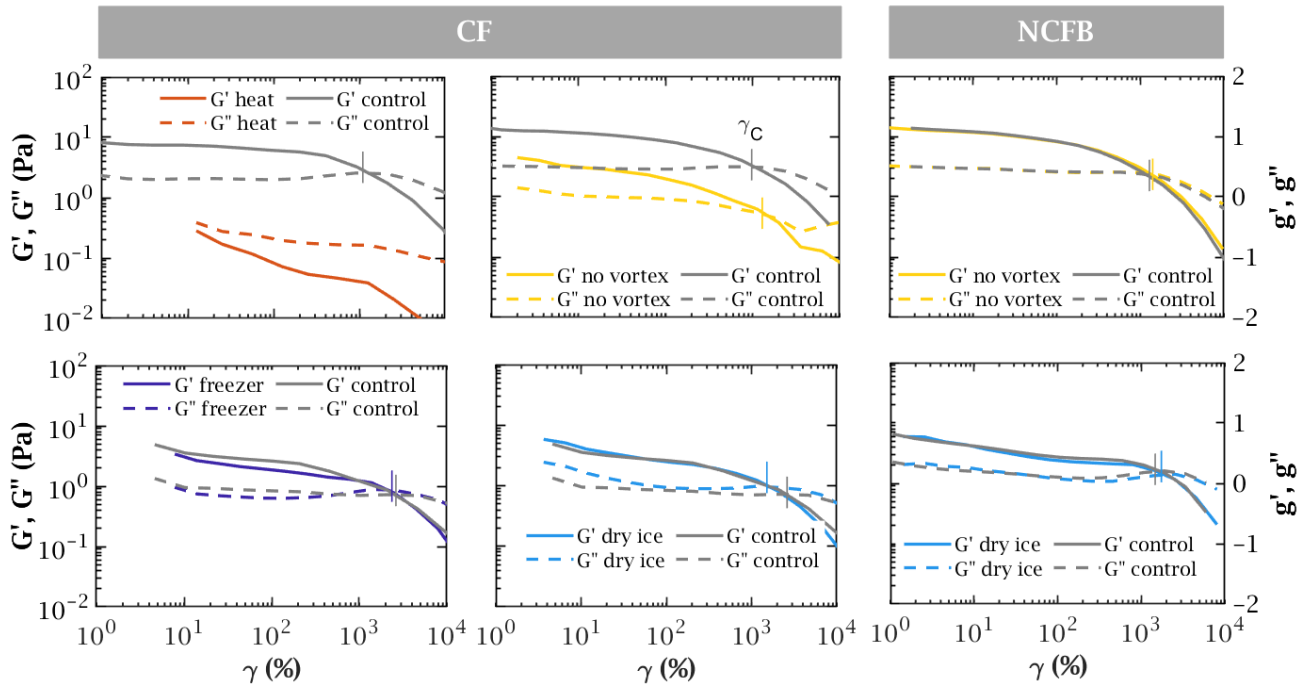


**Figure 1.** Representative strain sweeps for CF and NCFB sputa: evolution of  $G'$  (solid line) and  $G''$  (dashed line) with the exerted strain. Grey and coloured curves correspond to control and treated samples, respectively. The mark at the crossing of the curves denotes the critical point, where  $G' = G''$  at  $\gamma = \gamma_c$ . Measurement uncertainty lies within the line thickness.

behaviour in CF and NCFB sputa. Under low strain, sputa feature a constant linear viscoelastic regime (plateau in  $G'$  and  $G''$ ) with  $G' > G''$ , for strains up to several tens of percent. Increasing the strain,  $G'$  and  $G''$  gradually drop until intersecting at the critical strain  $\gamma_c$ , typically around 1000 %.

We summarise this general behaviour by four rheological quantities: the elastic and viscous moduli in the linear regime,  $G'_{5\%}$  and  $G''_{5\%}$ , and the critical strain and stress,  $\gamma_c$  and  $\sigma_c$ . In CF sputa,  $G'_{5\%}$  and  $G''_{5\%}$  typically range within 1–100 Pa and 0.3–30 Pa, respectively;  $\gamma_c$  within 300–3000 % and  $\sigma_c$  within 3–100 Pa, or equivalently  $g'_{5\%} \in [0, 2]$ ,  $g''_{5\%} \in [-0.5, 1.5]$ ,  $d_c \in [0.5, 1.5]$  and  $s_c \in [0.5, 2]$  in logarithmic scale (Figure 2). In NCFB expectorations,  $G'_{5\%}$  and  $G''_{5\%}$  range within 1–20 Pa and 0.5–5 Pa,  $\gamma_c$  within 900–3000 % and  $\sigma_c$  within 7–70 Pa, or  $g'_{5\%} \in [0, 1.5]$ ,  $g''_{5\%} \in [-0.5, 1]$ ,  $d_c \in [0.5, 1.5]$  and  $s_c \in [0.5, 2]$ . CF and NCFB sputa thus lie within the same magnitude range regarding these four rheological parameters.

#### Linear and flow rheology are poorly correlated

For both CF and NCFB expectorations, in the linear regime, the viscous and elastic moduli are highly correlated as the ratio  $G''_{5\%}/G'_{5\%}$ , referred to as the damping ratio  $\tan \delta_{5\%}$ , is consistently close to 0.3. The critical strain and stress are poorly correlated to  $G'_{5\%}$  as the slopes are flatter and the measured values are highly dispersed (Figure 2). In general, higher viscoelasticity comes with higher critical stress and lower critical strain. Lastly, we could not identify any correlation between  $d_c$  and  $s_c$ . We therefore focus, in the present study, on three weakly correlated or independent variables:  $g'_{5\%}$ ,  $d_c$  and  $s_c$ .

#### Sample and aliquoting variability

We have first divided 15 CF and 10 NCFB control samples into 2, 3 or 4 aliquots to assess sputum's inter-sample (between expectorations) and intra-sample (between aliquots) variability.

#### Rheometric variables are log-normally distributed

Figure 3 (a,b) depicts the distribution of the logarithmic values of the three quantities considered ( $g'_{5\%}$ ,  $d_c$  and  $s_c$ ), represented as quantile-quantile plot with normal distribution. Each data point corresponds to the average value per sample, identified by its colour; the associated standard deviations between aliquots are represented as error bars. All data sets are very well adjusted by normal distributions in accordance with Patarin *et al.*<sup>20</sup>. Shapiro-Wilk normality tests provide p-values of respectively 0.82, 0.61 and 0.37 for  $g'_{5\%}$ ,  $d_c$  and  $s_c$  for CF samples, and 0.63, 0.88 and 0.45 for NCFB samples. The normality is therefore verified. As a consequence, the effects of treatments were analyzed using log-transformed data. In particular, bilateral t-tests for mean

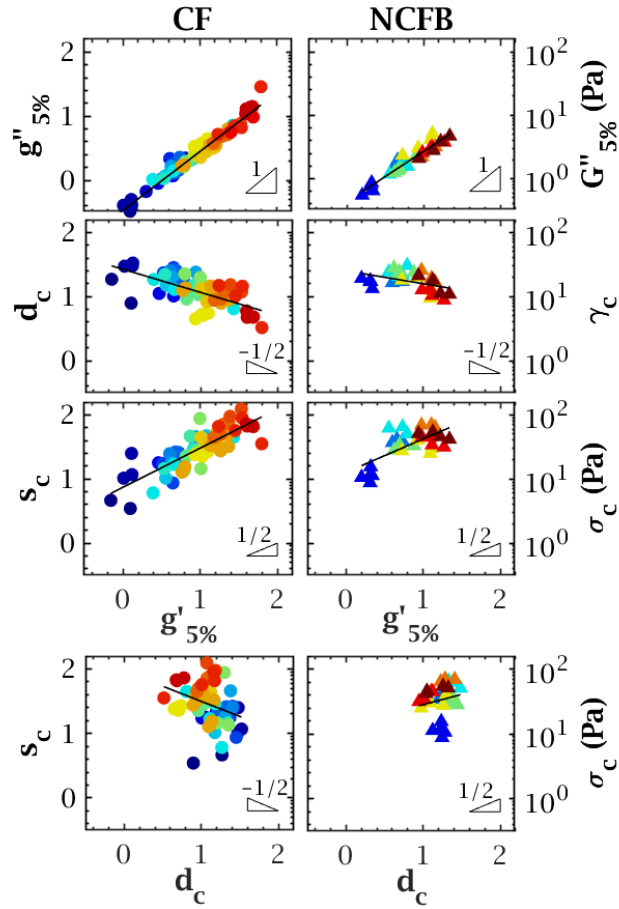


**Figure 2.** Top: Evolution of the logarithmic viscous modulus  $g''_{5\%}$ , critical strain  $d_c$  and critical stress  $s_c$  with the logarithmic elastic modulus  $g'_{5\%}$  for non-heated expectations of CF ( $N = 26$ ) and NCFB ( $N = 10$ ) patients. Each colour represents an expectation with its corresponding aliquots. The uncertainty on the moduli at 5 % strain is in the order of 0.6 Pa, smaller than the symbol size through most of the distribution.  $g'_{5\%}$  and  $g''_{5\%}$  are strongly correlated, and  $d_c$  and  $s_c$  are weakly correlated to  $g'_{5\%}$ . Bottom: Evolution of  $s_c$  with  $d_c$ . No correlation is found between these variables.

equality check are made on these transformed data. Note that by doing so, the tests check the equality of the geometric means of the scaled variables and not that of the arithmetic mean<sup>34</sup>, the latter being often biased by large outliers.

#### **Rheometry is reproducible within aliquots**

At the individual sample level, the standard deviation between aliquots quantifies the measurement reproducibility. Throughout the CF population, the distribution of standard deviations took a piecewise linear form, which corresponds to a bimodal probability distribution (Fig. 3 (c)). In the low-variability subpopulation, which encompasses 65–70 % of the samples, the aliquoting standard deviation remained below 0.12, between half and third of the inter-sample variability  $\sigma_p$  obtained in Figure 3 (a,b). In contrast, the distribution of standard deviations for NCFB samples (Fig. 3 (d)) followed a normal distribution (linear quantile plot) and all values stayed below 0.12. This lower variability in NCFB samples is consistent with their visually lower heterogeneity (Supplementary Figure S2).

Another remarkable feature is that the variability in each of the rheological variables is quite independent. For instance, the CF sample marked with an arrow in Fig. 3 (c) featured a high  $s_c$  standard deviation, while the standard deviations regarding the other two variables are small.

#### **Treatment effect**

We first analysed the effect of the treatments by qualitative inspection of the rheological curves of control and treated aliquots from the same sample (Figure 1). Then, we compared sample by sample the treated and control aliquots by calculating the difference between the corresponding logarithmic rheological values,  $\Delta X = X_{\text{condition}} - X_{\text{control}}$ , where  $X = g'_{5\%}$ ,  $d_c$  and  $s_c$ . The

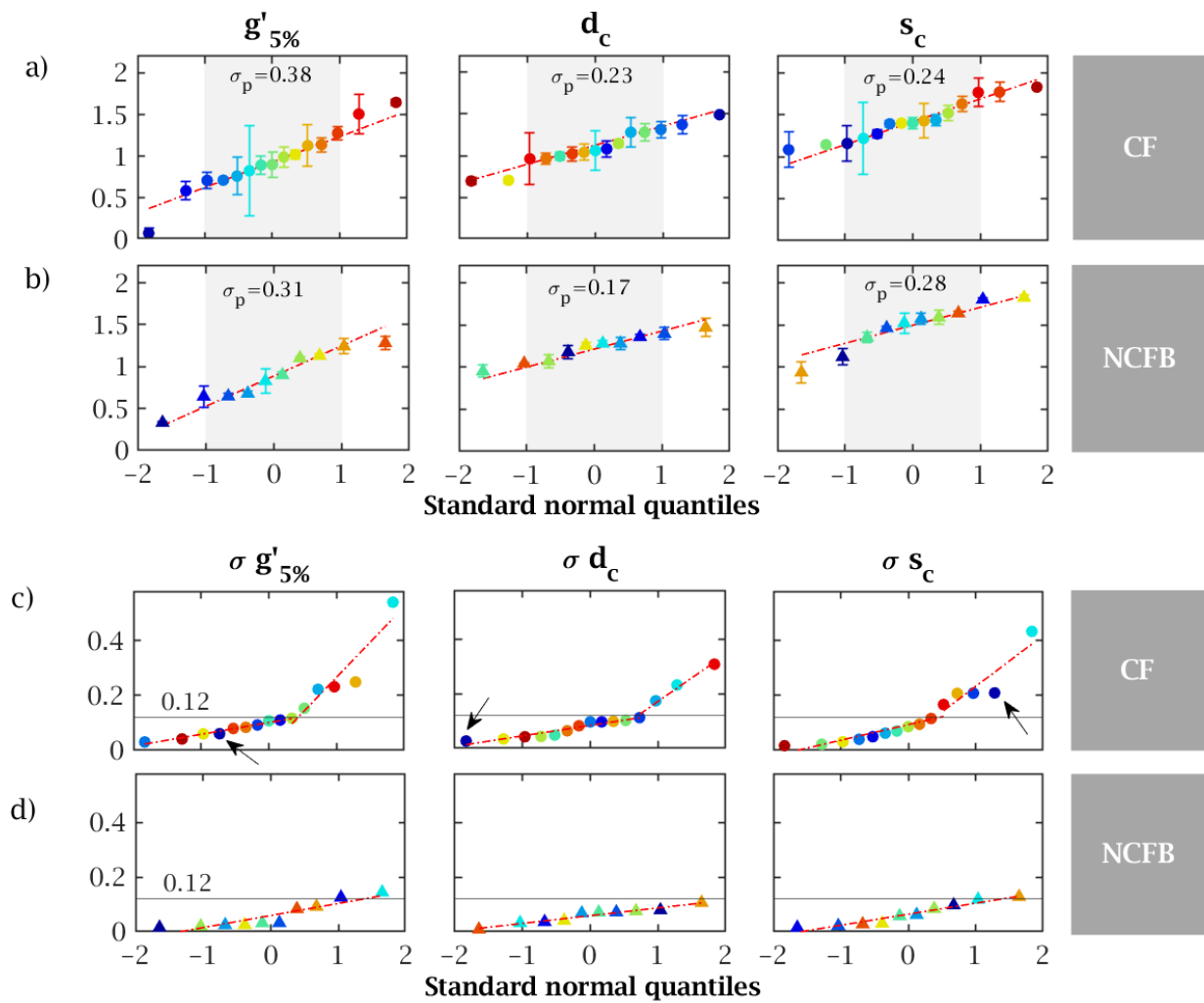


**Figure 3.** (a,b) Distribution of the logarithmic rheological quantities for the 15 CF (circles) and 10 NCFB (triangles) control expectorations. Each data point corresponds to the average value per sample, identified by its colour. The error bars correspond to the standard deviations due to sample aliquoting. The dashed line corresponds to a normal distribution; the grey area delimits 1 standard deviation around the mean. (c,d) Distribution of the standard deviations between the aliquots of the 15 CF (circles) and 10 NCFB (triangles) control expectorations.

obtained values for CF and NCFB samples are shown in Figure 4 as circles and triangles respectively. These results were statistically confirmed with bilateral t-tests to inspect mean equality between treated and control groups. The null hypothesis establishes mean equality between the groups while the alternative hypothesis considers mean inequality.

#### **Heating degrades the structure of sputum**

Heating sputum qualitatively modified its rheology (Fig. 1, top left). Samples became much more fluid-like ( $G'' > G'$ ) throughout the whole strain range, with viscoelasticity levels decreased by more than one order of magnitude, and lost their linear viscoelastic plateau. Only one of the three samples tested featured a critical point, observed at both lower strain and stress than the corresponding control (Figure 4). Structurally, this reversal from a mostly energy-conservative to a mostly energy-dissipative material means that the original backbone network of sputum has turned into non-cohesive elements, without recovering as the sample went cooled back to room temperature. These observations demonstrate the degradation of the gel network under heating.

#### **Freezing has no effect on sputum rheology**

Conversely, both CF and NCFB frozen samples were rheologically almost indistinguishable from their fresh counterparts (Fig. 1, bottom), although direct freezing caused slightly more variability than snap freezing in dry ice for the analysed CF

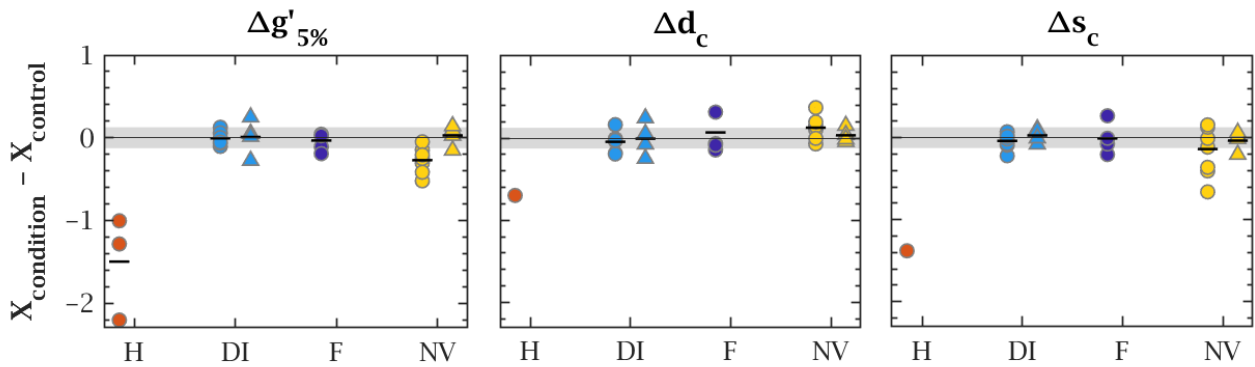


**Figure 4.** Comparison between the logarithmic rheological quantities of treated and control samples. H: heating, DI: Dry Ice, F: Freezing at  $-80\text{ }^{\circ}\text{C}$  and NV: not vortexed. Symbols correspond to individual CF (circles) and NCFB (triangles) samples. Only one of the three heated samples featured a crossover point, resulting in a single point in  $\Delta d_c$  and  $\Delta s_c$  for this condition. The small horizontal bar denotes the mean value of the considered condition. The grey band stands for  $\pm 0.12$ , the aliquoting standard deviation which separates low from high variability CF samples.

samples (Fig. 4). P-values (Supplementary Figure S3) for the freezing treatment were in all cases higher than 0.75, therefore the equality of means is very likely.

#### **Vortex preserves rheology and reduces variability**

Vortexing samples did not alter the qualitative shape of the rheological curves (Fig. 1, bottom right). However, non-vortexed CF samples featured weak variations of the mean: slightly lower  $g'_{5\%}$  and  $s_c$ , and slightly higher  $d_c$  (Fig. 4). Visual inspection of CF samples prior to measurement showed no difference in heterogeneity as shown in Supplementary Figure S2. We believe the lower viscoelasticity observed in non-homogenised samples could be due to the fact that the highly viscoelastic plugs would rather stay in the centre of the rheometer's geometry while the matrix flows towards the edge of the geometry. Since stresses at the outer edge of the plates have a dominant contribution to the overall torque generated, the measured response would then be mostly determined by the matrix, of comparatively low viscoelasticity. Conversely, vortex homogenisation breaks these inclusions and therefore allows to get a higher proportion of this viscoelastic material evenly distributed on the geometry, which could explain why homogenised samples are actually measured more viscoelastic. Statistically, we can reject the alternative hypothesis, different means ( $p > 0.05$ ) for all the samples (Supplementary Figure S3). However, the variation in rheological quantities was significantly higher than the aliquoting standard deviation after homogenisation (grey band in Figure 4) for the CF samples. Therefore, the effect of non-vortexing is more important than the aliquoting effect. This difference thus highlights the importance of homogenisation to get meaningful results, especially in samples which present large and thick mucous heterogeneities.

In contrast, vortex did not have any effect on NCFB expectorations and this result was consistent for all the analysed samples: all t-tests gave p-values over 0.75. This outcome was expected as, by sight, NCFB sputa are less heterogeneous than CF expectorations.

In summary, our results show no effect of freezing on sputum rheology, while heating is completely destructive. They also confirm the importance of carefully homogenising CF samples as their heterogeneity is a major factor of measurement variability. The specific effect of the vortexing protocol (e.g. duration, intensity) on this variability, especially in the samples with important aliquoting standard deviation in Figure 3 (b)), remains an open question.

#### **Ageing of sputum**

Biological samples evolve and should therefore be analysed immediately after collection. However, this temporal evolution is rarely quantified and it is therefore difficult to assess the sensitivity of samples to ageing. We characterised the rheological evolution of CF sputa when left at room temperature during 24 h by continuously monitoring their linear elastic and viscous moduli. Measurements started one hour after collection.

#### **Semi-purulent sputa are rheologically stable**

Sputa featured two distinct evolutions according to their purulence, estimated visually<sup>2</sup> (Figure 5). The semi-purulent samples ( $N = 2$ ) did not show any substantial rheological evolution as the values of  $G'_{5\%}$  and  $G''_{5\%}$  remained constant throughout the

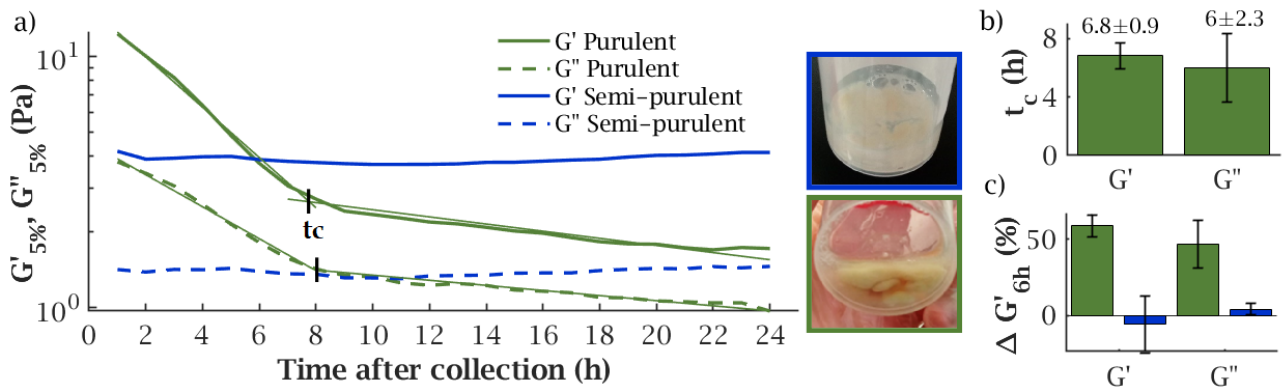


**Figure 5.** (a) Storage and loss moduli evolution in 24 hours for a purulent (green) and a semi-purulent samples (blue). The crossing point of the fits gives the characteristic time  $t_c$  (indicated with black marks) for the  $G'$  and  $G''$  drop found in purulent samples, obtained by intersecting the exponential fits to the two regimes (light green lines). (b) Mean values and standard deviations of  $t_c$  in  $G'$  and  $G''$  for purulent samples. (c) Mean values and standard deviations of the evolution of  $G'$  and  $G''$  after 6 hours,  $\Delta G'_{6h}$  and  $\Delta G''_{6h}$  for purulent and semi-purulent samples.

whole test.

#### Purulent sputa degrade in 6 hours

Conversely, in the purulent sputa ( $N = 4$ )  $G'_{5\%}$  and  $G''_{5\%}$  first dropped before an apparent stabilisation. The characteristic time to reach this steady state,  $t_c$ , was obtained by interpolation of the crossing point of two exponential fits in the two regimes found. It was very similar among the four samples,  $t_c = 6.8 \pm 0.9$  hours for  $G'$  and  $6.0 \pm 2.3$  hours for  $G''$  (Fig. 5 (b)). Moreover, the initial dynamics was also remarkably consistent among purulent samples. The reduction in moduli after 6 hours, defined as

$$\Delta G_{6h} = \frac{\Delta G_{5\%}(t = 1h) - \Delta G_{5\%}(t = 6h)}{\Delta G_{5\%}(t = 1h)},$$

was  $\Delta G'_{6h} = 59 \pm 5.7$  % and  $\Delta G''_{6h} = 47 \pm 16$  %. The difference between these two drops was not significant ( $p = 0.227$ ). Semi-purulent samples did not evolve significantly as  $\Delta G'_{6h} = -5.7 \pm 18.4$  % and  $\Delta G''_{6h} = 4.2 \pm 3.6$  % (Fig. 5 (c)).

A comparable decrease in CF sputum viscoelasticity, attributed to biological activity, was already reported at 37 °C, but not at 25 °C<sup>28</sup>. Conversely, Yuan *et al.* reported a two-fold increase of the viscoelastic moduli of healthy sputa under pure oxygen at 37 °C, attributed to an increase of mucin cross-links due to oxidation<sup>32</sup>. Our own results suggest that oxidation actually plays a minor role in ambient atmosphere as no stiffening is observed. The distinct evolution of the purulent samples tends to confirm that proteolytic degradation of the sample has a greater effect than oxidation as previously reported for acute asthma samples<sup>30</sup>. Practically, this evolution confirms that the delay between collection and rheometry should be minimised. However, semi-purulent samples are much less sensitive and a delayed rheological characterisation could still be considered meaningful.

## Discussion

In this paper, we have systematically investigated the effect on rheology of sample handling and storage of cystic fibrosis and non cystic fibrosis bronchiectasis sputa.

We first demonstrated that both CF and NCFB expectorations can be stored at  $-80$  °C without affecting substantially their rheological properties. Therefore, the rheological analysis of sputum samples can be performed without complicated logistic procedures. For instance, heating for preventive decontamination of the samples is not necessary as the possibility of freezing allows to wait for the results of microbial analyses prior to handle them.

While sputum samples are easy to obtain, their heterogeneity poses a concern about the repeatability of macrorheological measurements. We have shown how vortexing CF and NCFB sputum reduces the dispersion of rheological parameters, while keeping the mean values unchanged. The measurements carried out with NCFB samples, which are more homogeneous, showed low standard deviations. In contrast, we have found a larger effect of the heterogeneity of the CF samples which results in a greater dispersion. Moreover, the standard deviation between aliquots did not follow a Gaussian distribution in case of CF samples, but exhibited a long tail for the most heterogeneous ones. For these, the vortexing procedure was probably too short or too gentle to reach a complete homogenisation. A complementary study would clarify the influence of the homogenisation parameters, such as vortex duration, on the dispersion of rheological results in natively heterogeneous samples. At the structural

scale, microrheological investigations<sup>15–17</sup> would provide insight on the intimate mechanisms involved during homogenisation, for instance to better understand how the inclusions interleave within the matrix and how it affects the mechanical properties of mucus locally.

Finally, we also characterised the temporal evolution of CF sputa. While purulent samples see their elastic and viscous moduli reduced by about half in the first 6 hours, the semi-purulent samples remain unaffected. This contrasted result suggests that sputum degradation is mainly influenced by its biological load and not by its oxidation<sup>32</sup>. In particular, the presence of an immune response, evoked in this paper through the sample's purulence, was already identified as a key contributor to static rheology<sup>9</sup>. The observed drops of  $G'$  and  $G''$  in CF and NCFB sputum coincide with the rheological degradation on acute asthma expectorations measured by Innes *et al.*<sup>30</sup>. Moreover, the degradation of the gel's network was observed to break in the first 6 hours after collection. To understand this stabilisation, comparing these data with the evolution of the neutrophil and bacteria population could be insightful. Practically, this result stresses the importance of quickly analysing sputum samples, and especially the purulent ones, before structural evolution occurs. The importance of purulence also scores the limitation of the current protocol to determine it by visual inspection as it is yet estimated subjectively. Defining purulence through a quantitative scale would allow a more rational classification.

Sputum rheology provides objective and quantitative properties, with relatively low variability in the measured quantities, provided that samples are properly vortexed immediately after collection. While access to a rheometer may be a constraint in some laboratories, the ability to freeze samples at  $-80$  °C without losing their rheological properties makes it possible to overcome this limitation. Several practical points should also be taken into consideration when performing rheological measurements. First, samples should be correctly loaded into the rheometer as incorrect placement is a major source of measurement artefact. Second, measurements should be carried out promptly as mucus samples are prone to dehydration at physiological temperature, which greatly increases the variability of rheological measurements<sup>35</sup>. The use of commercially available solvent traps attenuates this difficulty<sup>35</sup>. Third, high shears at the upper end of the amplitude sweep protocol may partly drive the sample out of the geometries, making the rheological results unexploitable in this limit. This is the reason why we limit our analysis to the critical point, when the sample starts flowing, without considering the flowing region itself. All considered, practical difficulties can be quite easily overcome, making sputum rheology a reliable method that could be broadly exploited in biophysical and preclinical research.

Overall, the present investigation draws guidelines towards a justified protocol for sputum rheometry. The existence of such protocol would benefit to both fundamental and clinical studies as the results given by different groups could be easily contrasted and related without concerns about the methodology. For instance, understanding the relation between healthy and diseased mucus composition with its structure and flowing abilities could help first to understand the influence of viscoelasticity in mucus clearance. Then, the study of sputum rheology could also help to assess which elements from its composition (bacterial load, immune response, DNA, mucins, etc.) are abnormal. In clinical context, the personalised surveillance and monitoring of muco-obstructive lung diseases is still a major challenge due to the lack of quantitative biomarkers, especially on the early detection of exacerbations<sup>36</sup> and its immediate treatment. The demonstrated practical ability to perform unified rheological measurements could help tackling this challenge.

## References

1. Boucher, R. C. Muco-obstructive lung diseases. *New Engl. J. Medicine* **380**, 1941–1953, DOI: [10.1056/NEJMra1813799](https://doi.org/10.1056/NEJMra1813799) (2019).
2. Murray, M. P., Pentland, J. L., Turnbull, K., MacQuarrie, S. & Hill, A. T. Sputum colour: A useful clinical tool in non-cystic fibrosis bronchiectasis. *Eur. Respir. J.* **34**, 361–364, DOI: [10.1183/09031936.00163208](https://doi.org/10.1183/09031936.00163208) (2008).
3. François, A. & Héry-Arnaud, G. The microbiome in cystic fibrosis pulmonary disease. *Genes* **11**, DOI: [10.3390/genes11050536](https://doi.org/10.3390/genes11050536) (2020).
4. App, E. M. *et al.* Sputum rheology changes in cystic fibrosis lung disease following two different types of physiotherapy. *Chest* **114**, 171–177, DOI: [10.1378/chest.114.1.171](https://doi.org/10.1378/chest.114.1.171) (1998).
5. Shak, S., Capon, D. J., Hellmiss, R., Marsters, S. A. & Baker, C. L. Recombinant human DNase I reduces the viscosity of cystic fibrosis sputum. *Proc. Natl. Acad. Sci. USA* **87**, 9188–9192, DOI: [10.1073/pnas.87.23.9188](https://doi.org/10.1073/pnas.87.23.9188) (1990).
6. Zahm, J.-M. *et al.* Dose-dependent in vitro effect of recombinant human DNase on rheological and transport properties of cystic fibrosis respiratory mucus. *Eur. Respir. J.* **8**, 381–386, DOI: [10.1183/09031936.95.08030381](https://doi.org/10.1183/09031936.95.08030381) (1995).
7. King, M. Is cystic fibrosis mucus abnormal? *Pediatr. Res.* **15**, 120–122, DOI: [10.1203/00006450-198102000-00007](https://doi.org/10.1203/00006450-198102000-00007) (1981).

8. Puchelle, E., Jacquot, J., Beck, G., Zahm, J. M. & Galabert, C. Rheological and transport properties of airway secretions in cystic fibrosis—Relationships with the degree of infection and severity of the disease. *Eur. J. Clin. Invest.* **15**, 389–394 (1985).
9. Serisier, D. J., Carroll, M. P., Shute, J. K. & Young, S. A. Macrorheology of cystic fibrosis, chronic obstructive pulmonary disease & normal sputum. *Respir. Res.* **10**, 63, DOI: [10.1186/1465-9921-10-63](https://doi.org/10.1186/1465-9921-10-63) (2009).
10. Tomaiuolo, G. *et al.* A new method to improve the clinical evaluation of cystic fibrosis patients by mucus viscoelastic properties. *PLoS One* **9**, e82297, DOI: [10.1371/journal.pone.0082297](https://doi.org/10.1371/journal.pone.0082297) (2014).
11. Ma, J. T., Tang, C., Kang, L., Voynow, J. A. & Rubin, B. K. Cystic fibrosis sputum rheology correlates with both acute and longitudinal changes in lung function. *Chest* **154**, 370–377, DOI: [10.1016/j.chest.2018.03.005](https://doi.org/10.1016/j.chest.2018.03.005) (2018).
12. Norton, M. M., Robinson, R. J. & Weinstein, S. J. Model of ciliary clearance and the role of mucus rheology. *Phys. Rev. E* **83**, 011921, DOI: [10.1103/PhysRevE.83.011921](https://doi.org/10.1103/PhysRevE.83.011921) (2011).
13. Chatelin, R., Anne-Archard, D., Murriss-Espin, M., Thiriet, M. & Poncet, P. Numerical and experimental investigation of mucociliary clearance breakdown in cystic fibrosis. *J. Biomech.* **53**, 56–63, DOI: [10.1016/j.jbiomech.2016.12.026](https://doi.org/10.1016/j.jbiomech.2016.12.026) (2017).
14. Loiseau, E. *et al.* Active mucus–cilia hydrodynamic coupling drives self-organization of human bronchial epithelium. *Nat. Phys.* **16**, 1158–1164, DOI: [10.1038/s41567-020-0980-z](https://doi.org/10.1038/s41567-020-0980-z) (2020).
15. Duncan, G. A. *et al.* Microstructural alterations of sputum in cystic fibrosis lung disease. *JCI Insight* **1**, e88198, DOI: [10.1172/jci.insight.88198](https://doi.org/10.1172/jci.insight.88198) (2016).
16. Radiom, M. *et al.* Magnetic wire active microrheology of human respiratory mucus. *Soft Matter* **17**, 7585–7595, DOI: [10.1039/D1SM00512J](https://doi.org/10.1039/D1SM00512J) (2021).
17. Jory, M. *et al.* Mucus from human bronchial epithelial cultures: rheology and adhesion across length scales. *Interface Focus* **12**, 20220028, DOI: [10.1098/rsfs.2022.0028](https://doi.org/10.1098/rsfs.2022.0028) (2022).
18. Radtke, T. *et al.* Acute effects of combined exercise and oscillatory positive expiratory pressure therapy on sputum properties and lung diffusing capacity in cystic fibrosis: a randomized, controlled, crossover trial. *BMC Pulm. Med.* **18**, 99, DOI: [10.1186/s12890-018-0661-1](https://doi.org/10.1186/s12890-018-0661-1) (2018).
19. Nettle, C. *et al.* Linear rheology as a potential monitoring tool for sputum in patients with Chronic Obstructive Pulmonary Disease (COPD). *Biorheology* **54**, 67–80, DOI: [10.3233/BIR-17141](https://doi.org/10.3233/BIR-17141) (2018).
20. Patarin, J. *et al.* Rheological analysis of sputum from patients with chronic bronchial diseases. *Sci. Reports* **10**, 15685, DOI: [10.1038/s41598-020-72672-6](https://doi.org/10.1038/s41598-020-72672-6) (2020).
21. Broughton-Head, V. J., Smith, J. R., Shur, J. & Shute, J. K. Actin limits enhancement of nanoparticle diffusion through cystic fibrosis sputum by mucolytics. *Pulm. Pharmacol. Ther.* **20**, 708–717, DOI: [10.1016/j.pupt.2006.08.008](https://doi.org/10.1016/j.pupt.2006.08.008) (2007).
22. McElvaney, O. J., Gunaratnam, C., Reeves, E. P. & McElvaney, N. G. A specialized method of sputum collection and processing for therapeutic interventions in cystic fibrosis. *J. Cyst. Fibros.* **18**, 203–211, DOI: [10.1016/j.jcf.2018.06.001](https://doi.org/10.1016/j.jcf.2018.06.001) (2019).
23. Friedrich, R., Rappold, E., Bogdan, C. & Held, J. Comparative analysis of the wako  $\beta$ -glucan test and the fungitell assay for diagnosis of candidemia and pneumocystis jirovecii pneumonia. *J. Clin. Microbiol.* **56**, DOI: [10.1128/JCM](https://doi.org/10.1128/JCM) (2018).
24. Batéjat, C., Grassin, Q., Manuguerra, J.-C. & Leclercq, I. Heat inactivation of the severe acute respiratory syndrome coronavirus 2. *J. Biosaf. Biosecurity* **3**, 1–3 (2021).
25. Kim, Y. I. *et al.* Development of severe acute respiratory syndrome coronavirus 2 (SARS-CoV-2) thermal inactivation method with preservation of diagnostic sensitivity. *J. Microbiol.* **58**, 886–891, DOI: [10.1007/s12275-020-0335-6](https://doi.org/10.1007/s12275-020-0335-6) (2020).
26. Holz, O. *et al.* Freezing of homogenized sputum samples for intermittent storage. *Clin. & Exp. Allergy* **31**, 1328–1331, DOI: [0.1046/j.1365-2222.2001.01136.x](https://doi.org/10.1046/j.1365-2222.2001.01136.x) (2001).
27. Cuthbertson, L. *et al.* Implications of multiple freeze-thawing on respiratory samples for culture-independent analyses. *J. Cyst. Fibros.* **14**, 464–467, DOI: [10.1016/j.jcf.2014.10.004](https://doi.org/10.1016/j.jcf.2014.10.004) (2015).
28. Sanders, N. N. *et al.* Cystic fibrosis sputum: a barrier to the transport of nanospheres. *Am. J. Respir. Crit. Care Med.* **162**, 1905–1911, DOI: [10.1164/ajrcm.162.5.9909009](https://doi.org/10.1164/ajrcm.162.5.9909009) (2000).
29. Charman, J. & Reid, L. The effect of freezing, storing and thawing on the viscosity of sputum. *Biorheology* **10**, 295–301, DOI: [10.3233/BIR-1973-10302](https://doi.org/10.3233/BIR-1973-10302) (1973).
30. Innes, A. L. *et al.* Ex vivo sputum analysis reveals impairment of protease-dependent mucus degradation by plasma proteins in acute asthma. *Am. J. Respir. Critical Care Medicine* **180**, 203–210, DOI: [10.1164/rccm.200807-1056OC](https://doi.org/10.1164/rccm.200807-1056OC) (2009).

31. Cuthbertson, L. *et al.* Time between collection and storage significantly influences bacterial sequence composition in sputum samples from cystic fibrosis respiratory infections. *J. Clin. Microbiol.* **52**, 3011–3016, DOI: [10.1128/JCM.00764-14](https://doi.org/10.1128/JCM.00764-14) (2014).
32. Yuan, S. *et al.* Oxidation increases mucin polymer cross-links to stiffen airway mucus gels. *Sci. Transl. Medicine* **7**, 276ra27, DOI: [10.1126/scitranslmed.3010525](https://doi.org/10.1126/scitranslmed.3010525) (2015).
33. Agostini, P. & Knowles, N. Autogenic drainage: the technique, physiological basis and evidence. *Physiotherapy* **93**, 157–163, DOI: [10.1016/j.physio.2006.07.005](https://doi.org/10.1016/j.physio.2006.07.005) (2007).
34. Feng, C., Wang, H., Lu, N. & Tu, X. M. Log transformation: application and interpretation in biomedical research. *Stat. Medicine* **32**, 230–239, DOI: [10.1002/sim.5486](https://doi.org/10.1002/sim.5486) (2013).
35. Völler, M. *et al.* An optimized protocol for assessment of sputum macrorheology in health and muco-obstructive lung disease. *Front. Physiol.* **13**, DOI: [10.3389/fphys.2022.912049](https://doi.org/10.3389/fphys.2022.912049) (2022).
36. Wood, J. *et al.* A smartphone application for reporting symptoms in adults with cystic fibrosis improves the detection of exacerbations: Results of a randomised controlled trial. *J. Cyst. Fibros.* **19**, 271–276, DOI: [10.1016/j.jcf.2019.09.002](https://doi.org/10.1016/j.jcf.2019.09.002) (2020).

## Acknowledgements

This study was supported by the Centre de Ressource et de Compétence de Mucovisidose (CRCM) and the Institute of Biology and Pathology (IBP), without J. Quentin and L. Ponderand this research would not have been possible. We also thank Ioan Petrescu who helped in characterising some of the NCFB samples.

## Author contributions statement

Design of the study: HB, MRDSV, BD and MM.

Performed experiments: LEE.

Analysis: LEE, MRDSV and HB.

Writing: LEE and MRDSV.

Correcting/revision: all authors.

## Additional information

**Funding:** This work was partly funded by the Agence nationale de la recherche (ref. ANR-18-LCV2-0005) and the Association nationale de la recherche et de la technologie (ref. 20CUF8944).

**Competing interests:** LEE and MRDSV are full time employees of Rheonova, the company which designs and produces the rheometer used in this study. HB, MM and BD have no conflict of interests.

**Data availability:** The datasets used and/or analysed during the current study are available from the corresponding author on reasonable request.

## Supplementary material to *Sputum handling for rheology*

### Patients' data

We have included 36 expectorations collected from the “Centre de Ressource et de Compétence de Mucoviscidose” at the Grenoble Alpes University Hospital. 26 were obtained from adult CF patients and 10 from NCFB patients, who regularly come to the hospital for medical follow-up. Table S1 collects patients' data including gene mutations for the CF patients, demographic data as gender and age, body mass index (BMI), spirometry information: forced expiratory volume in one second (FEV1) and residual volume (RV) in percentage and expectoration's purulence by visual inspection as described by Murray *et al.*<sup>1</sup>

Patient	Genotype	Gender	Age	BMI (kg/m <sup>2</sup> )	FEV1 (%)	RV (%)	Purulence
CF1	DF508, DF508	M	23	21	72	208	Purulent
CF2	DF508, DF508	F	28	24	73	202	Purulent
CF3	DF508, DF508	F	34	20	75	–	Purulent
CF4	DF508, R1128X	M	25	16	41	382	Semi-purulent
CF5	DF508, R334W	F	29	17	62	232	Purulent
CF6	DF508, indetermined	F	31	17	27	252	Semi-purulent
CF7	DF508, L732X	M	23	20	46	213	Semi-purulent
CF8	DF508, DF508	M	52	20	37	193	Purulent
CF9	DF508, DF508	F	42	19	47	263	Purulent
CF10	DF508, DF508	F	36	18	29	256	Purulent
CF11	1717-1G>A, DF508	M	30	24	79	197	Purulent
CF12	DF508, DF508	M	27	21	75	95	Purulent
CF13	DF508, DF508	F	26	22	58	267	Purulent
CF14	1717-1G>A, 3849G->A	M	34	23	107	144	Purulent
CF15	DF508, A455E	M	46	23	24	196	Purulent
CF16	DF508, R1128X	M	25	16	45	257	Semi-purulent
CF17	DF508, DF508	F	26	22	56	191	Purulent
CF18	2118del4, S902R	F	50	22	38	221	Purulent
CF19	DF508, V232D	M	52	23	99	85	Purulent
CF20	DF508, DF508	F	29	24	72	193	Semi-purulent
CF21	DF508, A455E	M	46	22	22	203	Purulent
CF22	DF508, 1811+1	M	19	18	62	190	Semi-purulent
CF23	DF508, DF508	M	28	25	129	155	Semi-purulent
CF24	DF508, DF508	M	31	20	94	17	Purulent
CF25	DF508, A455E	M	46	23	26	218	Purulent
CF26	DF508, DF508	F	27	22	80	143	Purulent
NCFB1		F	28	20	44	188	Purulent
NCFB2		F	37	20	44	85	Semi-purulent
NCFB3		F	19	25	86	113	Purulent
NCFB4		F	45	25	73	138	Purulent
NCFB5		F	37	25	58	124	Purulent
NCFB6		F	29	20	30	210	Purulent
NCFB7		F	45	24	75	132	Purulent
NCFB8		F	29	20	45	–	Semi-purulent
NCFB9		F	23	19	37	155	Semi-purulent
NCFB10		F	29	24	41	146	Purulent

**Table S 1.** Cystic Fibrosis (CF) and NCFB (NCFB) patients included in this study. The table gives data of patients' demographic, spirometry and purulence.

### Vortex procedure

The collected expectorations were vortexed with Vortex Genie™ 2 from Scientific Industries SI™. The sample was vortexed gently increasing the stirring intensity until the sample visually takes the shape of a torus and starts flowing (see Figure S1). Therefore, the maximal speeds used were dependent on the sample but ranged from 1000 to 3000 rpm. This vortex intensity was then maintained during 30 s.

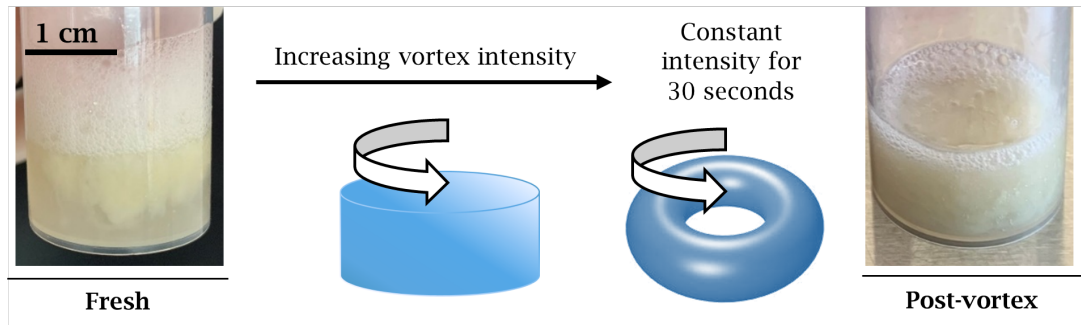


**Figure S 1.** CF sputum sample collected during a physiotherapist session in the CHU Grenoble Alpes before and after vortex. A schematic image shows the torus shape created when slowly increasing the vortex intensity. Once this torus is obtained, the intensity is kept constant during 30 seconds.

### Expectorations

Figure S2 presents typical photographs of the fresh collected expectorations, ordered from lower to higher  $g'_{5\%}$  standard deviations between replicates. The CF high variability samples do not seem visually more heterogeneous. Therefore, the vortex protocol should be optimised to reduce the high variability between replicas even when the differences in heterogeneity are not perceptible at sight.

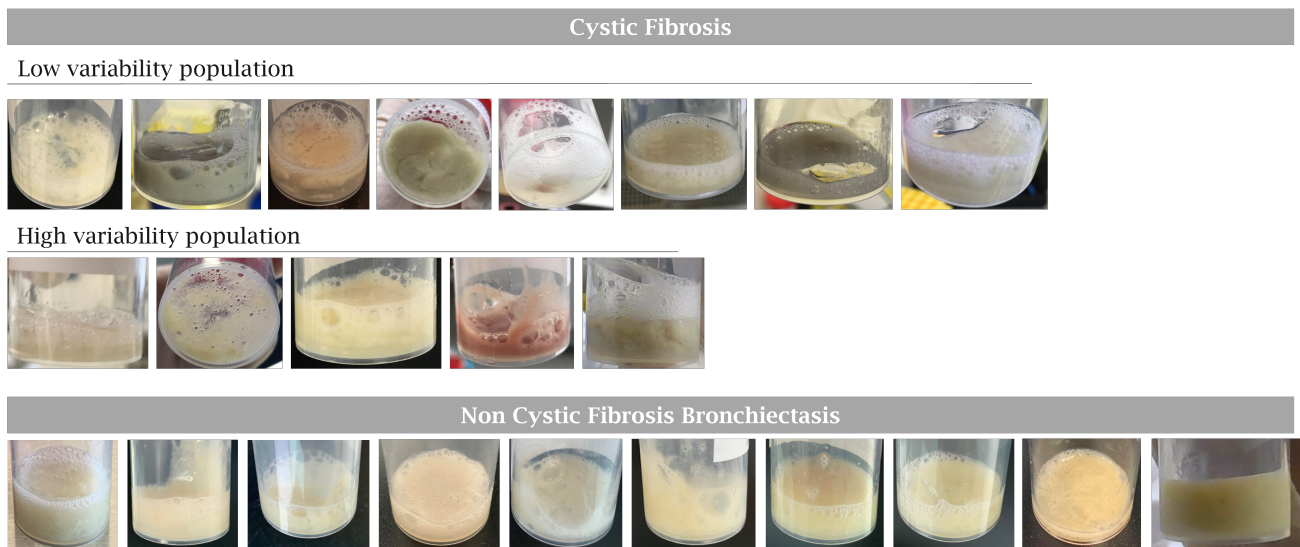


**Figure S 2.** Typical images of the fresh expectorations after collection, ordered by increasing dispersion in elastic modulus.

### Treatment mean equality

We have carried out bilateral t-tests to study the mean equality between control (non-heated, non-frozen and vortexed) samples with treated samples. Heated samples have not been included as only one sample out of three showed a crossover, therefore  $d_c$  and  $s_c$  values are only available for this single sample.

Figure S3 displays whiskers plots for control (white) and treated samples (coloured). The p-values for the t-tests are indicated for each variable and condition. We can statistically accept no significant differences between the control and treated groups considering a confidence of 0.1. However, it is clear that, while the freezing methods show high p-values ( $> 0.75$ ), the effect of not vortexing CF expectorations leads to values much closer to the acceptance level and therefore a relatively high risk of wrongly rejecting the alternative hypothesis (mean inequality).

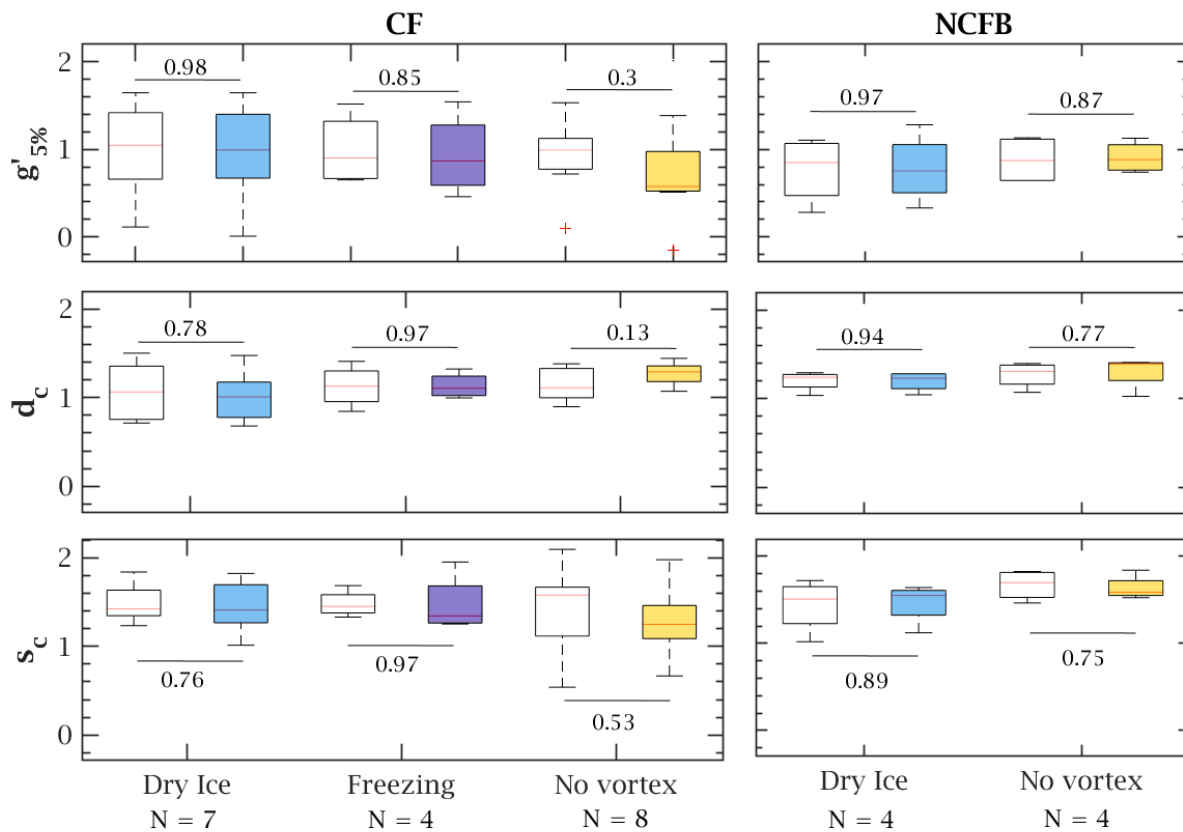


**Figure S3.** Whiskers plots comparing control (white) and treated (coloured) samples. The central mark shows the median and the borders of the box designate the first and third quartile (25 and 75 % of the values). The obtained p-values for the mean equality bilateral t-tests are displayed for each condition.

### References

1. Murray, M. P., Pentland, J. L., Turnbull, K., MacQuarrie, S. & Hill, A. T. Sputum colour: A useful clinical tool in non-cystic fibrosis bronchiectasis. *Eur. Respir. J.* **34**, 361–364, DOI: [10.1183/09031936.00163208](https://doi.org/10.1183/09031936.00163208) (2008).

In the presented article we have investigated the correlations between the rheological variables and the distribution of 26 CF and 10 NCFB expectorations. Since then, more patients have been included in the study, which allows us to verify the robustness of our conclusions. Therefore, we here present the measurements for 59 CF and 22 NCFB expectorations following the protocol previously validated.

We confirmed the rheological variables follow log-normal distributions through the Q-Q plots in Fig 3.1 and through the Shapiro-Wilk normality test which gave p-values over 0.05 in all cases. The values were 0.81, 0.77, 0.05 and 0.44 for  $g'$ ,  $g''$ ,  $s_c$  and  $d_c$  for CF samples, and 0.79, 0.73, 0.16 and 0.43 for NCFB samples. Moreover, while CF and NCFB follow similar distributions (see Fig 3.1), we observed a change of slope for  $s_c$  at around 1.3 ( $\sigma_c = 20$  Pa in the linear domain) which is more pronounced for CF samples. We will see in chapter 7 how the most severe patients presented  $\sigma_c > 20$  Pa.

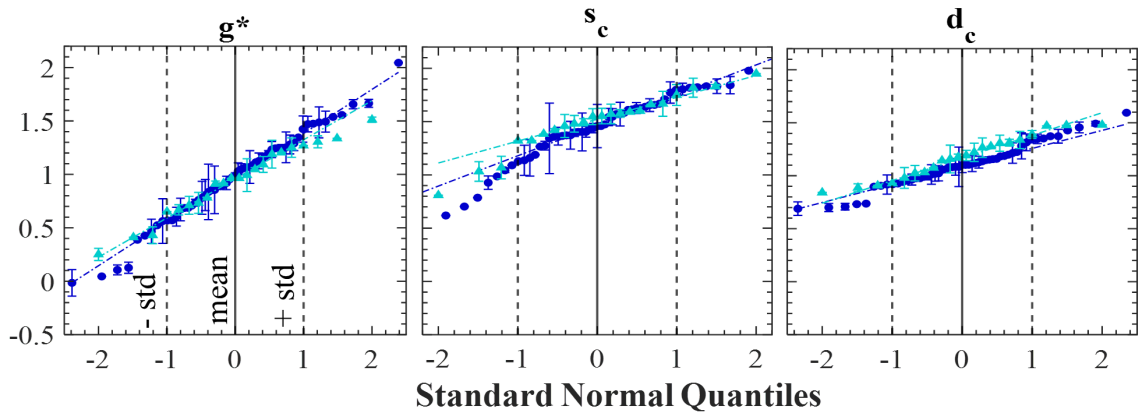


Figure 3.1: Distribution of the logarithmic rheological quantities for 59 CF (circles) and 22 NCFB (triangles) expectorations. The dashed-dotted line corresponds to a normal distribution; the vertical dashed lines delimit 1 standard deviation around the mean (solid line).

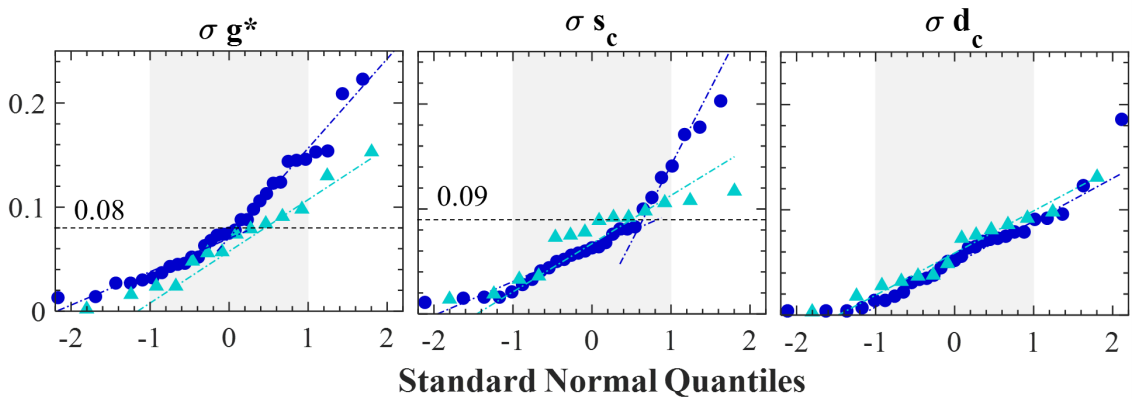


Figure 3.2: Aliquoting standard deviation for 33 CF (circles) and 14 NCFB (triangles) expectorations. The grey region delimits  $\pm$  a standard deviation of the plotted population and the horizontal dashed lines mark the limit between low and high variation found for CF samples.

Then, we investigated the aliquot variability in Fig 3.2 and once again found

a bimodal distribution for CF samples for  $\sigma g^*$  and  $\sigma s_c$  with 52% of the samples for  $g^*$  and 73% for  $s_c$  in the low-variability region with values under 0.09 which corresponds to less than a third of the population's standard deviation,  $\sigma_p(g^*) = 0.4$  and  $\sigma_p(s_c) = 0.29$ .

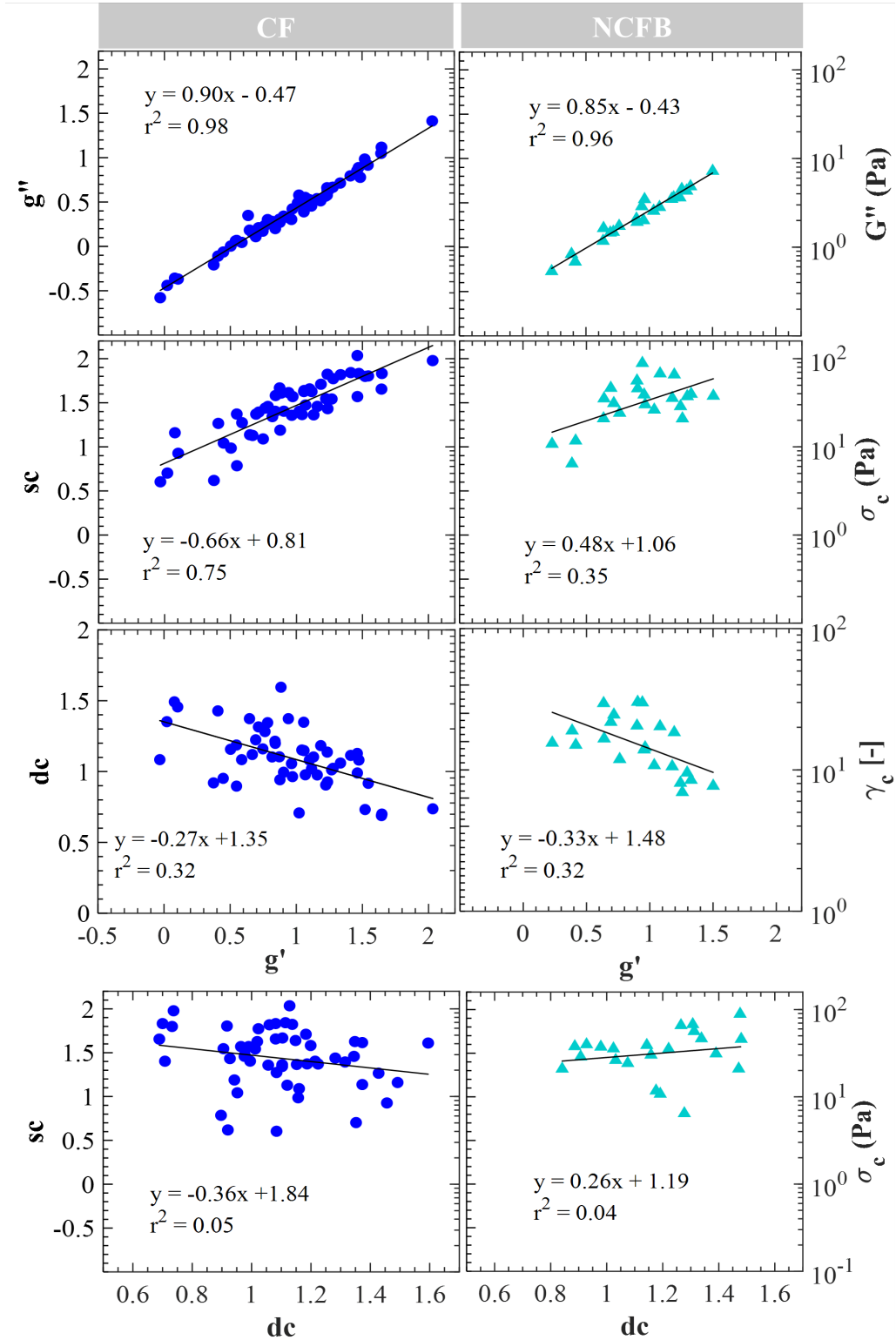


Figure 3.3: Top: Evolution of  $g''$ ,  $s_c$  and  $d_c$  with  $g'$  for 59 CF and 22 NCFB expectorations. Bottom: Evolution of  $s_c$  with  $d_c$ .

Lastly, in Fig 3.3, we observed the same correlations than in the article's Figure 2 confirming the study of the three poorly correlated variables: two from the large deformation region ( $s_c$  and  $d_c$ ) and  $g'$  from the linear domain.

# Chapter 4

## Vortex effect

Sputum samples are highly heterogeneous with plugs ranging from the millimetre to the centimetre in a viscoelastic matrix (Figure 4.1). In the previous chapter this heterogeneity was found to be the cause of having disparate measurements in macro rheology between aliquots coming from the same sample. If the sample contains particles of the same order of magnitude than the gap between the rheometer plates, the sample will not react uniformly to shear [24] and continuous mechanics does not apply. For this reason, a first step of homogenisation is necessary to ensure the accuracy and consistence of the measurement.

The classical methods to break the sputum plugs and homogenise them are chemical through the addition of reduction agents [34], or mechanical as repetitive pipetting or the use of shakers or vortex systems. We have rejected the idea of using chemical products as they break the disulphide bridges of the proteins destroying the gel structure of the sputum. We have therefore focused on the study of the mechanical techniques.

Firstly we have compared what happens when pipetting or vortexing a viscoelastic gel to find out if the driving mechanism is a macroscopical fragmentation or a mixing of the two phases. Secondly, we compared the effect on rheology of these two techniques to determine if they are destructive. Lastly, we quantified the vortex mixing efficiency to find the optimal vortexing protocol to obtain homogeneous samples.

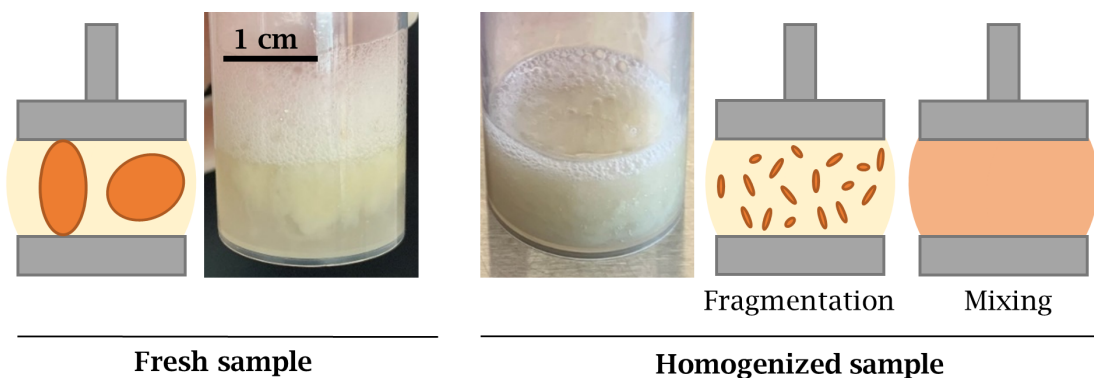


Figure 4.1: CF sputum sample collected during a physiotherapist session in the CHU Grenoble Alpes before and after homogenisation.

## 4.1 Heterogeneity of sputum

At the macroscale, sputum samples are mainly composed of a light translucent phase which we will refer to as matrix and a coloured phase which we will call plug (see Figure 4.2).

An expectoration from a CF adult patient was collected with its two phases perfectly separated. The volume of the plug was 350  $\mu\text{l}$  and the matrix was 500  $\mu\text{l}$ . We first measured the rheology of each phase to quantify their viscoelasticity contrast. Strain sweeps at 1 Hz and frequency sweeps at 5% deformation were applied to each phase. The matrix was measured with the DHR3 rheometer (TA Instruments) while the plug was analysed with the ARES-G2 rheometer (TA Instruments).

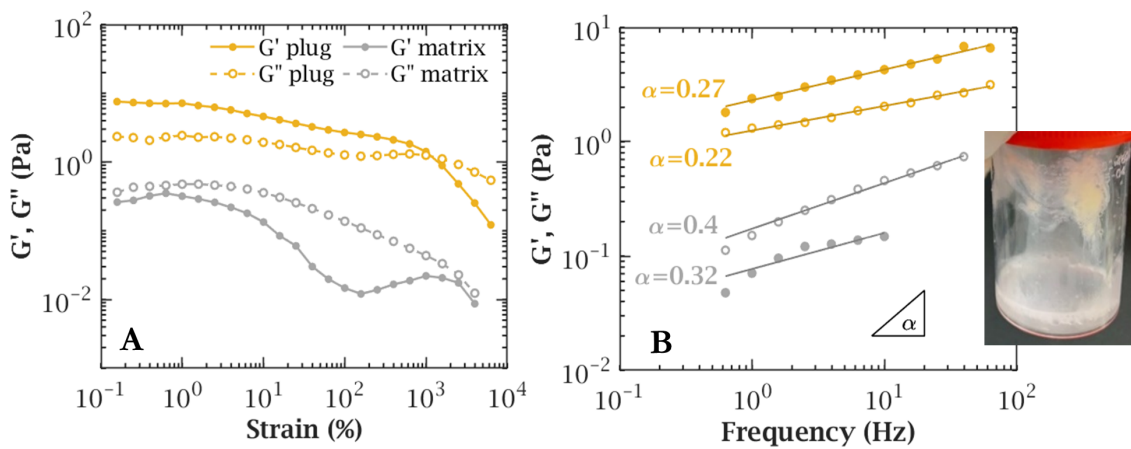


Figure 4.2: Right: photo of a collected CF expectoration with both phases separated: the coloured plug on the top part and the translucent matrix in the bottom of the tube. A and B: strain and frequency sweeps for the plug (orange) and the matrix (grey).  $G'$  is plotted with filled markers and continuous line and  $G''$  is represented with empty markers and discontinuous line.

The plug showed a high elastic response at low strains ( $G' > G''$ ) followed by a drop at mid-strains and a final flowing phase in which the viscous modulus exceeds the elastic modulus ( $G'' > G'$ ), see Figure 4.2 A. The measured elastic and viscous moduli in the plateau were 7 and 2 Pa and the crossover point was reached at 1169% strain, corresponding to a stress of 1.2 Pa. In contrast, the matrix (which remarkably elongated when pipetting from the tube) featured a viscous dominated behaviour along all the measured strain range. The frequency sweeps (Figure 4.2 B) confirm the elastic character of the plug between 1 and 100 Hz while the matrix has a viscous dominated behaviour with  $G''$  larger than  $G'$ . In both cases  $G'$  and  $G''$  increase with the frequency but at different speeds. The slopes in the plug measurements are lower than the ones for the matrix, the plug is less affected by the increasing speed of the solicitation, therefore has a more solid-like behaviour.

When comparing the rheology of the plug in Figure 4.2 with the strain sweeps of sputum samples as shown in Figure 2.6, we remark sputum and the measured plug have the same behaviour. Therefore, when measuring sputum samples the plug is dominating the rheological measurements.

## 4.2 Mixing procedures

As patient expectorations are limited and have small volumes we have worked with the viscoelastic model fluid described in the material and methods chapter (chapter 2). Once we have measured the rheology of the different parts of a sputum sample, we can correctly choose the polyacrylamide concentrations which will give us similar viscoelasticity contrasts.

We have mimicked the matrix and plug phases by using different Flopaam concentrations to cover a range of viscoelasticity contrasts, always keeping the plug with the higher elasticity. For visualization, the plug phase was coloured with graphite and the matrix was kept transparent. We systematically recreated 1.5 ml sputum samples by adding 75% v/v of transparent Flopaam (matrix) and 25% v/v of the coloured Flopaam (plug) in a flat bottom tube, see Fig 4.3.

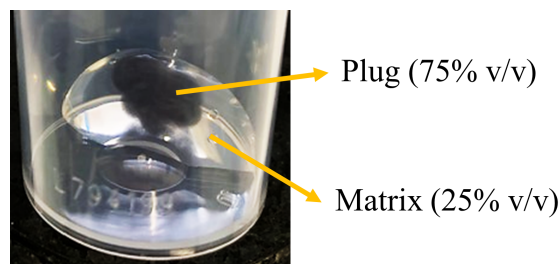


Figure 4.3: Model sputum composed of 25% v/v of coloured Flopaam to mimic the plug and 75 % v/v of transparent Flopaam to mimic the sputum's matrix.

First, we compared the effect of mixing the two phases of the model expectation using either a vortex or a positive displacement pipette. For each diphasic sample three replicates were carried out.

- **Vortex:** The sample is vortexed in the flat bottom tube, gently increasing the stirring speed until the sample takes the shape of a tore and starts rotating at the tube's base. This vortex intensity is then maintained for 30 seconds. Then the resulting fluid is cautiously poured in a rectangular 1.5 ml well stuck on a coverslip and placed between a camera (JAI BM-500 GE) and a white LED panel for imaging. This same operation is repeated 9 times.
- **Pipetting:** The whole model expectation is pipetted once with a positive displacement pipette in the flat bottom tube and then poured into the imaging setup. After imaging it is poured again into the flask and pipetted again. To compare with the vortex, the pipetting was carried out 9 times.
- **Control:** The pouring effect has also been looked up to make sure it did not have a big effect on the homogenising outcomes. Therefore, the sample was simply poured from the tube into the rectangular frame and the opposite way for 9 times.

Figure 4.4 presents the evolution of the inclusion along time due to the different mixing processes. In the first column, we have the control situation in which we address the effect of pouring the sample from the tube to the visualisation frame. We consider the pouring has no effect on the mixing and that the differences between the first and last images are negligible. In the second column the effect of

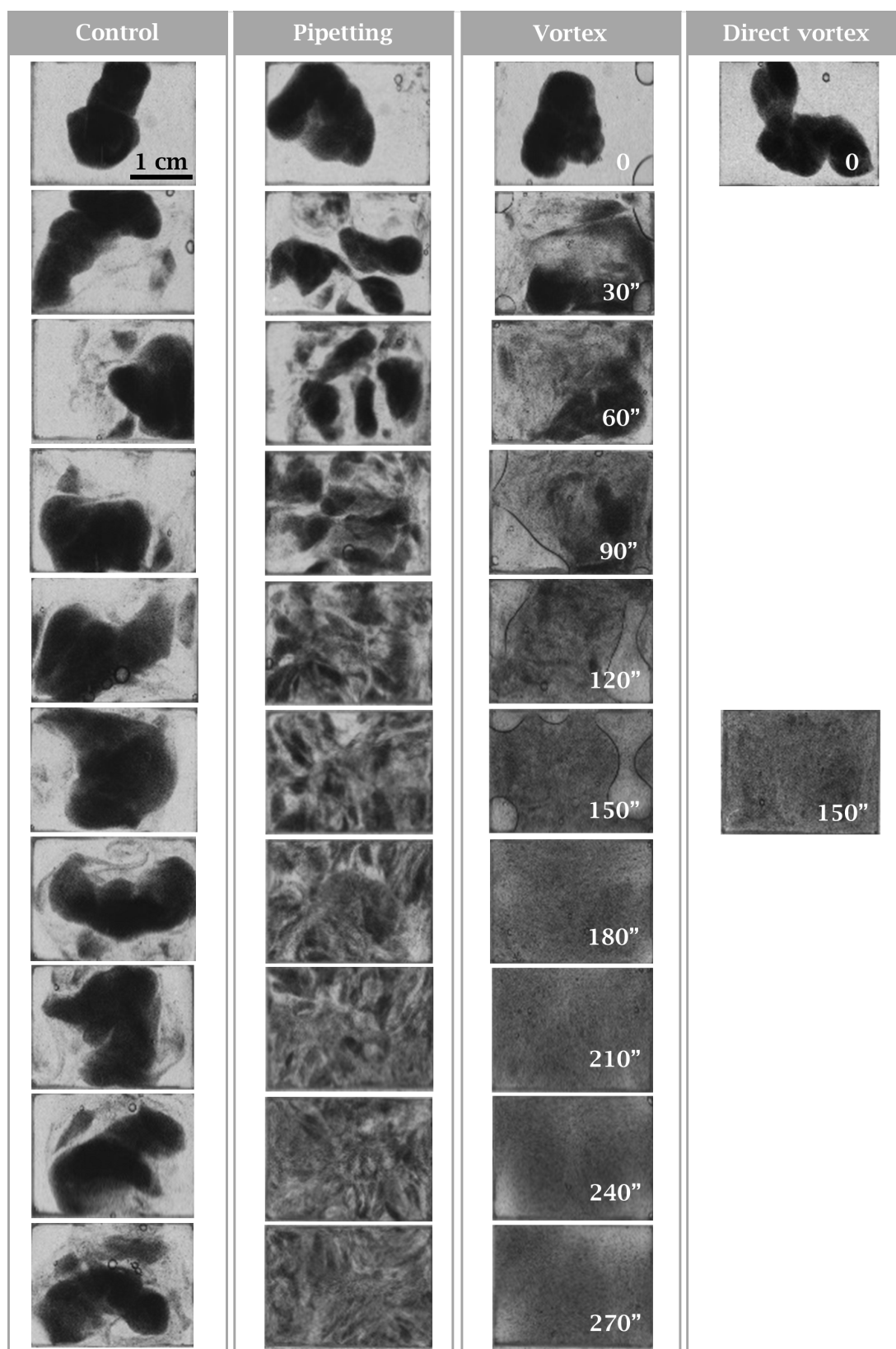


Figure 4.4: Vortex and pipetting effect in a diphasic Flopaam sample. The matrix's concentration is 0.5% and the inclusion is 1% to simulate a sputum sample.

pipetting is followed through 9 strokes of the pipette cone. The inclusion fragments

into smaller pieces with each stroke. In the third column images show the effect of increasing vortexing time. A significant difference was found macroscopically between homogenising by active mixing with a vortex and pipetting with the positive displacement pipette. While vortexing diffuses the inclusion in the matrix, pipetting breaks it into smaller pieces.

We are therefore focusing our study to the effect of vortex as mixing with the vortex lead to homogeneous samples without fragments. However, in practice the vortex process will be continuous and not with intervals of 30 seconds so we also tested continuous vortexing (last column in Figure 4.4) to see if we could directly reach the homogeneous situation by increasing the vortexing time. The outcome is not different when vortexing for 150 seconds without stop than vortexing 5 times for 30 seconds as shown in the example of Figure 4.4.

### 4.3 Vortex mixing efficiency

Through visual inspection of the captured images we can qualitatively estimate the homogenisation efficiency. However, the use of a quantitative value will lead to an objective criteria. We have therefore defined a mixing index (MI) by using the intensities of the pixels of the grey-scale images. For each image we obtained the variance  $S^2$  [35, 36] of the pixel intensities, defined as:

$$S^2 = \frac{1}{N} \sum_{i=1}^N |I_i - \bar{I}|^2,$$

where  $I_i$  is the pixel intensity,  $\bar{I}$  is the average intensity and  $N$  is the total number of pixels. The mixing index is defined as the ratio between the analysed mix and the homogeneous situation:

$$MI = \frac{S_0^2 - S^2}{S_0^2 - S_1^2},$$

where  $S_0^2$  is the variance of the unmixed system,  $S_1^2$  the variance of the perfect mix and  $S^2$  the variance of the analysed image.  $S_0^2$  corresponds to the first image taken in which the plug has just been placed in the matrix and  $S_1^2$  is 0 as in the perfect mix all pixels will show the same value. This way, MI is equal to 1 when the sample is perfectly homogeneous, and 0 when no homogenisation has taken place.

The tested viscoelastic contrasts ( $G_{\text{plug}}^*/G_{\text{matrix}}^*$ ) ranged from 2.4 to 44 and  $\sigma_{\text{cplug}}/\sigma_{\text{cmatrix}}$  ranged from 2 to 27 Pa. The mixing index for all the samples studied was adjusted to an exponential saturation  $MI = 1 - \exp^{-bt}$  with different increasing speeds  $b$  (see Figure 4.5 A) until reaching a plateau at  $MI = 1$ . The characteristic lag times ( $1/b$ ) ranged from 41 to 66 s and all samples reached a mixing index over 0.95 after 3 minutes of vortex, even in the less favourable case.

We investigated if the lag times obtained through the fit from Figure 4.5 were related to the contrast between rheological variables of the plug and the matrix. In Fig 4.6 A and B the lag time is plotted against  $G_{\text{plug}}^*/G_{\text{matrix}}^*$  and  $\sigma_{\text{cplug}}/\sigma_{\text{cmatrix}}$ . The points are randomly distributed along the lag time with no particular tendency in both variables. Therefore, the mixing efficiency is not dependant to the contrast between the two phases.

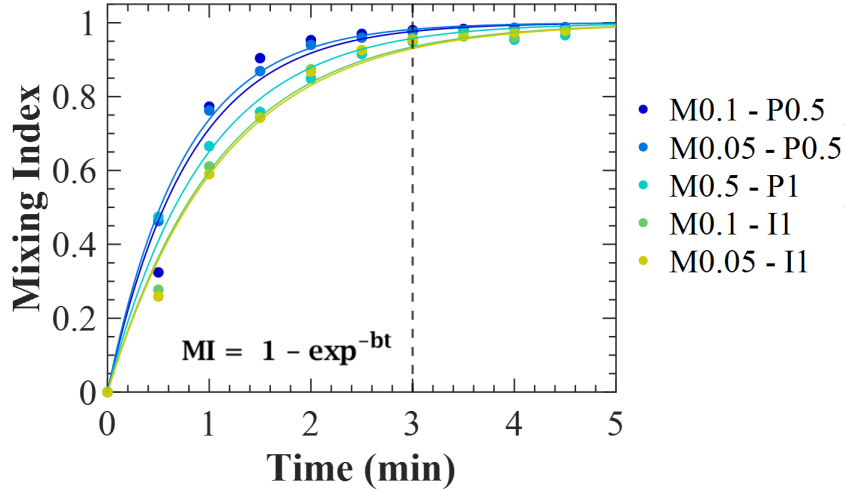


Figure 4.5: Evolution of the mixing index along increasing vortex time for 5 viscoelastic contrasts.

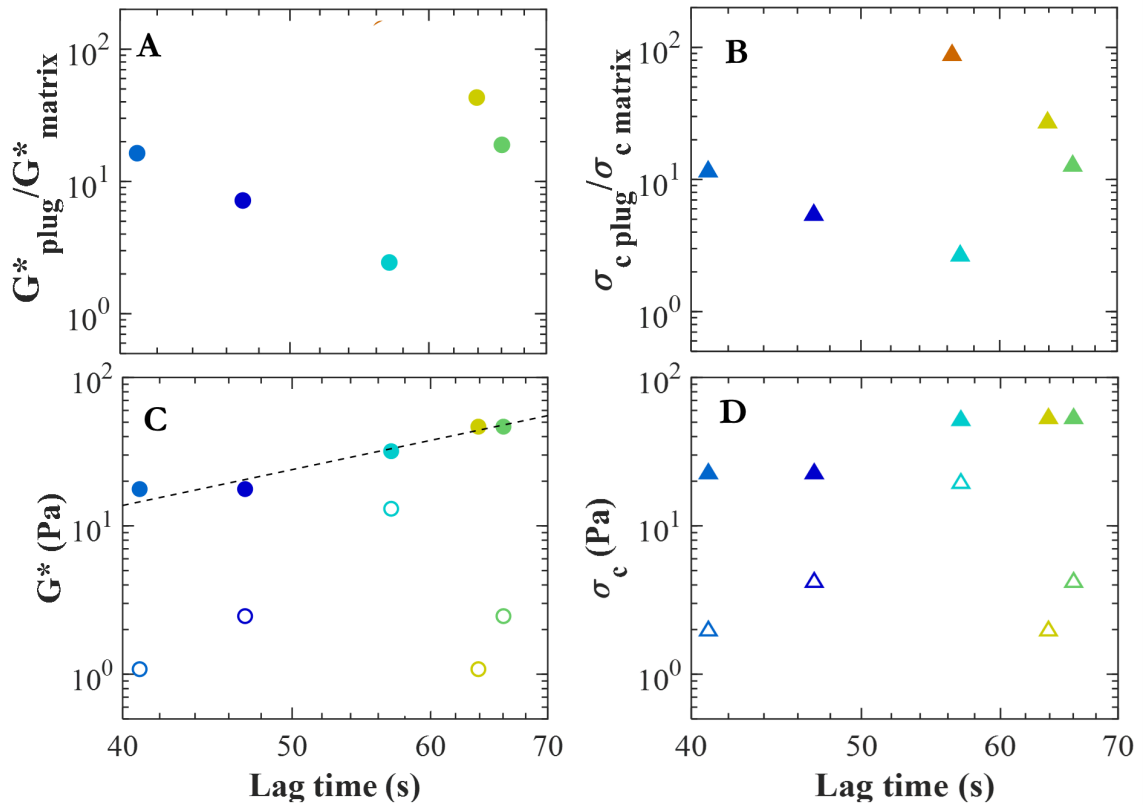


Figure 4.6: A and B:  $G^*$  and  $\sigma_c$  contrast between the plug and the matrix phase as a function of the mixing lag time. C and D:  $G^*$  and  $\sigma_c$  of the plug (filled markers) and the matrix (empty markers) as a function of the mixing lag time.

On the contrary, the mixing index was found to be dependent of the plug's viscoelastic modulus and its critical stress 4.6 C and D. The higher  $G^*$  of the plug, the longer lag times indicating slower mixing as plotted in Figure 4.5. This observation is consistent with the findings of Ramsay et al. (2016) [37] findings. The vortex

agitation leads to different shear rates in different points of the fluid which will have varied relaxation times leading to elastic instabilities. Therefore, mixing is driven by the plug's elasticity which elongates and stretches increasing the contact surface between the two phases.

The current concern is to confirm whether vortexing has any impact on the rheology of the samples. We therefore investigate this further in the following section.

#### 4.4 Vortex effect on rheology

We have compared the rheology measured before and after vortexing to evaluate its effect on the sample's rheology. As shown in Figure 4.7 A, while vortex does not lead to high differences of the crossover point, the plateau values of  $G'$  and  $G''$  after vortex (blue curve) were slightly higher than the fresh sample (green curve). In the sputum handling chapter (chapter 3) we obtained the same outcome when vortexing sputum samples. We argue that when placing the samples on the rheometer's geometry the plug had a tendency to stay in the centre of the plate while the matrix stays on the border. This effect is reduced when placing vortexed samples as the highly viscoelastic plugs, which have been integrated into the matrix, are now evenly distributed on the geometry reaching its edge. Parallel-plate captors calculate the shear stress in the outer radius, as a consequence, there is a higher viscoelastic response when the plug is mixed with the matrix. Therefore, the effect in rheology was minor for the sample of Figure 4.7 A.

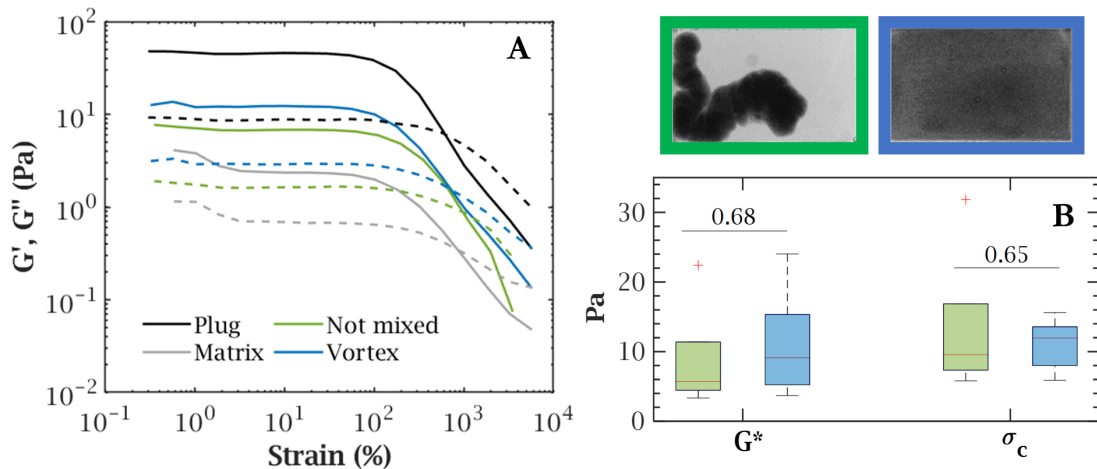


Figure 4.7: A: Strain sweeps of the plug with 1% concentration (black), the matrix with 0.1% (grey), the diphasic sample without mixing (green) and the homogenised sample (blue) after 5 minutes of vortex. B: Boxplots of not mixed (green) and vortexed (blue) samples. The p-values from a bilateral T-student test are exhibited for each condition.

When comparing the  $G^*$  and  $\sigma_c$  for all the viscoelastic contrasts testes, we observe in Figure 4.7 C that in average, samples after vortex present higher  $G^*$  and  $\sigma_c$ . However, the p-values for a bilateral T-test showed no significant difference between the fresh and vortexed samples.

In Figure 4.8 we have represented the contrast of the viscoelastic modulus and the critical shear stress as a function of their evolution before and after vortexing,

$\Delta G^*$  and  $\Delta\sigma_c$ , calculated as:

$$\Delta X = \frac{X \text{ vortexed}}{X \text{ not mixed}} - 1$$

We observe that the higher the rheological contrast between the plug and the matrix, the stronger the vortex effect on rheology. As we previously explained, we believe this increase is due to the fragmentation and spreading of the plug over all the rheometer's geometry after vortexing.

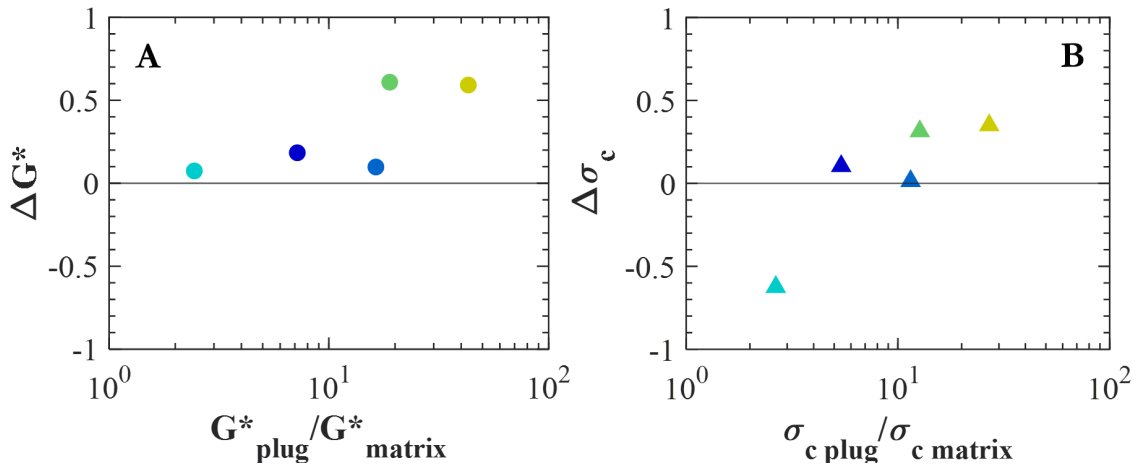


Figure 4.8: Evolution before and after vortexing,  $\Delta X$  of the viscoelastic modulus ( $G^*$ ) and the critical shear stress ( $\sigma_c$ ) as a function of the contrast between the plug and the matrix phase

## 4.5 Conclusions

In this chapter we have studied the efficiency of homogenising shear thinning viscoelastic fluids with a vortex system in order to homogenise sputum samples before rheometry. We have proved with a biphasic model fluid, that vortex mixes the samples while pipetting fragments it. Moreover, we have demonstrated the vortex method reaches an efficiency of 95% mixing within 3 minutes for all the viscoelastic contrasts measured. In addition, we observed that the plug's elasticity had an inverse effect on the mixing efficiency, with higher  $G^*$  resulting in longer lag times and slower mixing. Lastly, we found that the higher the viscoelastic contrast between the two phases, the more important the effect on rheology.

Anyhow it is surprising that rheology or its contrast hardly modulates the characteristic time. We expected to find strong differences between samples with high viscoelastic contrast and samples with smooth contrast. These results have been approved for Flopaam 6035S and it is not certain that they can be extended to sputum and mucus samples. Moreover, it raises the question about the size scales involved. The seeding of the plug's phase with graphite limits the results to the macroscopic scale as they are too big to investigate the mixing quality at the microscale. Further studies should be done by, for instance, the addition of fluorescent microscale particles to investigate their mixing as well as the possible ruptures and rheological modifications in the sample's network.

In this chapter we have therefore confirmed we can improve the mixing efficiency of shear-thinning viscoelastic polyacrylamide by increasing the vortexing time. However, 3 minutes can be a lot of time if a person is required to hold the beaker on the vortex. For this reason, in the following chapter we introduce a passive homogenisation system we have developed to minimise the user variability.

## Chapter 5

# Homogenisation of viscoelastic fluids

In the previous chapter we have studied the mixing efficiency of pipetting and vortexing as well as its effect on the rheology of sputa. Nonetheless, these methods are manual and will therefore be user-dependent. In clinical and biological research, having a non user-dependent homogenising protocol with high mixing efficiency in short times is crucial for many processes. We have therefore developed a simple passive channel with a porous section and studied the homogenisation of shear thinning viscoelastic fluids flowing through it with the idea of integrating it into the rheometer. However, we soon realised the system was not compatible with sputum samples due to the large volumes required to go through, as well as for the complexity of cleaning sputum in the channel. As a consequence, this chapter remains as a study of the behaviour of viscoelastic heterogeneous fluids through porous media which will not be applicable for sputum samples.

The efficient mixing of viscoelastic fluids poses a challenge due to the fluid's complex rheology [38]. When different components with varying viscoelastic properties are mixed together, their individual properties can affect the overall mixing process. For example, if one component has a high elasticity and another has a low elasticity, they may not mix well together and may separate into distinct phases. These variations in viscosity and elasticity can lead to uneven distribution of the components in the mixture, making it difficult to achieve a homogeneous mixture. Moreover, homogeneous mixing achieved only by diffusion takes long times, this is why extra energy needs to be injected to generate turbulence and chaotic advection [35, 39]. The existing systems can be categorised in two groups: active and passive mixers [40]. Active mixers require an external source of energy and are normally more efficient while being complex systems. Passive mixers do not need external energy supply and consist of different geometries and obstacles in microchannels to alter locally the flow rate and achieve the folding and stretching of the fluids.

We have injected a diphasic viscoelastic fluid through a channel with a porous section which will disperse and/or break the inclusions. In view of simulating the mixing of sputum inclusions within its matrix, we use shear-thinning polyacrylamide solutions at different concentrations so as to study a wide range of viscoelasticity contrasts (relaxation time of the matrix higher, lower or the same than the inclusion's relaxation time). Then, we explore the mixing performance of the porous medium at different shear rates by characterising the aspect of the dispersed phase after it

went through it.

## 5.1 Experimental set up

The homogenising system consists on a porous section, as the SMX (Shear and Mixing eXtruder) mixers, but from a 2D approach to properly analyse what is the effect of the porosity. The channel is 3D printed on an ABS like resin and has two glass windows (before and after the porous medium) for a good imaging. The device has an inlet section with two conduits (one for the continuous phase and another one for the dispersed phase), a porous media area with a typical pore size of 0.5 mm and an outlet area (see Figure 5.1). The set-up is composed of a syringe driver (PHD 22/2000), an electro-pneumatic regulator (rs-232c) controlled by a MATLAB script to regulate injection time and pressure, the designed channel, a white LED panel, a camera (JAI BM-500 GE), a lens (Nikon AF-S DX 18-70mm f/3.5-4.5 G IF) and capillaries to connect the different parts. The matrix and inclusion phases consist of polyacrylamide solutions of Flopaam 6035S (see section 2.5 for details). The inclusion is marked with graphite particles to allow visualising its propagation within the matrix.

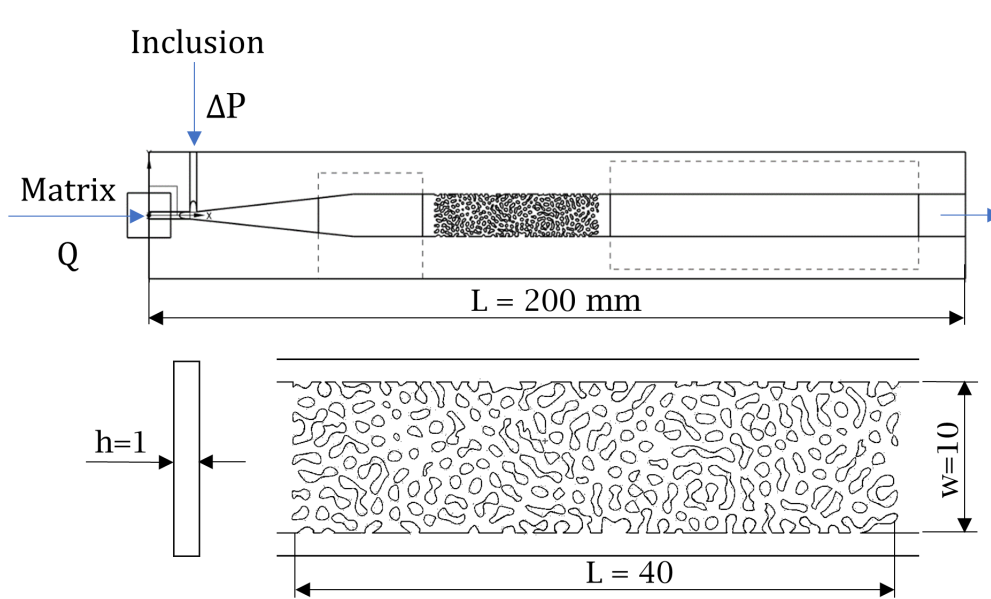


Figure 5.1: Homogenisation channel and a close up of the porous section. All the displayed measurements are in mm.

The matrix is injected through the syringe pump by a continuous flow and the coloured inclusion is added by a pressure pulse. Once the inclusion is created, the continuous matrix flow forces the coloured inclusion to go through the porous region. After the porosity the inclusion breaks in some situations, and it stays as a whole at high flow rates (see 5.2). We hypothesise these two outcomes will depend on:

- the imposed flow rate ( $Q$ ), which will influence the shear rate ( $\dot{\gamma}$ )
- the fluids rheology, which depends on the polyacrylamide concentration and will influence the relaxation time ( $\lambda$ ) of the sample and,

- the inclusion's size, the bigger the inclusion the easier it will be to break into several pieces.

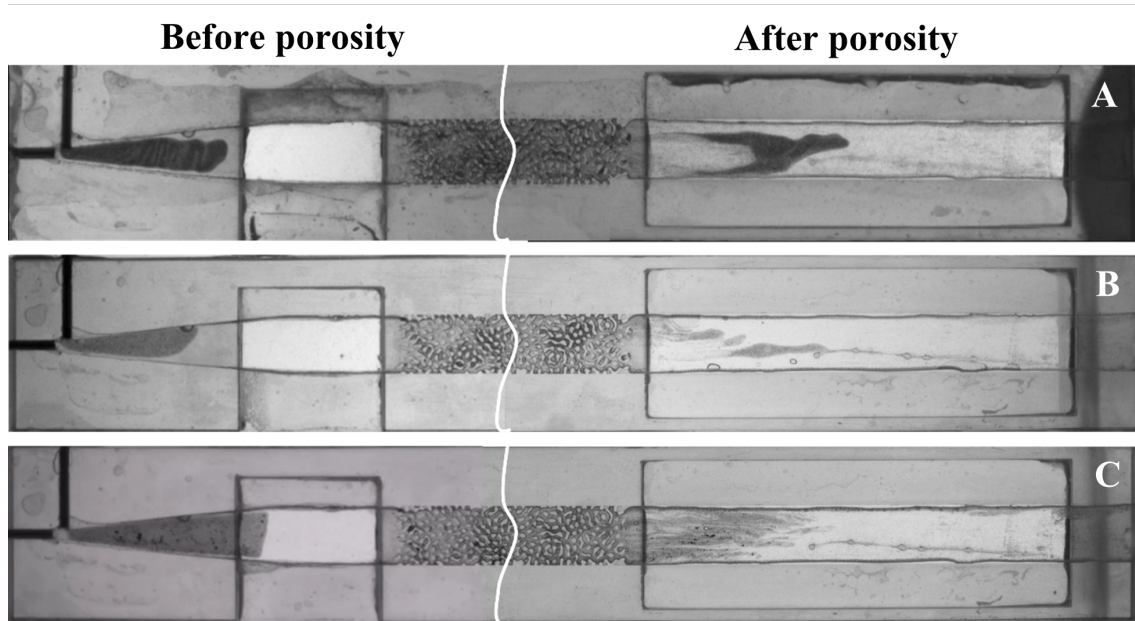


Figure 5.2: Three inclusions before and after the porous region. A: the plug comes out as a whole. B: the plug breaks into smaller pieces. C: the plug stretches into filaments forming a diffused cloud.

### 5.1.1 Flow rate

The shear rate in a rectangular channel with both sides of the same order of magnitude is calculated as a function of the imposed flow rate and the geometric parameters of the channel as described by Son Y. et al. [41].

$$\dot{\gamma} = \frac{6Q}{ab^2} \left(1 + \frac{a}{b}\right) f^* \left(\frac{a}{b}\right)$$

where  $a$  is the smaller dimension of the rectangular section of the channel,  $b$  is the larger dimension and  $f^*$  is an aspect-ratio function of the  $a/b$  ratio (see Figure 5.1).

Along the porous area, which dominates the breakup mechanism, the highest shear rate will be in the narrowest section. Therefore  $a$  is the typical distance between two obstacles in the porosity ( $a = 0.7$  mm) and  $b$  is the height of the channel ( $b = 1$  mm). Entering in Table 1 from Son Y. et al. [41], we can extract the  $f^*$  value for an aspect-ratio  $a/b = 0.7$ . This value is  $f^* = 0.6085$ . Moreover, between two obstacles, the section is reduced and  $Q$  increases. We have therefore divided these values by 7 which is the typical number of empty ways the fluid can go through in the porous medium. We can now calculate  $\dot{\gamma}$  as a function of the flow rate using the obtained  $f^*$ . In our experiments  $\dot{\gamma}$  typically ranges from 15 to 3016  $\text{s}^{-1}$ .

### 5.1.2 Relaxation time

Pure elastic solids immediately relax when releasing an exerted stress, whereas viscoelastic fluids take some time to react. This delay in the material's response is known as relaxation time ( $\lambda$ ). For elastic fluids, the thinning of the fluid column can be followed by measuring the minimal diameter ( $D_{\min}$ ) along time ( $t$ ). For highly elastic fluids, the diameter evolution follows an exponential law defined by Bazilevsky et al. [42].

$$D_{\min}(t) \propto \exp\left(\frac{-t}{3\lambda}\right)$$

We have used the Haake CaBER-1 extensional rheometer (Thermo Haake GmbH) with parallel plates of 6 mm diameter. The stretching of the fluid until the breaking point was recorded with a high speed camera (Photron Fastcam Mini UX100) and a light source.

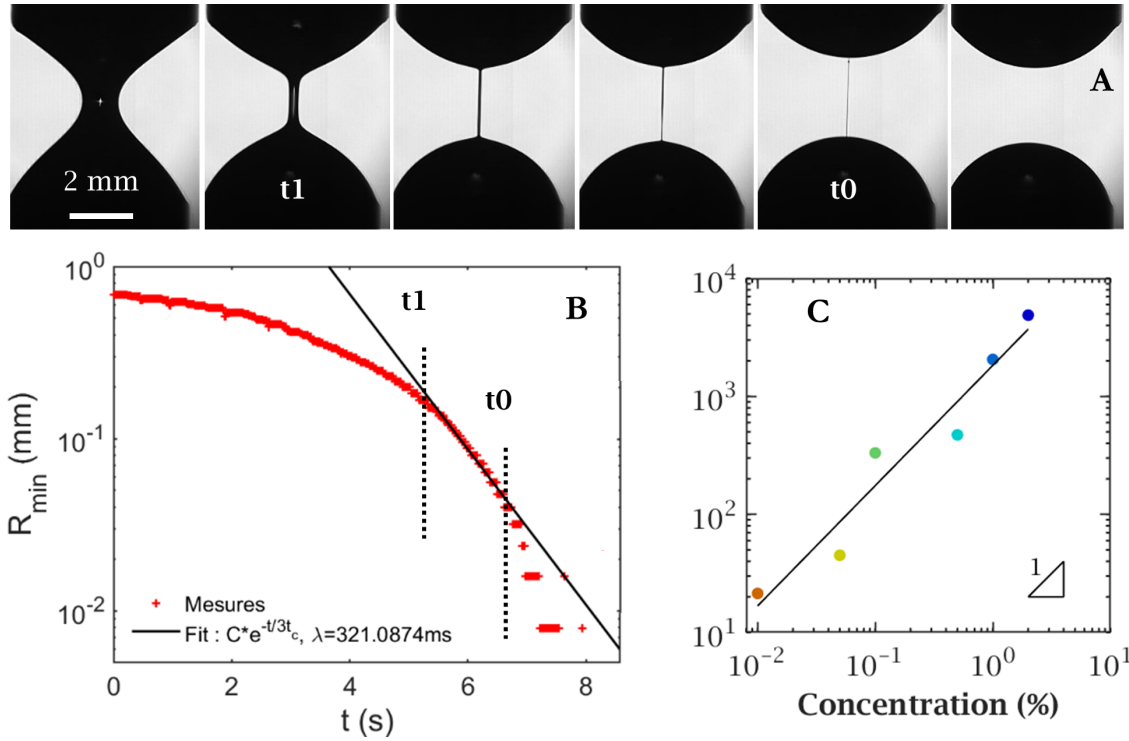


Figure 5.3: A: Capillary breakup rheometry process captured with a high-speed camera showing the temporal evolution of Flopaam 0.1% placed between the CaBER plates. B: Minimal diameter evolution along time for the 0.1% Flopaam solution. C: Relaxation time as a function of the concentration of Flopaam.

First, a droplet of fluid is placed between the two parallel plates. Second, the top plate slowly rises thinning the fluid until creating a cylindrical column between the geometries ( $t_1$  in Figure 5.3). Lastly its diameter will decrease exponentially with time (Figure 5.3 B) before it starts breaking at  $t_0$ . We have then processed the captured images in Matlab to obtain the relaxation time by fitting the diameter's drop along time to the exponential section.

We have obtained the relaxation times for the different Flopaam concentrations studied (Figure 5.3 C) which increases linearly with the concentration with a slope of 1. Therefore, the higher the polymeric content, the longer the relaxation time.

In the concentrations used,  $\lambda$  ranges from 0.06 to 2.1 s and is therefore higher than the typical shear time ( $1/\dot{\gamma} \in [0.1, 66.3]$  ms). Therefore flow is too fast to allow full relaxation of the polymers.

## 5.2 Results

We first analysed the simplest case in which the matrix and the plug have the same concentration, and we keep the size of the plug approximately fixed. In this first situation there are only two parameters: the fluid's rheology and the flow rate. Then, we studied the effect of viscoelastic contrast between the two phases. In this second study we consider three variables: the rheology of the matrix, the rheology of the plug and the flow rate.

### 5.2.1 No viscoelastic contrast between matrix and inclusion

When working with the same concentration in the matrix and in the plug, we observed three different outcomes when the imposed flow rate and the viscoelasticity contrast of the plug and matrix were altered:

- the inclusion does not break and continues as a whole after going through the porous medium (triangles in Figure 5.4),
- the inclusion breaks into pieces in the matrix (circles in Figure 5.4),
- the inclusion stretches showing a diffused cloud after the porous section (squares in Figure 5.4).

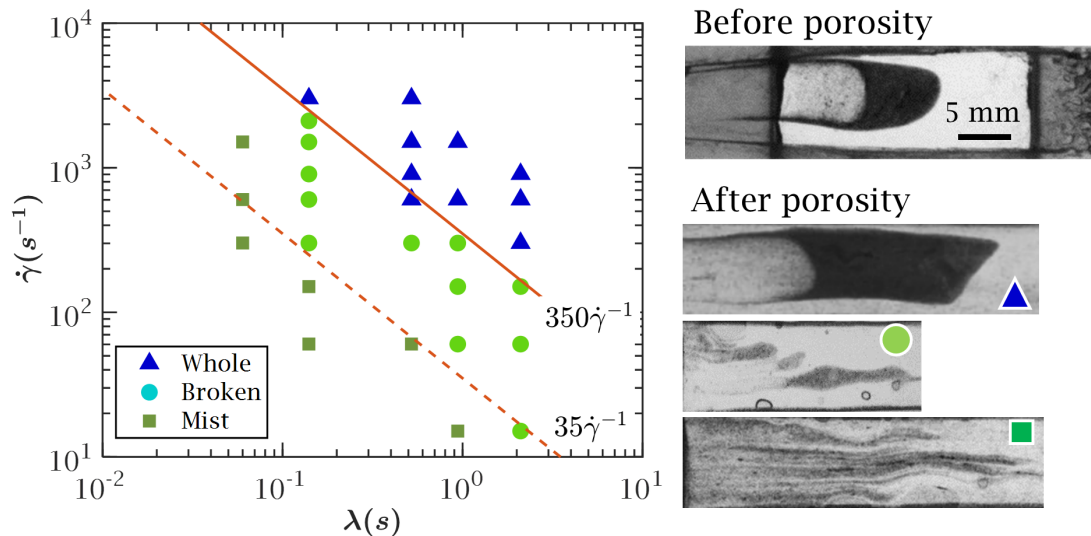


Figure 5.4: Phase diagram showing the outcome after the porous media for the same fluid as matrix and plug. The plugs' size is 25% the area of the inlet section.

We plotted these three regimes in a phase diagram with the relaxation time in the abscissa and the shear rate in the ordinate. We found the transition between these regimes followed straight lines of slope -1, therefore, the product  $\dot{\gamma}\lambda$  equals

a constant value. This product is known as the Weissenberg number ( $Wi$ ) and is defined as the ratio between elastic and viscous forces as follows:

$$Wi = \frac{\text{elastic forces}}{\text{viscous forces}} = \dot{\gamma}\lambda$$

For our experimental data we find a boundary at  $Wi \simeq 350$  separating between the breaking and non-breaking situation. Moreover, when descending to  $Wi$  numbers lower than 35, the inclusion does not break in separated blocs but elongate and spread in the matrix. It is interesting how these two boundaries have one decade difference between each other.

Fluids with higher elastic modulus and consequently, longer relaxation times, reach the breaking situation at lower flow rates. In other words, for elastic fluids, lower flow rates are convenient for fragmenting the inclusion which initially seems contra intuitive. Conversely, the lower  $G'$ , the easier it is to break the inclusion.

The explanation we propose is that when the inclusion reaches an obstacle, elasticity and shear rate compete. If the  $Wi$  number exceeds a critical  $Wi$  value, the inclusion will continue its way as a whole, being pulled by its own elasticity. However, when the  $Wi$  number is lower than the critical  $Wi$ , the inclusion breaks as the elasticity is not enough to compensate the shearing (see Figure 5.5). This interpretation is consistent with the fact that the transition occurs at constant  $Wi = 350$ .

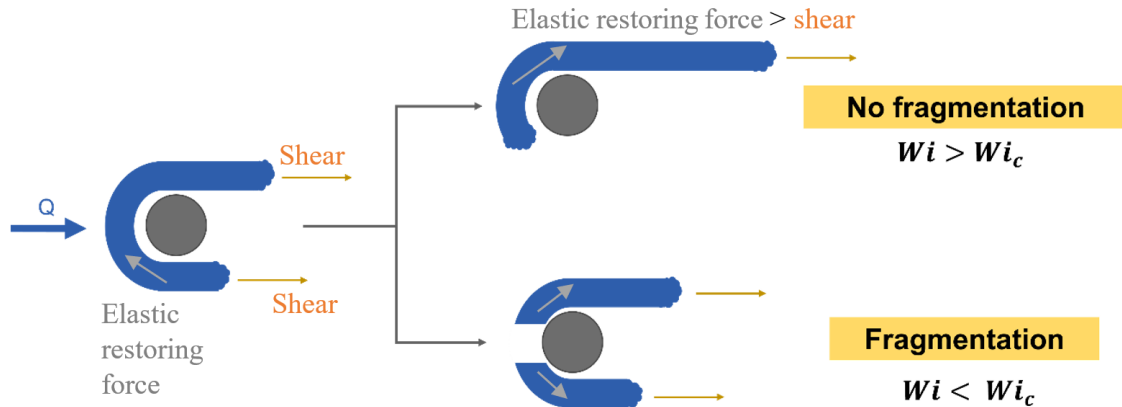


Figure 5.5: Proposed mechanism for the outcome of Flopaam inclusions in a Flopaam matrix going through a porous region.

As the rheology of both phases is the same in these experiments, it is not clear if this proposed mechanism is driven by the matrix phase or the inclusion phase. Therefore, we carried out the same experiments with viscoelasticity contrast between the phases.

### 5.2.2 Viscoelastic contrast between matrix and inclusion

We will now study how two contrasting phases react after the porous medium when altering the flow rate. In Fig 5.6 we have plotted the relaxation time ratio between the matrix and the plug against the  $Wi$  number of the plug (A) and the matrix (B). The ratio between relaxation times of the matrix to the plug is lower than one

when the plug is more elastic than the matrix, and higher than one in the opposite situation.

In this case, while the diffused regime found in the monophasic phase was not retrieved, we did find some conditions at which the plug was not breaking after the porosity. As in Fig 5.4, at high  $Wi$  numbers (triangles in Fig 5.6), the plugs came out of the porous region as a whole without splitting into smaller pieces. While this outcome was observed both when  $\lambda_{\text{matrix}} < \lambda_{\text{plug}}$  and in the opposite case, the limit between breaking and not breaking Moreover, when  $\lambda_{\text{matrix}} < \lambda_{\text{plug}}$  we could not characterise the porous flow at moderate  $Wi$  as inclusions stayed blocked before the porous section and did not manage to go through the pores. We attributed this blockage to the upstream configuration of the channel, as at low  $Q$ , inclusions flow asymmetrically along one side wall after their formation.

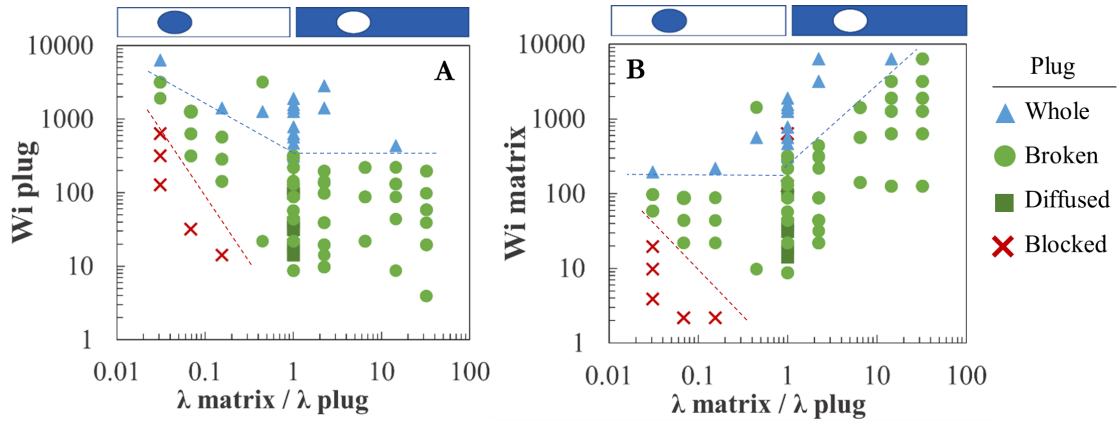


Figure 5.6: Phase diagram showing the outcome after the porous media for samples with a viscoelastic contrast between matrix and plug. The inclusions' size is 25% the area of the inlet section.

### 5.2.3 Size dependency

The proposed mechanism in Fig 5.5 should present different outcomes depending on the plug's size. We expected that larger plugs, would tend to fragment more than small ones. Small plugs would simply reach the obstacle and be dragged by its elastic force while larger plugs will surround the obstacle and divide its elastic restoring force into different directions leading to its fragmentation.

We have therefore tested some points in the phase diagram with smaller and larger plugs. The smaller plugs have sizes of  $\sim 15\%$  of the inlet surface while the larger ones are  $\sim 40\%$ . In Fig 5.7 we present the obtained phase diagrams for the monophasic and biphasic samples for smaller and larger plugs.

Surprisingly no differences are observed compared to the  $\sim 25\%$  plugs studied previously. The limit between fragmented and not fragmented stayed at  $Wi = 350$ .

The proposed mechanism cannot be fully validated as it appears to be too simplistic and fails to explain the consistent transition between the two regimes when altering the size of the plug. To enhance this study, additional tests should be conducted to explore the impact of a single isolated inclusion. It would also be beneficial to generate smaller plugs of a comparable order of magnitude as the obstacle or the

pore, as in the current study, the plug may be too large compared to the obstacle and may not be representative.

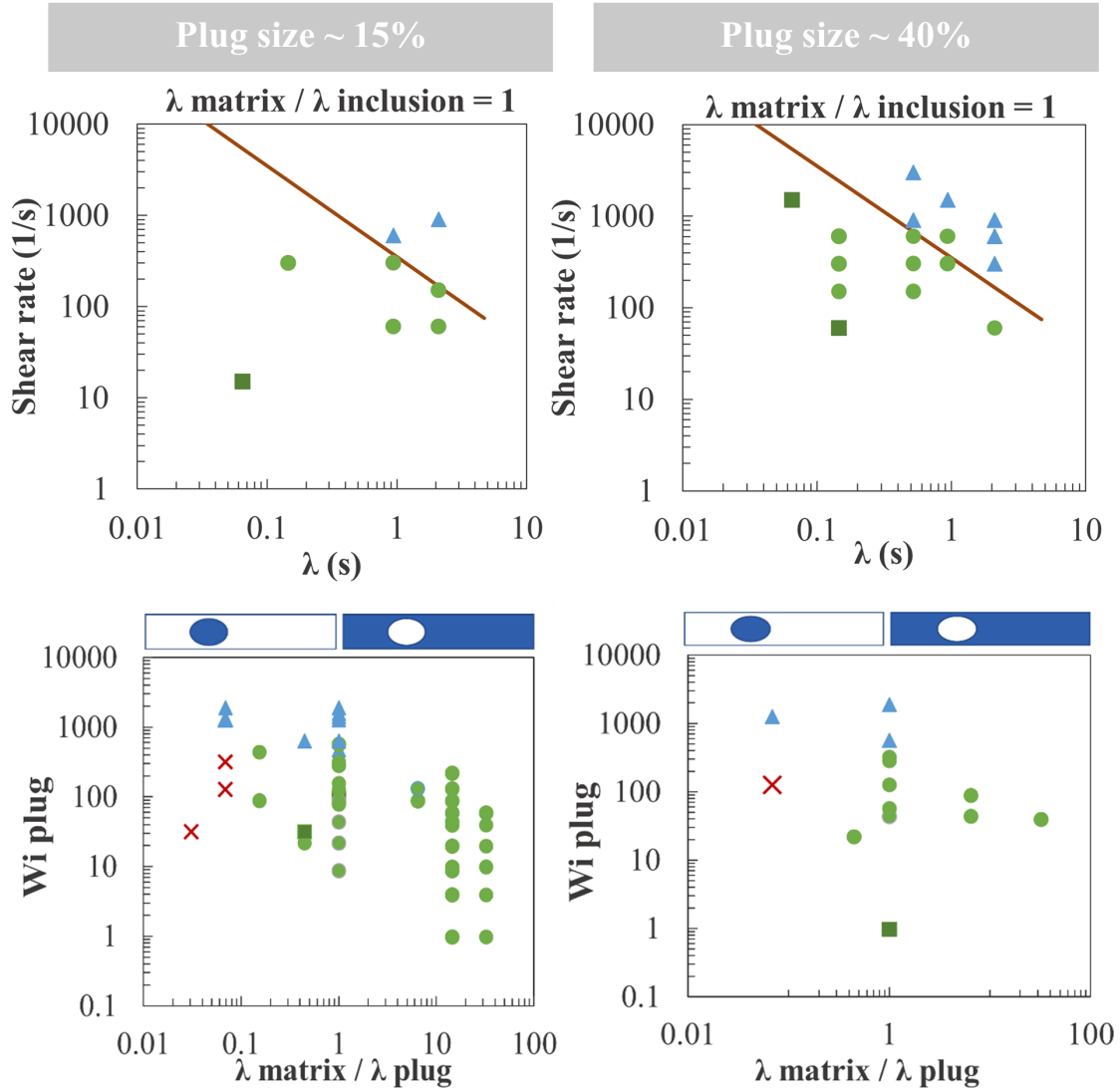


Figure 5.7: Phase diagrams for plugs of  $\sim 15\%$  (left) and  $\sim 40\%$  (right) of the inlet section. The two graphs at the top are the results from monophasic samples with both phases having the same concentration. The two graphs at the bottom are for diphasic samples with a contrast of viscoelasticity between plug and matrix different to 1.

### 5.3 Conclusions

In this chapter the aim was to build a passive non-user dependent system to break mucus plugs found in sputum into smaller pieces or homogenise them with the matrix. However, we soon found several practical problems to apply the system to sputum samples. For instance, the volume of sputum samples is not enough to fill up the channel. Moreover, a method to push the last part of the fluid into the porous medium should be implemented. For this reason, these experiments have finally

stayed as a study of the flow of viscoelastic fluids through a passive homogenisation system composed of a porous region.

The designed channel led to two main outcomes when injecting two viscoelastic fluids: the plug does not break, or the plug breaks into smaller pieces in the matrix. These regimes seem to be the response of a competition between the fluids elasticity and the imposed shear. Nevertheless, we have built two phase diagrams for monophasic and biphasic fluids and have found a range of flow rates at which we can always break our plugs. It is remarkable how the non-fragmentation regime takes place at high  $Wi$  numbers, indicating that slower flow rates improve the fragmentation. This result is contra-intuitive as we normally expect to improve the fragmentation and mixing by increasing the speed. At high flow rate, thus high  $Wi$  number, the elastic restoring force of the plug is stronger than the applied shear, pulling the samples around the obstacle and coming out from the porous region as a whole.

Future experiments will be carried out as a new PhD project with a modified upstream design, to circumvent the blocking of samples with plugs more viscoelastic than the matrix at low  $Wi$ . It would also be interesting to investigate lower  $Wi$  numbers to find the limit at which chaotic flow begins. Lastly, the dependence of the porous medium, in particular, its characteristic size, should be explored as different pore size will strongly alter the shear stress.

# Clinical findings

In the previous part we have developed the correct protocol to obtain consistent and reproducible rheological measurements of sputum samples. From now on, all the measurements presented will follow the methods and specifications indicated in the previous section. Sputum samples will refer to the ones collected in the Grenoble University Hospital unless otherwise stated. Therefore, sputum samples analysed here have all been aliquoted and vortexed after removing the saliva and stored in a  $-80\text{ }^{\circ}\text{C}$  freezer maximum one hour after collection.

This part will focus on the comprehension of sputum's behaviour and how do these features relate to the patient's clinical state. In chapter 6 we will start by characterising sputum's rheology investigating both the small and large deformation regimes and we will be able to extract some information about its structure. We will then continue to analyse the composition of sputum samples to understand the correlations between sputum's content and its mechanical properties. In the following chapter (7), we correlate sputum's composition and rheology with sputum's purulence. Then, we look into the elements involved in infection as bacteria colonisation and immune response to try to understand their influence on sputum's rheology. Moreover, along this chapter we also look at the patient's severity and how does it evolve as a function of rheology, composition and infection.

## Chapter 6

# Solid concentration influence on rheology

The rheological properties of viscoelastic fluids are related to their composition and microstructure. A viscoelastic fluid can be viewed as a complex network of interconnected particles, fibres, or polymers that interact with each other to determine the fluid's overall behaviour. At low concentrations, polymer chains are free to move independently and the viscoelasticity of the solution will be dominated by the viscoelasticity of the solvent. As the concentration increases, the number of polymer chains per unit volume also increases and chains start entangling leading to increased viscoelasticity. In addition to the sample's composition, the microstructure of viscoelastic fluids can be altered by external factors such as shear or strain. Applying certain forces on a viscoelastic fluid can cause the network to deform and restructure, which can result in modifications to its mechanical properties. Studying the relationship between sputum's composition, microstructure, and rheological properties is important to obtain a better understanding of the system's behaviour and how it will react to different factors.

In this chapter we therefore investigate sputum's composition and structure and its influence on its rheology. First, we quantify sputum's solid concentration distinguishing between organic and inorganic matter and analysing how they are correlated with sputum's mechanical properties. Then, we study what happens when we apply high strain to sputum and if the behaviour can be a criteria to distinguishing between diseases or patient's severity. Lastly, we will address the recovery capacity of sputum when we remove the applied effort and if it recovers, in what quantity it returns to its initial properties.

### 6.1 Sputum composition

Healthy mucus is a hydrogel composed of  $\sim 97.5\%$  water, a network of high molecular weight glycoproteins ( $\sim 4$  MDa) called mucins, salt and globular proteins [8, 43]. Pathological mucus, can also have other biological material such as DNA, cell debris, bacteria, inflammatory cells, etc.

Viscoelasticity has been shown to correlate to its solid fraction in mucus collected from human epithelial cells (HBE) [15] and differences have been reported on the relation between solid matter and osmotic pressure between healthy and diseased

sputum [17]. However, it remains unclear whether the anomalous viscoelasticity in pathological expectorations is primarily driven by organic (mucins, DNA, cell debris, etc.) or inorganic (salts) content. In this section we study separately these two influences in CF and NCFB sputum samples.

### Solid matter

We measured the solid fraction of 32 CF and 19 NCFB expectorations. Samples were weighted in a precision balance before and after drying at 37°C during 24h to ensure all the water was evaporated as some samples took longer than others to completely dry (see Fig 6.1). For these measurements we used volumes between 50 to 100  $\mu\text{l}$  depending of the total volume of the sample.

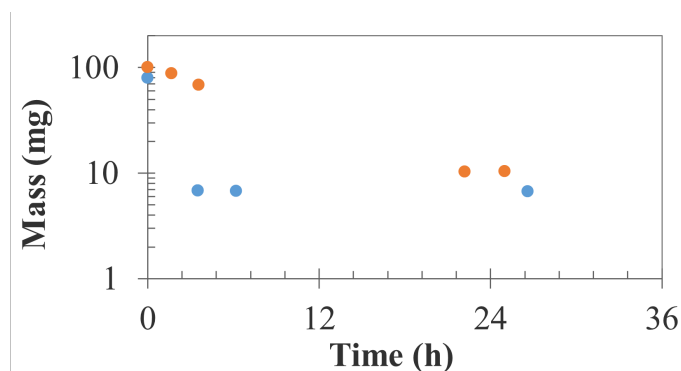


Figure 6.1: Measured mass as a function of time of two sputum samples during drying at 37°C.

Then, we measured the salt concentration of 22 CF and 19 NCFB samples by measuring its conductivity. For each sample, we diluted 15  $\mu\text{l}$  of sputum in 1.5 ml of ultra-pure water by mixing with the positive displacement pipette and then used the sensION+ EC5 DL conductivity meter. With the calibration curve we transformed the conductivity values into salt concentration.

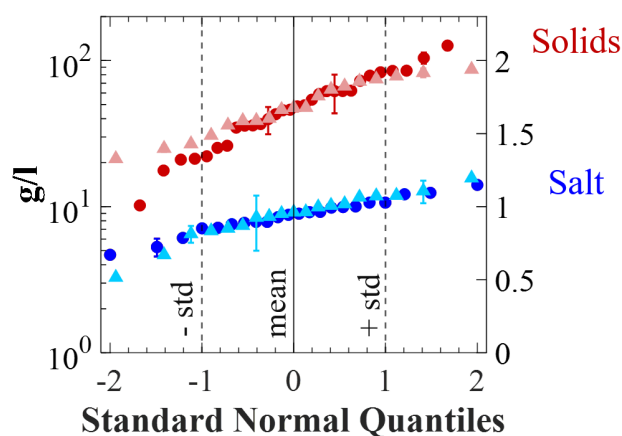


Figure 6.2: Distribution of solid and salt concentration (g/l) for CF (circles) and NCFB (triangles) sputum samples. Left axis follows a linear scale while the right axis shows the logarithmic values.

The distribution of the measured total solid and salt concentrations are displayed in Fig 6.2 for CF (circles) and NCFB (triangles). The solid fraction ranged from 8.42 to 138.96 g/l for the CF expectorations and from 21.3 to 86.96 g/l for NCFB samples. The populations followed log-normal distributions with mean  $\pm$  standard deviation values in the logarithmic domain of  $1.64 \pm 0.29$  for CF and  $1.68 \pm 0.19$  for NCFB samples. Thus, mean solid concentrations in the linear domain correspond to 44 g/l for CF and 48 g/l for NCFB. The salt concentration also followed log-normal distributions with mean  $\pm$  standard deviations of  $0.94 \pm 0.12$  and  $0.94 \pm 0.16$  for CF and NCFB samples respectively. In the linear domain, the mean salt concentration was 8.6 and 8.7 g/l for CF and NCFB, with values ranging from 5.29 to 10.66 g/l for CF and from 3.28 to 15.69 g/l for NCFB sputum. Therefore, in both diseases the dry mass is  $\sim 5 \pm 0.5$  % w/w, higher than for normal sputum which is around 3% [44]. Contrarily, the salt concentration ( $\sim 0.9 \pm 0.1$  %) is the same than for healthy sputum [8].

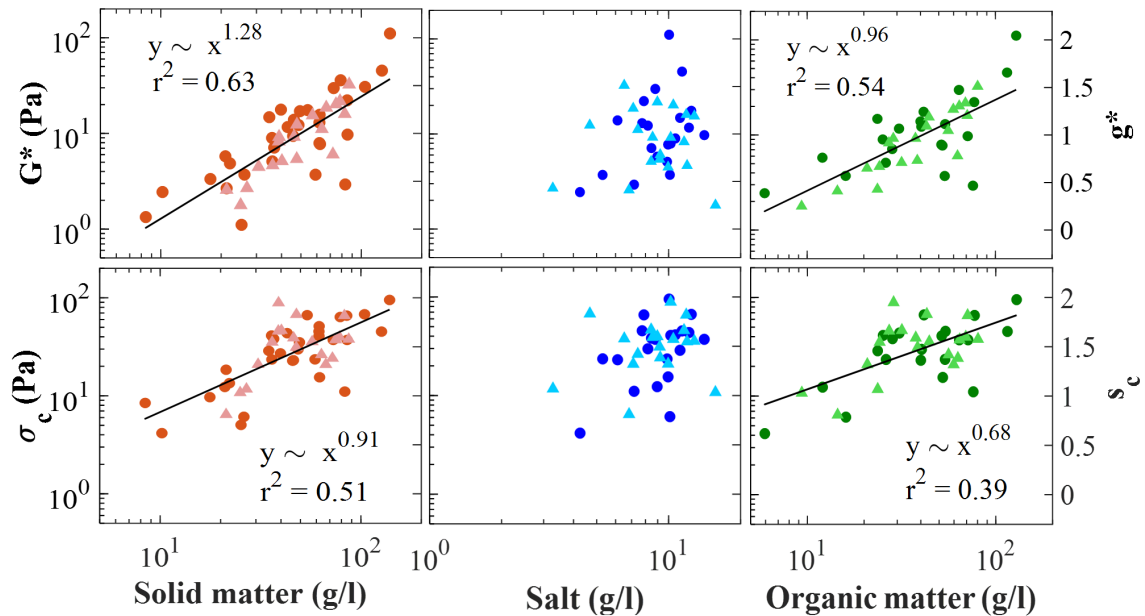


Figure 6.3: Correlations between  $G^*$  and  $\sigma_c$  with the solid, salt and organic matter concentration. CF samples are represented by circles and NCFB sputum by triangles.

We also carried out strain sweeps with the sputum samples and crossed these measurements with their dry mass and salt concentrations in Fig 6.3.  $G^*$  and  $\sigma_c$  are directly correlated to the solid concentration with power laws of 1.28 and 0.91 respectively as best fits. The higher the solid matter in the sputum sample, the higher its viscoelasticity and its critical stress. Interestingly, other studies have also reported 1.2 as the power law factor of  $G^*$  as a function of solid concentration [8]. On the contrary, we observed no correlation between the rheological measurements and the salt concentration. The salt concentration did not vary greatly along the measured sputa, all the plotted points stay around the same region without a tendency (see Fig 6.3). Moreover, the salt concentration retrieved in our samples did not differ from the values found in literature for healthy subjects [8, 43], thus we did not expect to see a significant influence on pathological sputum rheology.

We still wanted to verify if the salt concentration was dependent of the solid matter but as shown in Fig 6.4, where we plot  $G^*$  as a function of the solid and salt concentration, we did not found any tendency.

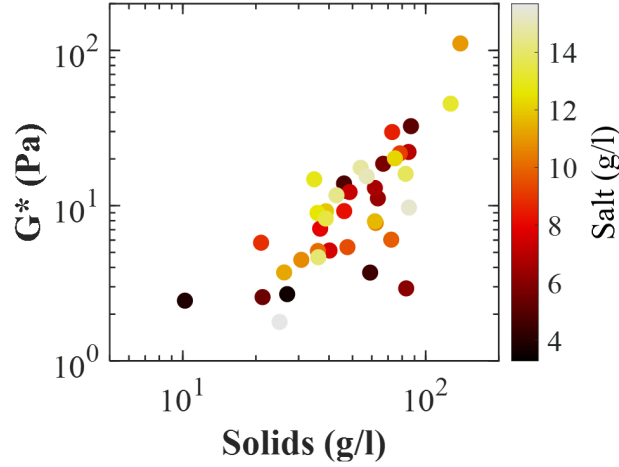


Figure 6.4: Correlations between  $G^*$  and solid concentration with the salt concentration as a colourmap.

We therefore subtracted the salt concentration to the total solid concentration obtaining the organic matter (right graphs in Fig 6.3). Without salt,  $G^*$  and  $\sigma_c$  reduced the slope of the correlation with the organic concentration to 0.96 and 0.68 exponents.

In contrast, previous studies had reported a reduction in the pore size of saliva when adding free calcium [45] due to the creation of crosslinks with MUC5B. This could be explained, as it has already been speculated by Lai et al. [46], by the fact that macrorheology is not capable of describing the adhesive properties and that the ionic content of mucus has an influence in the adhesion between mucins.

Our results however show a clear correlation between the solid fraction and the viscoelastic modulus. The viscoelastic modulus for a fully swollen gel has been defined [47] as:

$$G^* \sim \frac{n}{N}kT$$

where  $n$  is the number density of the solid matter,  $N$  the average number of monomers per strand and  $kT$  the thermal energy in the polymeric network [48]. As we do not know the number density we will reformulate the previous formula with the Avogadro number ( $N_A$ ), the molecular weight ( $M_w$ ) and the solid's density ( $\rho$ ) through:

$$n = \frac{N_A}{M_w}\rho$$

$$G^* \sim kT \frac{N_A}{M_w} \frac{\rho}{N}$$

Therefore,  $G^* \sim \rho$ . Similarly, Rubinstein et al. [47] also predicted  $G^*$  dependence with the concentration without salt as  $G^* \sim c^{5/6}$ , with the same logic as before we reformulate this expression as  $G^* \sim \rho^{5/6}$ .

We have therefore tested these two correlations with our data in Fig 6.5 and plotted the resulting fits as dashed lines. Rubinstein fits describe correctly our data.

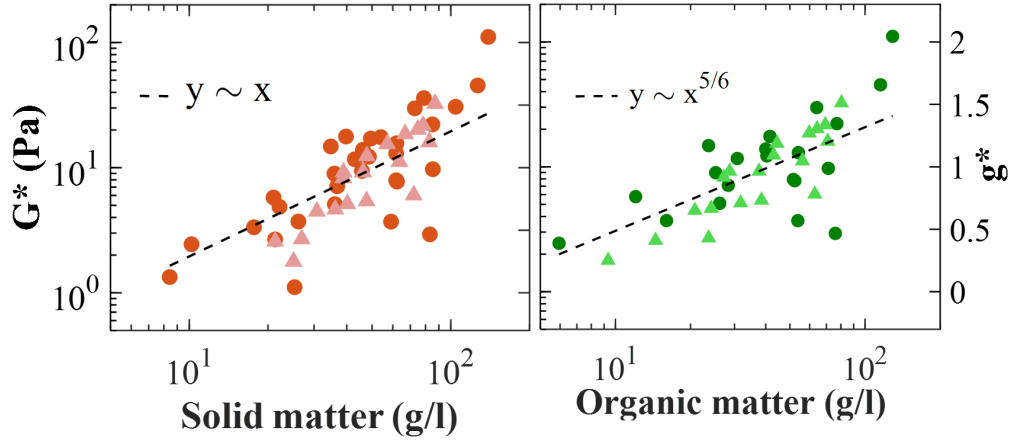


Figure 6.5: Rubinstein fits (dashed lines) [47]  $G^* \sim \rho_{\text{solids}}$  and  $G^* \sim \rho_{\text{nosalt}}^{5/6}$ .

Moreover, Hill et al. [8] measured the osmotic pressure ( $\Pi$ ) of mucus from epithelial cells (HBE mucus) and found the organic concentration at which polymers start overlapping,  $\rho^*$ . Diluted HBE mucus have mucins far away from each other with no contact, when increasing the concentration, mucins will start touching.

The concentration of the fully swollen gel is proportional to the overlapping concentration [49],  $\rho \propto \rho^* \propto N/R_g^3 \propto N^{1-3\nu}$  therefore,

$$G^* \sim kT\rho^{3\nu/(3\nu-1)}$$

where  $R_g$  is the radius of gyration and comes from the size of the mucins and  $\nu$  is related to the chain size ( $R_g \sim N^\nu$ ) [50] and is governed by the interaction between the solvent and the polymeric chains [49]. In our case,  $\nu = 1/3$ , which corresponds to strong attractive interactions between polymer segments and poor solvent influence [49].

The osmotic pressure follows the following expression [8]:

$$\Pi = RT \frac{\rho}{M_w} + RT \frac{\rho^*}{M_w} \left( \frac{\rho}{\rho^*} \right)^\alpha$$

In the diluted situation, the osmotic pressure grows as a function of  $\Pi \sim \rho$  while after  $\rho^*$ , the concentration dependence takes a larger exponent,  $\Pi \sim \rho^\alpha$ , with  $\alpha > 1$ . As  $RT = kTN_A$ , the viscoelastic modulus is proportional to the osmotic pressure, then  $G^* = (a\rho + b\rho^\alpha)/N$ .

We consider the same overlapping organic concentration as Hill et al. [8] as we do not know the molecular mass of the organic matter in our samples. They consider  $M_w = 10^8$  g/l ( $\sim 100$  MDa) and  $R_g = 400$  nm for mucins and  $\rho_{\text{mucins}}^*$  can be calculated as then  $\rho_{\text{mucins}}^* = 0.6$  g/l. The concentration of mucins account for  $\sim 50\%$  of the organic concentration [8], thus  $\rho^* = 1.8$  g/l.

The resulting Fig 6.6 shows the resulting fit. Although this equation is effective at high organic concentrations, at lower concentrations, the data points do not exhibit as significant of a reduction in  $G^*$  as the fit suggests. Contrary to mucus collected from human epithelial cells which only contains mucins and globular proteins, sputum samples also present pathogens, cell debris and DNA which could help to the overlapping of its network at lower organic concentrations.

We also observe how all of our samples are in the region where  $\rho > \rho^*$ , we therefore will explore the diluted region in the following section.

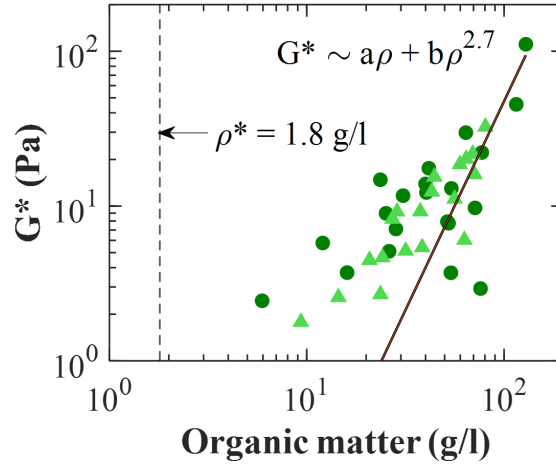


Figure 6.6: Overlapping organic concentration  $\rho^*$  at which the gel passes from a diluted to a semi-diluted state. The dotted line follows  $G^* = a\rho + b\rho^\alpha$  with  $a = 6.97 \cdot 10^{-5} \text{ m}^2/\text{s}^2$  and  $b = 2.57 \cdot 10^{-5} \text{ Pa}$  and  $\alpha = 2.7$ .

The two models tested, correctly describe our data. However, Rubinstein's model does not account for samples that strongly increase their  $G^*$  at high organic concentrations, while Hill's approach performed better for such cases.

### Hydration test

To study the diluted regime with  $\rho < \rho^*$ , we hydrated a sputum sample, keeping isosalinity, and analysed the evolution of its rheology.

We collected a big volume expectoration from a NCFB patient. First, we measured its rheology and quantified its solid and salt concentration of 500  $\mu\text{l}$ . The sample had a viscoelastic modulus  $G^* = 32.15 \text{ Pa}$  and a critical stress of  $\sigma_c = 35.5 \text{ Pa}$  and was composed of 87.19 g/l of solid matter and 6.5 g/l of salt. Then, we prepared 2, 4, 10, 100 and 1000 fold dilutions gently mixing the corresponding sputum volume with salted water with the positive displacement pipette. Salt concentration was kept constant.

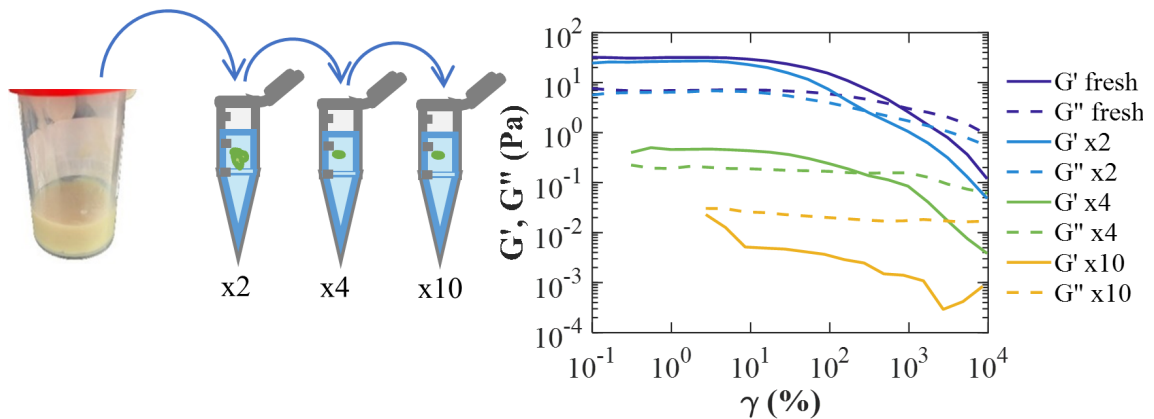


Figure 6.7: Strain sweeps for the hydration test with a NCFB expectoration.

When diluting, the plateau values decreased keeping  $G' > G''$  until the ten-fold dilution at which the elastic character was lost ( $G' < G''$ ), see Fig 6.7. From this dilution on, the sample was very liquid and the signal of the rheometer had too much noise. The first dilution (x2) does not present a strong drop compared to the fresh sample. We were not surprised of this result as this dilution was not properly homogenised, the sample was very thick and we did not manage to completely homogenise it with the salted water following the same mixing procedure as for the rest of the dilutions. Yet, the crossover point decreased at each dilution.

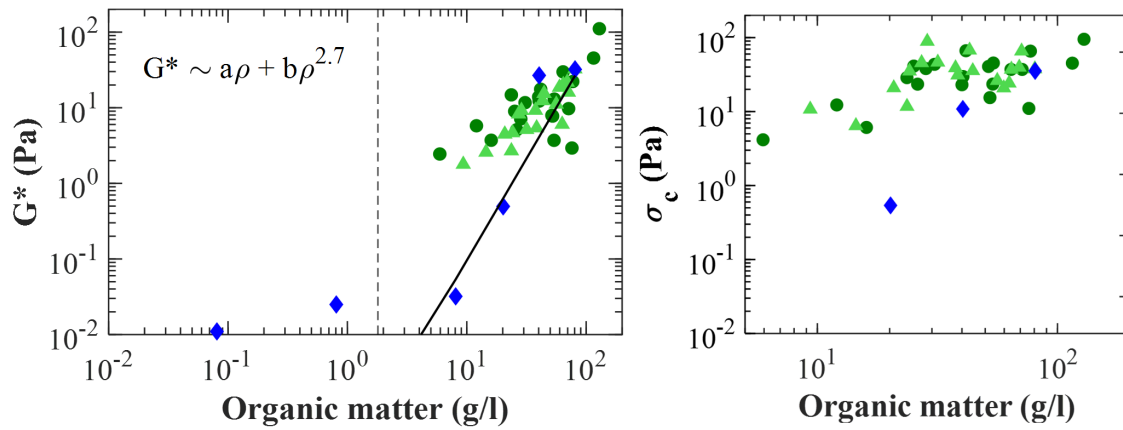


Figure 6.8: In blue diamonds we have plotted the measurements of the rheology and solid content of a NCFB fresh sample and its 2, 4, 10, 100 and 1000 fold dilutions. The full line is the best fit we could do for the sputum sample data and the dashed line correlates  $G^*$  with the solid concentration to the power of 2.7 as proposed by Hill et al. [8].

The plateau values of  $G^*$  and  $\sigma_c$  are plotted in Fig 6.8 represented by blue diamonds. Although both variables decreased their values when hydrating, the drops seemed more drastic than for the 51 sputum samples. However, it is remarkable how well the diluted samples follow Hill's fit, increasing  $G^*$  with the organic matter to the power of 2.7 at high concentrations ( $\rho \gg \rho^*$ ) where elements in the network are in contact and mucin bundles entangled. This implies that some entanglements are maintained during hydration (in the  $\rho \gg \rho^*$  region), causing a significant swelling of the network. The sharp decrease in  $G^*$  may be attributed to the fact that diluted samples retain regions with strongly entangled mucins while the majority of the system is highly diluted. This hypothesis could also account for the reduction in  $\sigma_c$ , since the dominant phase has fewer entanglements, thereby requiring lower strains to make the fluid flow.

Moreover,  $G^*$  shows a breakpoint somewhere between 1 and 10 g/l coinciding with the overlapping concentration determined by Hill et al. [8] ( $\rho^* = 1.8$  g/l). After  $\rho^*$ , the diluted sputum presents does not evolve as much with  $G^*$ . This could be explain by the fact that elements in the network are not in contact anymore and are highly dispersed in the solvent therefore we only measure the solvent's viscoelasticity.

## 6.2 Sputum under large strain

When manipulating the sputum *ex vivo* by pipetting, vortexing or loading on the rheometer we are applying shear and stresses to the sample and interfering on its internal network. These stresses can also appear *in vivo* in the respiratory tract during the mucociliary clearance of pathological mucus by coughing which involves large deformations. If these efforts are small we have already seen  $G'$  and  $G''$  of sputum samples will not react. Nevertheless, when the shear is increased, these values start dropping until reaching a critical point at which the structure is able to flow.

In chapter 3 we have presented the measurements from classical rheometry, Small Amplitude Oscillation Shear (SAOS), which obtain their values from the analysis of a single sinusoidal. Contrary to Large Amplitude Oscillation Shear (LAOS) analysis, SAOS does not consider the deformation of the signal at high strain. We have seen in the methods chapter (chapter 2) how through the decomposition of the signal into its harmonics, we can obtain some information about the system's behaviour under high efforts. We have therefore tested this LAOS approach on data transferred by the Montpellier University Hospital.

47 patients provided sputum as part of a clinical trial, which was characterised with oscillatory strain sweep tests. These samples corresponded to 12 patients with COPD, 8 exacerbated COPD, 22 cases of NCFB and 5 samples from exacerbated NCFB.

### Identification of the large strain domain

In each experiment we record sinusoidal signals measured from the top and bottom captor of the rheometer. By decomposing these signals, we obtained the intensity of each harmonic,  $I_3$  and  $I_1$  along the applied strain. Then, we found the beginning of the nonlinear regime as the point where the coefficient  $Q$  stopped being constant and plotted the corresponding strain value for different types of samples in Fig 6.9 A. When comparing the mean strain value of the samples from patients with COPD with and without exacerbation, no significant differences were found. In contrast, a significant difference ( $p$ -value = 0.005) was observed between the NCFB patients: the exacerbated cases reached the nonlinear domain at higher strain values. This means stronger deformations need to be applied to start deforming exacerbated NCFB sputum. However, this observation is based on a small sample size of only 5 samples, which may limit its robustness.

Moreover, we also calculated the strain at which  $G'$  and  $G''$  cross which is the critical or crossover point. When this point is reached, samples start flowing and are able, for instance, to advance in the respiratory tract. Exacerbated samples presented higher  $\gamma_c$  than non-exacerbated in Fig 6.9 B, still these differences were not statistically significant. Lastly, by comparing these two graphs we see the large deformation domain (once the measured signal is no more a perfect sinusoidal) covers more than one decade for sputum, with  $\gamma$  ranging from 100% to 3000%.

The LAOS analysis can also bring light into the structural conformation of the polymeric network. For sputum, the coefficient  $Q$  drops after the linear domain as shown in Fig 2.3 in the methods chapter which Hyun et al. [26] observed was a signature of untangled polymers. In fact, Fass et al. [9] describe MUC5B as linear polymers while MUC5AC have a three-dimensional network forming bundles.

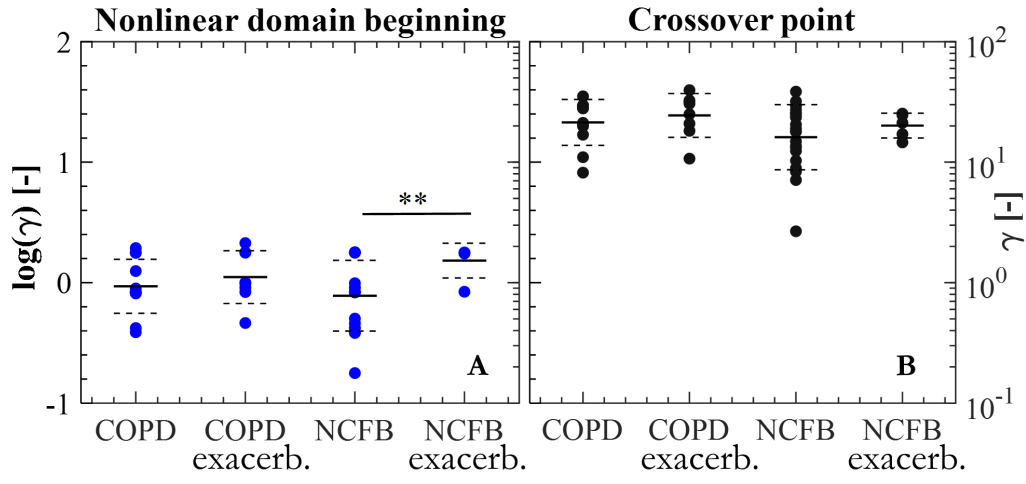


Figure 6.9: A: Strain at the first point of the nonlinear domain for 12 COPD and 22 NCFB expectorations as well as their exacerbated cases ( $N_{\text{COPD}} = 8$  and  $N_{\text{COPD}} = 5$ ). \*\* indicates a p-value of 0.005. B: Strain at the critical point  $\gamma_c$ . Solid lines represent mean values and dashed lines standard deviation.

Therefore, it seems sputum's network is not strongly crosslinked but is an heterogeneous system with multiple elements in contact. This finding could be explained with the several observations in literature who talk about untangled mucus insoluble "flakes" [51] composed of mucins organised with a granular appearance [52].

### Sputum's response to large strain

We have already identified the beginning of the nonlinear domain, now we will quantify the macroscopical reaction of sputum during large strain.

We calculated the elastic and viscous coefficients of the Chebyshev polynomial,  $e_3/e_1 = G'_3/G'_1$  and  $v_3/v_1 = G''_3/G''_1$  for the COPD and NCFB expectorations and confirmed the strain stiffening ( $e_3/e_1 > 0$ ) and shear thinning ( $v_3/v_1 < 0$ ) behaviour of sputum (Fig 6.10 A and B). Still, this behaviour is not constant along the applied strains. Once the nonlinear domain starts, sputum becomes stiffer and less viscous with increasing strain until reaching a maximal  $e_3/e_1$  value and a minimal  $v_3/v_1$  from which the stiffening and thinning rate decreases. Therefore the nonlinearities are more and more important until reaching the maximal and minimal values, then the third harmonic starts losing importance. We have not found any description of this observation in the literature even if this same behaviour has been reported [53, 54]. Still, this could simply be explained by the fact that the intensity of the third harmonic ( $I_3$ ) is zero in solid and liquid-like materials. At low strains, sputum stores the energy and does not create nonlinearities in the measured signal. On the contrary, at very high strains it takes a liquid-like behaviour flowing when overpassing the critical point. After this point, the material liberates all the energy completely deforming with the strain.

We also notice that the values of  $e_3/e_1$  and  $v_3/v_1$  start being non-zero before the onset on the nonlinear regime (dashed lines on Fig 6.10), and dropped after the critical point (solid lines on Fig 6.10). In fact, this behaviour was not observed as a generality.

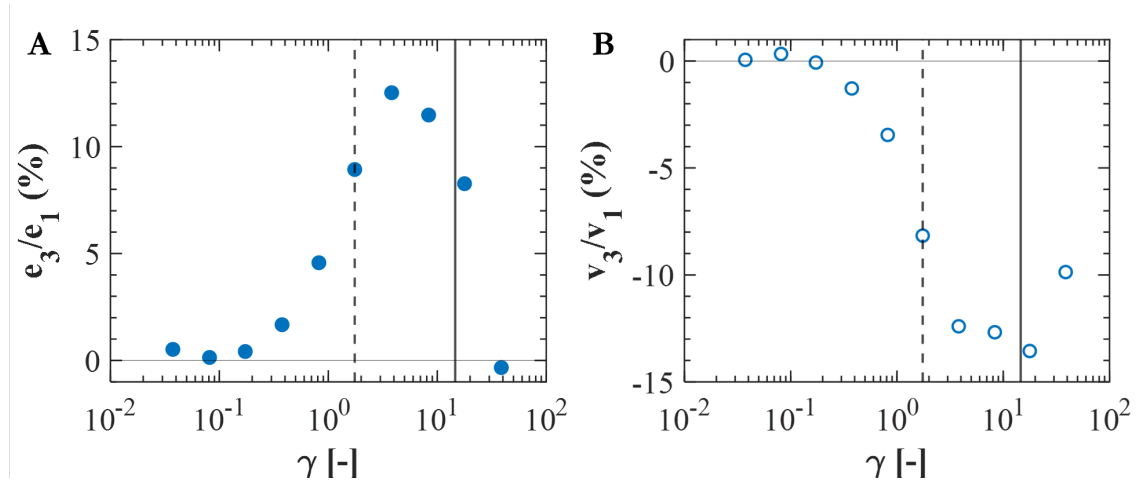


Figure 6.10: LAOS response of an exacerbated NCFB sample. The dashed line indicates the first point in the nonlinear domain and the solid line marks  $\gamma_c$  for this sample. A: Intracycle elastic coefficients are positive revealing the strain stiffening response. B: Intracycle viscous coefficients are negative indicating a shear thinning behaviour.

In Fig 6.11 we plotted the strains for the maximal  $e_3/e_1$  (blue full line) and the minimal  $v_3/v_1$  (blue dashed line) along with the beginning of the nonlinear regime (black dashed line) and the critical strain (black full line). Along all the analysed samples we observed the two outcomes in Fig 6.11, some presented the maximal  $v_3/v_1$  at  $\gamma > \gamma_c$  (A) and others at  $\gamma < \gamma_c$  (B). We could not explain this observation as it was not found to be a singular feature of a certain group of samples.

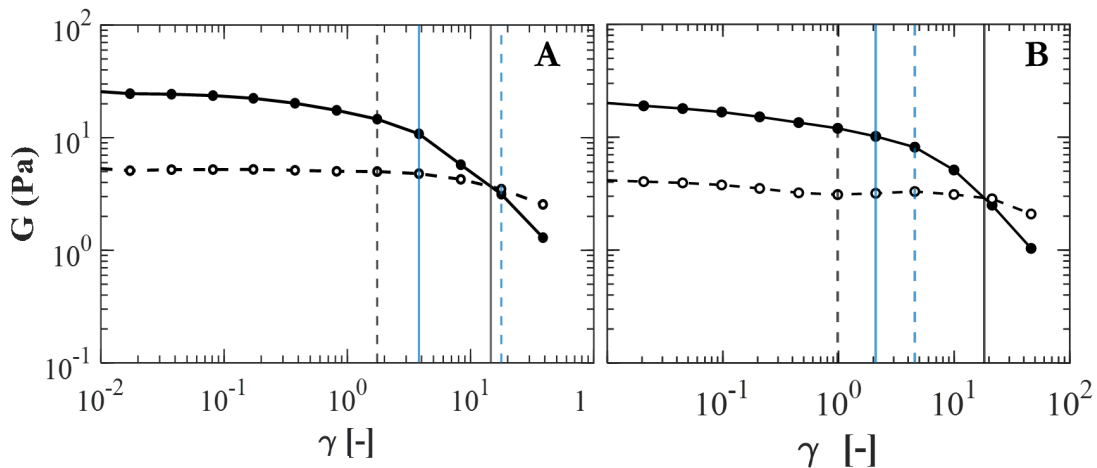


Figure 6.11: Stain sweeps for an exacerbated NCFB sample (A) and an exacerbated COPD expectoration (B). The black vertical lines indicate the beginning of the nonlinear domain (dashed lines) and the critical point  $\gamma_c$  (full lines). The blue lines mark strains for the maximal  $e_3/e_1$  (full lines) and the minimal  $v_3/v_1$  (dashed lines).

We therefore compared the maximum and minimum values within the 47 expectorations trying to find any particularities for each disease (see Fig 6.12). We observed a significant difference (p-value = 0.03) between exacerbated and non-

exacerbated NCFB samples for the strain of the maximal  $e_3/e_1$ : the values for non-exacerbated NCFB are lower. Still, exacerbated NCFB expectorations consistent only of 5 samples which limits the t-test robustness. The strain at which the minimal  $v_3/v_1$  is reached was similar in all the expectorations. However, the exacerbated cases showed increased values but the mean differences were not statistically significant.

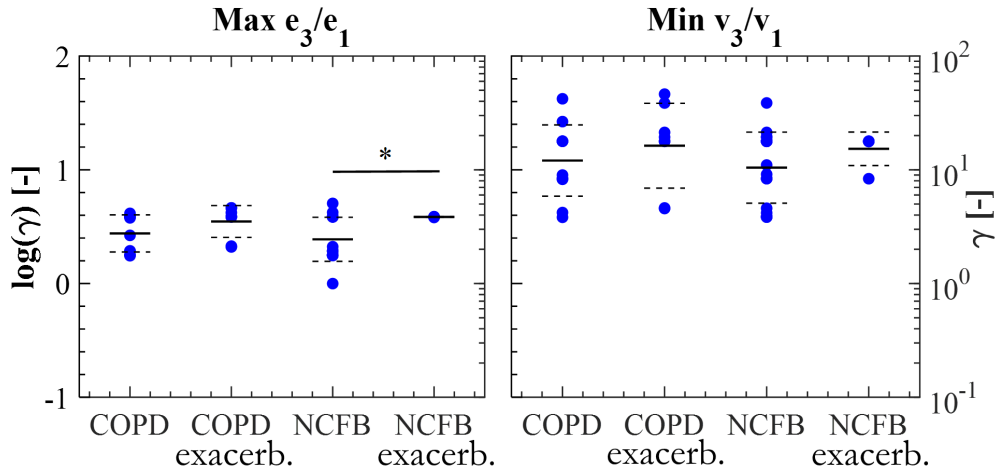


Figure 6.12: Strain of the maximal and minimal values of  $e_3/e_1$  and  $v_3/v_1$  obtained for the 12 COPD, 8 exacerbated COPD, 22 NCFB and 5 exacerbated NCFB expectorations. The p-value for \* is 0.03.

We have seen in this section that the LAOS analysis does not provide clear markers of mucus clearance that could be related to any specific factor. Thus, we will keep the  $\gamma_c$  and  $\sigma_c$  variables to characterise the large deformation regime in the subsequent analysis since they can be easily obtained by extending the SAOS analysis to the entire strain sweep rheological curve.

## 6.2.1 Recovery

Cough is generated to produce a strong shear force on the clogged mucus, which moves it towards the mouth and clears it from the respiratory tract. This mechanism induces strong shear stresses of around 14 Pa [55]. Therefore, to move mucus, large deformations must be applied and the critical point is reached. As we have seen in the previous section, sputum reduces its viscoelasticity at high strains showing a liquid-like behaviour which helps to its clearance. Although coughing generates a strong shear stress, it is not constant and a series of repetitive pulses are needed to clear obstructed mucus. As such, we aim to investigate whether sputum is capable of regaining its gel-like structure when the applied stresses are ceased. If this was the case, we want to know first if this recovery is instant or if there is a lag time and second, if it is able of completely recovering its original viscoelasticity or it can be cleared again applying lower strains. Studying the rheological recovery of sputum is interesting because it can provide insights into the dynamics of mucus clearance in the lungs.

## Healthy sputum

To setup the measuring protocol we started by analysing an expectoration from a smoker volunteer. We placed the sample in the ARG2 rheometer and protected it from drying isolating it in an anti-evaporation trap with an injection of saturated air. Then, we applied consecutive strain sweeps and time sweeps. The strain sweeps went from 0.1 to 5000% to make sure we passed the crossover point, then the time sweeps were carried out at a fixed strain of 5%, value in the linear  $G'$  and  $G''$  plateau. This way we are first altering the sample's network through the application of a strong strain and when we release the effort, we immediately look at the time it takes to stabilise. This same process was repeated 6 times.

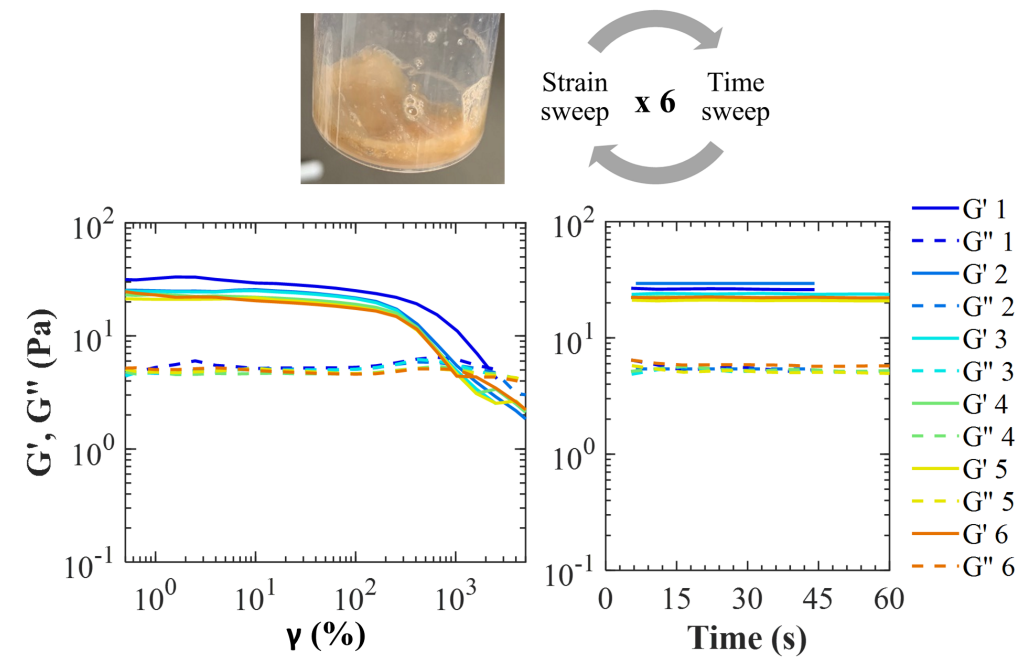


Figure 6.13: Recovery protocol applied to a sputum sample from a smoker donor. It consisted on: (1) a strain sweep passing the crossover point followed by (2) a time sweep at small strain. The same process was repeated 6 times.

We observed the recovery was instantaneous as both  $G'$  and  $G''$  are stable from the first measured point in the time sweep when releasing the large strain (see Fig 6.13). However, a difference was observed in the plateau values between the first and the following strain sweeps. There was a slight drop of  $G'$  and  $G''$  in the linear domain as well as an advancement of the critical strain  $\gamma_c$ .

Figure 6.14 shows the plateau values of  $G'$  and  $G''$  at 5% strain along the 6 strain sweeps performed. While the loss modulus does not evolve, the storage modulus suffers a smooth drop as previously noticed in the strain sweep curves (Fig 6.13).  $G'$  drops its value 19.3% and  $G''$  8.2%. On the right side of the figure, the same evolution for the variables at the crossover are displayed.  $\sigma_c$  reduces 49.4% its value from 156.25 Pa to 69.8 Pa while  $\gamma_c$  drops 51.84% from 2122.5% to 992%. Therefore, with the first strong strain we are distorting a part of the sputum's network which is not able to completely recover: it is still able to recuperate its gel structure almost completely but it will start flowing at substantially lower strains (reduced by a factor of more than 2).

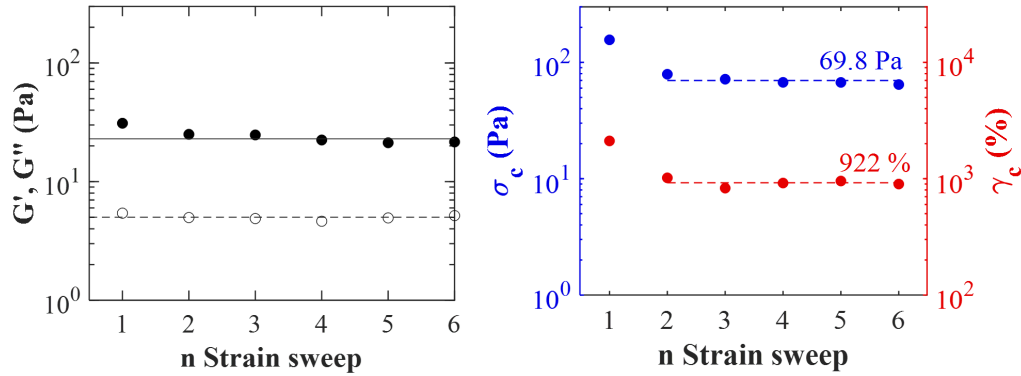


Figure 6.14: Evolution of the plateau values of  $G'$ ,  $G''$  at 5% strain,  $\sigma_c$  and  $\gamma_c$  along the consecutive amplitude sweeps for the smoker sputum sample.

### CF and NCFB sputum

As we had observed sputum immediately recover its gel form we decided to systematically measure three consecutive strain sweeps in 34 CF and 15 NCFB expectorations to quantify the evolution of the rheological variables.

Figure 6.15 shows the two outcomes found. 25 out of 34 CF and 10 out of 15 NCFB samples showed a drop in  $G'$  and  $G''$  while 9 CF and 5 NCFB samples showed an increase of these variables. However, there was a consistent drop of  $\gamma_c$  and  $\sigma_c$  as previously seen in the healthy sputum.

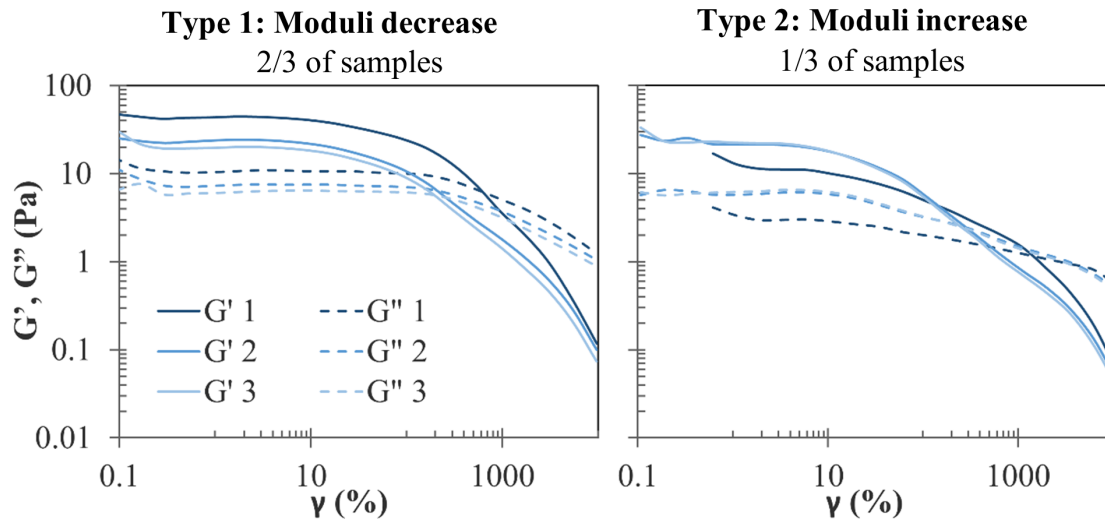


Figure 6.15: Representative strain sweep curves measured in CF and NCFB expectorations for three consecutive tests. Three strain sweeps were carried out, they are indicated from darker to lighter colour.

We first investigated the evolution of the linear domain. In Fig 6.16 we represent the first drop (filled markers) or increase (empty markers) of  $G'$  for the 34 CF and 15 NCFB samples as a function of their initial elastic modulus,  $G'_1$ . In Fig 6.16 we see how the increase or reduction of  $G'_2$  was not strongly correlated to the sample's initial elastic modulus. The only particularity was that all the samples with  $G'_1$

$> 20$  Pa (dashed line in Fig 6.16) always dropped their elastic modulus after large strain.

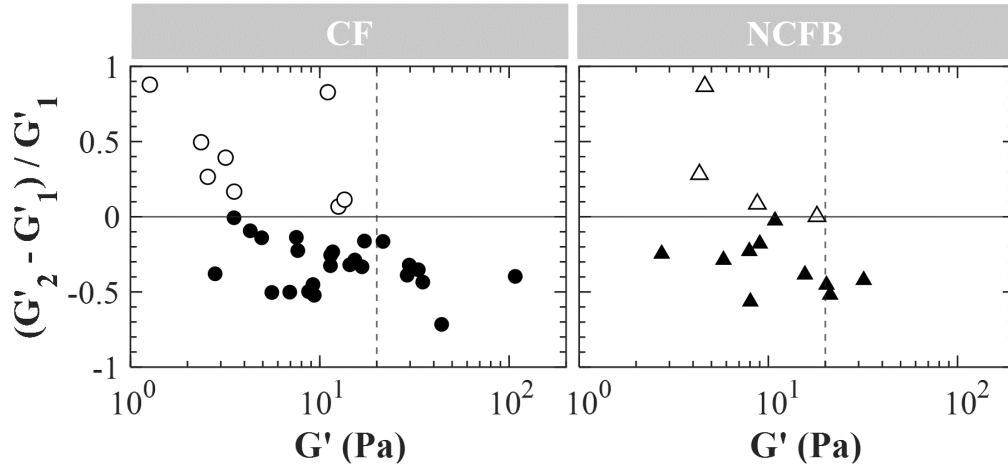


Figure 6.16: Variation of  $G'$  between the first and second strain sweep for  $G'$  for the 34 CF (circles) and 15 NCFB (triangles) expectorations as a function of  $G'$  from the first strain sweep.  $G'$  drop as filled markers and  $G'$  increase as empty markers.

We then plotted in Fig 6.17 the same points as a function of their purulence addressed by their transparency ( $v$ ) calculated following the procedure described in section 2.4 and we coloured each point with the sample's colour obtained through image processing.

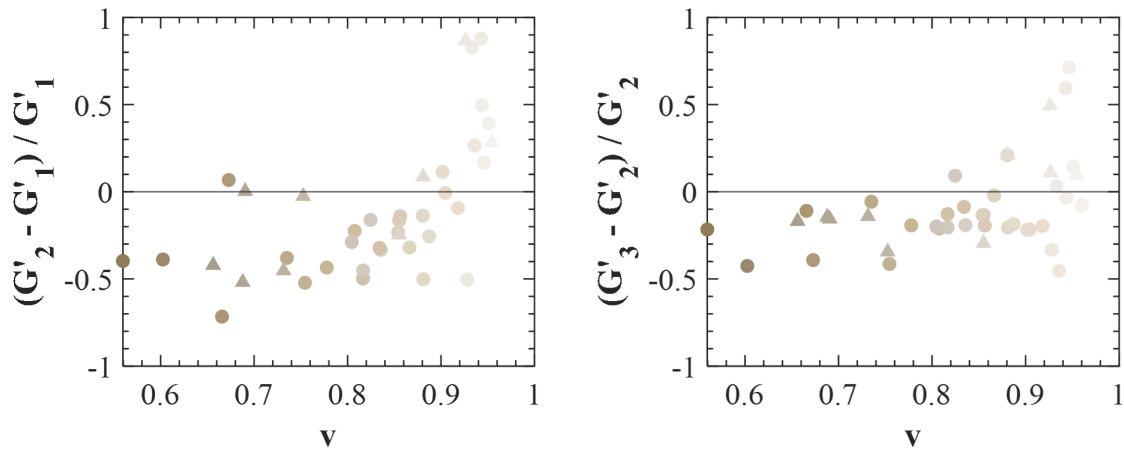


Figure 6.17: Variation of  $G'$  between the first and second strain sweep and between the second and third strain sweep for the CF and NCFB expectorations as a function of sample's purulence.

The expectorations which increased their  $G'$  after the first strong deformation were all light samples. As we will see into detail in chapter 7, sputum's colour or purulence is known to be an indicator of infection and solid concentration. Our results show how darker samples become less viscoelastic after strongly deforming, while lighter samples increase their viscoelasticity.

In average, type 1 samples dropped  $G'$   $32.6 \pm 16.2\%$  for CF and  $33.1 \pm 16.7\%$  for NCFB expectorations after the first strain sweep and  $19.9 \pm 11.6\%$  and  $19.9 \pm 7.2\%$

after the second strain sweep. The second drop was significantly smoother than the first one with p-values of 0.0011 for CF and 0.023 for NCFB samples. The 9 CF samples that did not decrease their plateau values (Type 2 in Fig 6.15), presented increases of  $G'$  after the first strain sweep ranging from 6.8% to 757.1% and from 0.3% to 263.8% for the 5 NCFB samples. The second increases were not as strong with values ranging from 3.2% to 71.36% for CF and from 2.1% to 49.4% for NCFB samples.

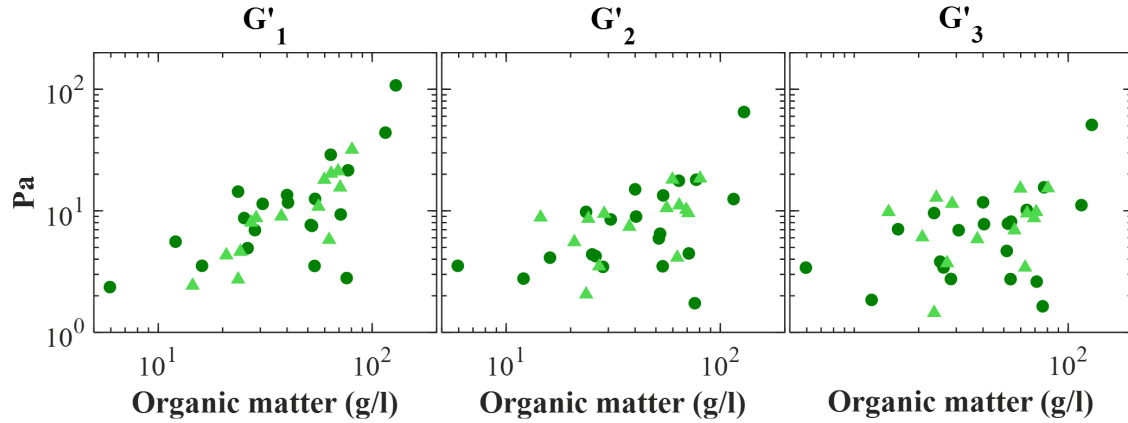


Figure 6.18: Plateau values of the elastic modulus  $G'$  for the first, second and third strains sweeps as a function of organic concentration.

In rheometry, it is common practice to apply a pre-shear to the sample in order to remove any prior history effects and to establish a consistent starting point for all samples, and therefore enabling reliable comparisons. We have investigated if applying strong strains to our samples improved the correlation between organic concentration and the viscoelastic modulus in Fig 6.18. We noted that  $G'_2$  and  $G'_3$  exhibit flatter distributions and weaker correlations with the organic matter. Moreover, pre-shearing does not align the data points or reduce their dispersion as expected.

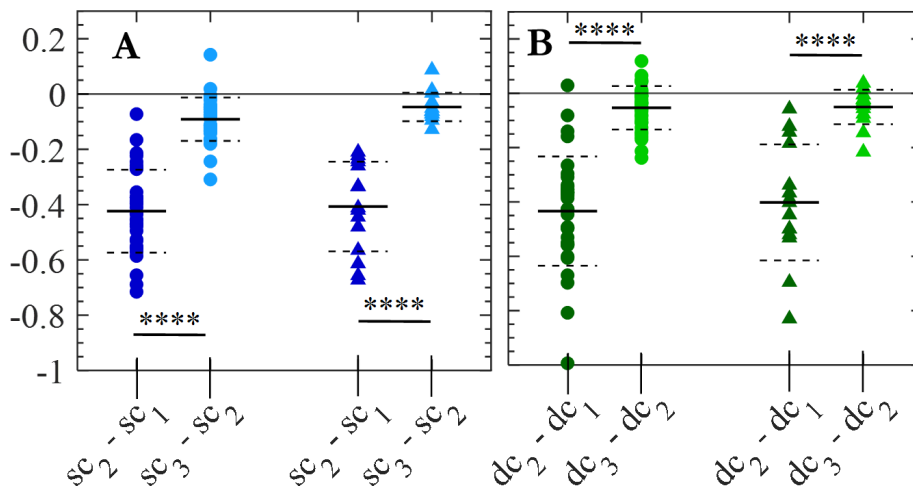


Figure 6.19: Variation between consecutive strain sweeps for  $s_c$  (A) and  $d_c$  (B) for the 34 CF (circles) and 15 NCFB (triangles) expectorations. \*\*\*\*: p-value < 0.0001.

Contrarily, the evolution of the critical stress and strain were consistent along all the analysed samples. The 34 CF and 15 NCFB expectorations respectively reduced their  $\sigma_c$  value by  $60.0 \pm 14.5\%$  and  $58.3 \pm 14.4\%$  after the first strain sweep and  $20.1 \pm 11.18\%$  and  $14.2 \pm 5.1\%$  after the second strain in average, see Fig 6.19 A. Similar outcome was observed for  $\gamma_c$  with reductions of  $61.3 \pm 15.7\%$  and  $55.8 \pm 21.3\%$  after the first strain and  $16.6 \pm 11.7\%$  and  $12.7 \pm 10.7\%$  after the second strain (Fig 6.19 B).

The strongest effects when applying high deformation to both CF and NCFB sputum have been in the crossover variables ( $\sim 60\%$ ). Moreover, the evolution after the second large deformation is milder than the first one with drops of  $\sim 5\%$  for the crossover variables and  $\sim 33\%$  in  $G'$  for dark sputum and increases of  $\sim 20\%$  for lighter sputum.

## 6.3 Conclusions

Rheology is driven by the structure and composition of the sample. Therefore through rheometry we can obtain some information about the internal network of our samples. In this chapter we have first quantified the solid concentration of sputum samples and found CF and NCFB expectorations contain  $\sim 5\%$  w/w of solid matter. Moreover, while salt concentration seems to have no effect on macrorheology, the organic fraction is directly correlated with sputum rheology. Hence the organic matter was analysed separately finding sputum increases its  $G^*$  with increasing solid concentration following power law fits with exponents higher than 1. Diluted sputum samples on the contrary do not vary as much their viscoelasticity. This outcome might be because at high concentration, the network has multiple contact points increasing  $G^*$  while in diluted samples we measure mainly the solvent's response as the solids are isolated and dispersed.

Sputum is often submitted to large strains both *in vivo* and *ex vivo*, for example when coughing or pipetting samples for analysis. We have therefore studied its behaviour under large strain. Through LAOS analysis we found sputum samples are formed of untangled polymeric chains, reinforcing the observations that mucins group in bundles or flakes [51, 52]. Furthermore, we have confirmed sputum has a strain stiffening and a shear thinning behaviour. In particular, exacerbated NCFB sputum started deforming at higher strains than non exacerbated NCFB and COPD samples.

After a period of large deformation and flow, sputum recovers its gel-structure immediately. However, the recuperation is not complete and  $G'$  evolves differently depending on the sample's purulence. While dark sputum become softer after applying strong efforts reducing  $G'$  to a third of its initial value, light samples increase their  $G'$  plateau values around 20%. Nonetheless, all sputum samples increased their flowing capability by reducing their critical strain and stress ( $\sim 60\%$ ), therefore less effort is required to make it flow. When subjected to a second large deformation, sputum samples exhibit similar trends, but with milder evolution.

Studying the composition, structure, and rheology of sputum is important for several reasons as it can provide insights into the underlying disease mechanisms and it can aid in the diagnosis and monitoring of respiratory diseases. Changes in sputum composition, structure, or rheology can be indicative of disease progression or response to treatment. In this chapter we have seen how purulence which, as pre-

viously mentioned has been related to infection, alters sputum's recovery capacity. The colonisation of mucus by pathogens triggers the immune response [1] as well as an overproduction of mucins, in particular MUC5AC [9]. Thus, the organic solid matter is expected to increase in muco-obstructive patients aligned with their severity. In the upcoming chapter, we will explore the impact of purulence on rheology and the clinical condition of the patient, with a particular focus on discerning the effects of pathogens and inflammatory mediators.

# Chapter 7

## Infection

Patients with muco-obstructive lung diseases often suffer infections [56, 57, 58] increasing mucus secretion and purulence. The respiratory system is defended from pathogens through mucus clearance and through the activation of the immune response [1]. When the mucus layer is too thick and viscoelastic, the beating of the cilia from the epithelial cells is not enough to clear the mucus, leading to the colonisation of pathogens and chronic infections. Mucus networks are ideal for bacterial and fungal growth as they constitute at the same time a source of nutrients and a structure to keep spreading [59]. Some types of pathogens can form biofilms which are viscoelastic accumulations of bacteria protected from the surrounding by extracellular polymeric substances [60].

We have already showed in the previous chapter how the viscoelastic properties of sputum are influenced by the concentration of organic matter. In this chapter we will study the impact of these pathogens and neutrophils produced during the immune response on rheology.

### 7.1 Purulence

When sputum samples arrive to the bacteriology team in the hospital, a purulence classification is given to each sample through visual inspection or by comparison with a colour chart [21, 32] as explained in chapter 2. Samples can be categorised as purulent, semi-purulent and salivary.

During pulmonary infection, the inflammatory response recruits neutrophils which contain myeloperoxidase granules, a green protein which could be giving the darker purulent colour to mucus [20, 21]. Moreover, some bacteria as *Pseudomonas aeruginosa* release coloured pigments which could be also contributing to purulence [19, 20]. Therefore, it is not completely clear which is the origin of the increased purulence of sputum. We will therefore start by investigating how is purulence related to the patient's severity and infection.

Patient's severity is typically characterised by the Forced Expiratory Volume  $FEV_1$ , the volume of air that an individual can exhale in 1 second during a forced breath. A classification of lung functioning has been set by Pellegrino et al. [61] as a function of the predicted % as follows:

- **Mild** > 70 %
- **Moderate**: 60 - 69 %

- **Moderately severe:** 50 - 59 %
- **Severe:** 35 - 49 %
- **Very severe** < 35 %

From the 67 CF collected samples, 78% were purulent, 19% semi-purulent, 1% salivary and 1% contaminated with blood (hemato-purulent). In the case of NCFB samples 75% were purulent, 17% semi-purulent and 8% salivary. In Fig 7.1 we compare the amount of neutrophils, the total bacterial colonies and the FEV<sub>1</sub>(%) from purulent (P) and semi-purulent (SP) sputum. We have not included the salivary and hemato-purulent samples as they were only 3 and 1 samples which do not make a large enough group to statistically compare between groups.

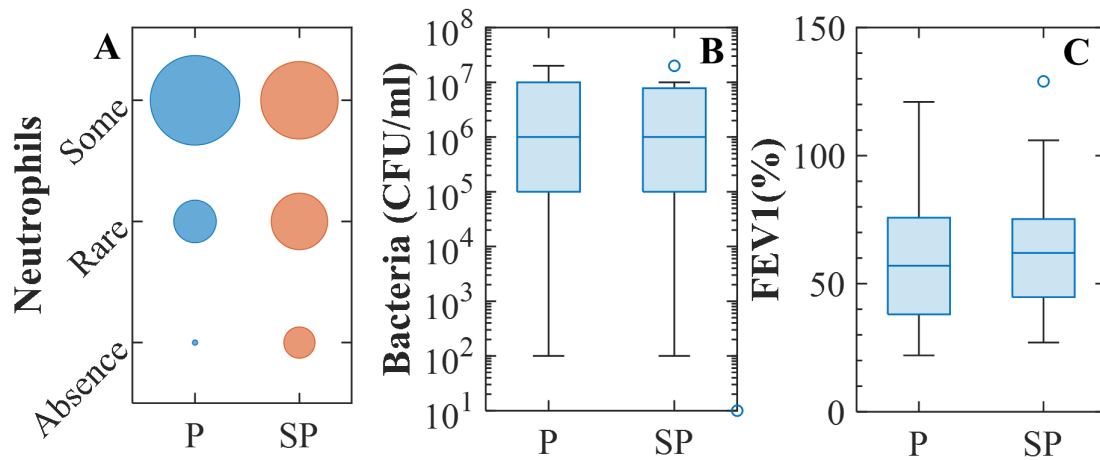


Figure 7.1: Differences between purulent (P) and semi-purulent (SP) CF and NCFB samples due to: (A) neutrophil count, where the size of the marker indicates the proportion of samples, (B) the amount of bacterial colonies and (C) FEV<sub>1</sub> (%). No significant differences are observed.

All the purulent expectorations had neutrophils but still the difference with the semi-purulent samples is not as strong as suggested in literature [21, 20]. For bacterial load and FEV<sub>1</sub> no differences can be found between the purulent and semi-purulent groups. These result contrasts previous studies [20, 19] in which purulent samples always showed a correlation with severe FEV<sub>1</sub> and bacteria.

Looking closer to the boxplots presented in 7.1, we can see that the error bars are large.

Indeed, if we consider the real colour of samples obtained through the imaging process described in chapter 2 and take  $v = 0.85$  (the dashed line in Fig 2.5 F) as the threshold to differentiate between mucoid ( $v > 0.85$ ) and purulent ( $v < 0.85$ ) expectorations, we reduce the variability of the colour chart classification. The error bars of Fig 7.2 are smaller than the ones previously found in Fig 7.1.

On the one hand, 14 out of the 16 purulent samples tested had some neutrophils while in only 1 sample it was rare to find them and in 1 other sample there were none. On the other hand, mucoid samples were more varied, some neutrophils were found in 17 out of 29 samples while in 7 it was rare to find them. Therefore, even though neutrophils could be found in mucoid samples, there is a higher probability

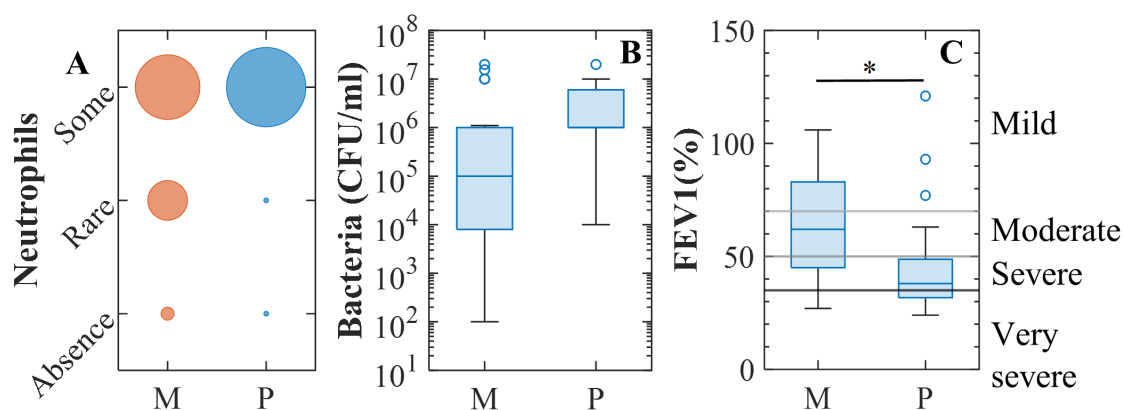


Figure 7.2: Differences between mucoid (M) and purulent (P) CF and NCFB samples due to: A: neutrophil count, where the size of the marker indicates the proportion, B: the amount of bacterial colonies (p-value = 0.465) and C: FEV<sub>1</sub> (%) (p-value = 0.030).

of retrieving neutrophils in purulent samples. Furthermore, while no significant differences were observed related to the amount of bacteria (p-value = 0.465), a significant decrease of the FEV<sub>1</sub> was found in purulent samples (p-value = 0.03). Then, patients with purulent sputum (see Fig 7.3) have a severe or very severe lung function while patients with mucoid expectorations have a moderate or mild pulmonary functioning.

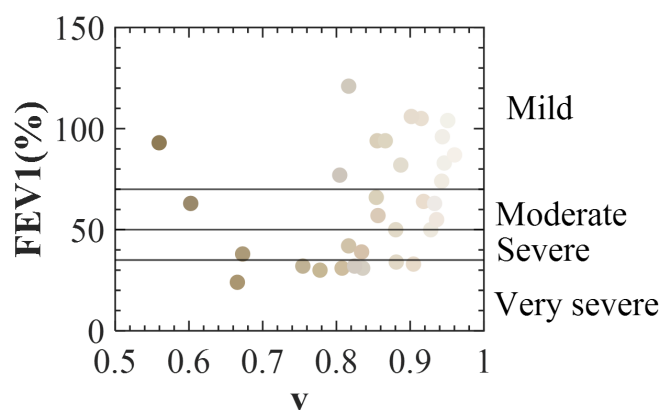


Figure 7.3: FEV<sub>1</sub> (%) as a function of the colourimetry parameter  $v$ .

To sum up, our colour-based quantification of purulence allowed us to retrieve the expected link between purulence, neutrophil contents, bacterial load, and pulmonary function. Now that we have seen the clinical implications of sputum's purulence, we will investigate which is its origin. In the following sections we will firstly address the effects of sputum composition on purulence and its mechanical properties and we will secondly study the role of bacteria and neutrophils on these alterations.

## 7.2 Infection effects on sputum properties

When patients suffer infection, there is an increase of mucus secretion and sputum becomes thicker. Several studies have shown how the production of MUC5AC [51] and MUC5B is raised during infection [62, 63]. Moreover, larger DNA concentrations have also been reported [51]. Therefore, added to the organic matter of pathogens and the immune response, we expect to see differences in the solid fraction between purulent and semi-purulent sputum.

Fig 7.4 confirms this hypothesis, purulent samples have increased solid matter. When using the hospital's visual inspection classification (Fig A) the difference is significant with a p-value of 0.02, while categorising with our image treatment (Fig B) leads to a even stronger difference (p-value < 0.0001). Moreover, we found solid mass is inversely correlated to the  $v$  value through an expression coherent with Beer Lambert's law, the darker the sample, the higher the solid content in sputum. Therefore, the solid fraction can be estimated through the colourimetry test.

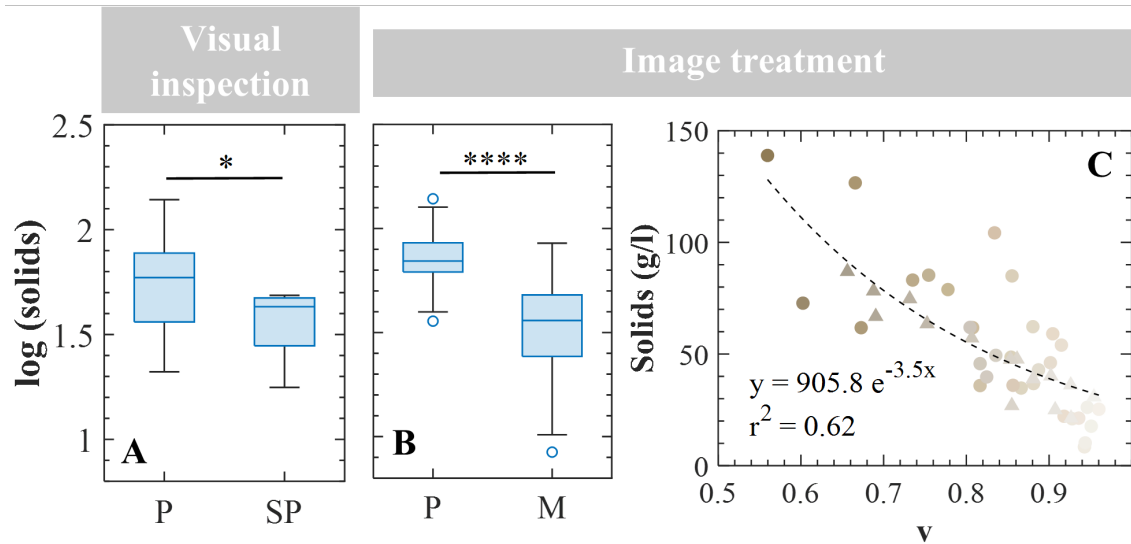


Figure 7.4: Solid concentration as a function of purulence. The logarithmic values have been used for the statistical analysis. A: purulence classification through visual inspection. B: purulence addressed through image treatment. C: CF (circles) and NCFB (triangles) solid fraction is correlated to its colour.

The increased solid concentration must be translated in changes in sputum's mechanical properties following the direct relation between solid fraction and  $g^*$  found in the previous chapter. We compared the hospital's sample's purulence with  $g^*$ ,  $s_c$  and  $d_c$  for all the collected samples in Fig 7.5 A, B and C and observed a significant increase of  $g^*$  in purulent expectorations (p-value = 0.002) and a decrease of  $d_c$  (p-value = 0.027). Then, we investigated the evolution of these rheological properties along the colour gradient in Fig 7.5 D and E. The viscoelastic modulus is inversely related to the colour transparency as expected from the similar relation retrieved with the solid content in Fig 7.4. Purulent dark expectorations are harder, they have a higher  $g^*$  and they start flowing at lower deformations.

Therefore, we have confirmed purulent samples are more viscoelastic and contain larger amount of solids. The question now is to know which pathogens are responsible for these rheological alterations or if they are just caused by the mucin and

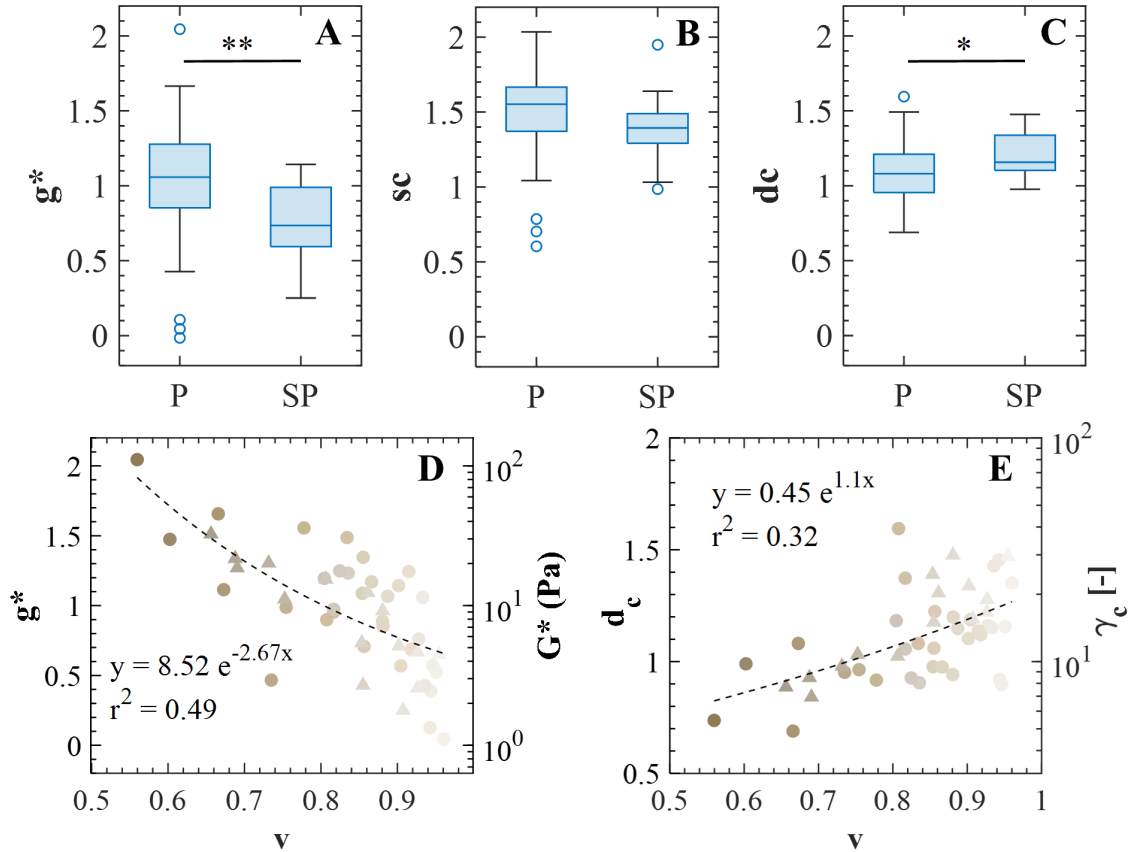


Figure 7.5: Rheological variables  $g^*$ ,  $s_c$  and  $d_c$  as a function of the purulence found in CF and NCFB sample. 63 samples are purulent (P) and 13 semi-purulent (SP). Significant differences are observed in  $g^*$  and  $d_c$ , p-values 0.002 and 0.027, respectively.

DNA overproduction.

## 7.3 Bacteria

The most common pathogens in CF mucus are *Pseudomonas aeruginosa* (PA) and *Staphylococcus aureus*. When the disease advances, *Haemophilus influenzae*, *Achromobacter xylosoxidans* or *Burkholderia cepacia* [2] can also be found. In NCFB expectorations we find similar colonies, with also *Pseudomonas aeruginosa* and *Staphylococcus aureus* the most abundant strains [64].

Bacterial infections have been reported to have an influence on sputum's viscoelasticity [22, 51]. Landry et al. [60] showed how *P. aeruginosa* adheres to mucins reducing their mobility and forming thick aggregates which inhibit antibiotic penetration. In particular, mucoid *P. aeruginosa*, a phenotype which can be viewed in Fig 7.6, produces alginate creating biofilms protecting the bacteria from host defences and antibiotics [65]. Moreover, the sputum from adults with muco-obstructive lung diseases often contains drug resistant bacterial strains as Methicillin resistant *Staphylococcus aureus* (MRSA) due to the exposure to antibiotics which complicates their treatment [2].

We started by investigating the effect of the total bacteria on rheology as we

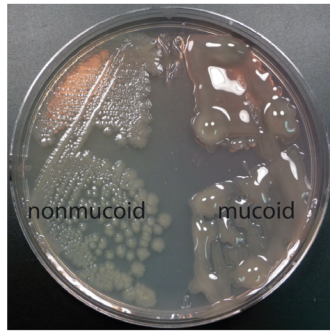


Figure 7.6: *P. aeruginosa* non mucoid and mucoid phenotypes. Image from Damron et al. 2012 [65].

expected to find viscoelastic purulent samples highly colonised, and semi-purulent light expectorations uninfected.

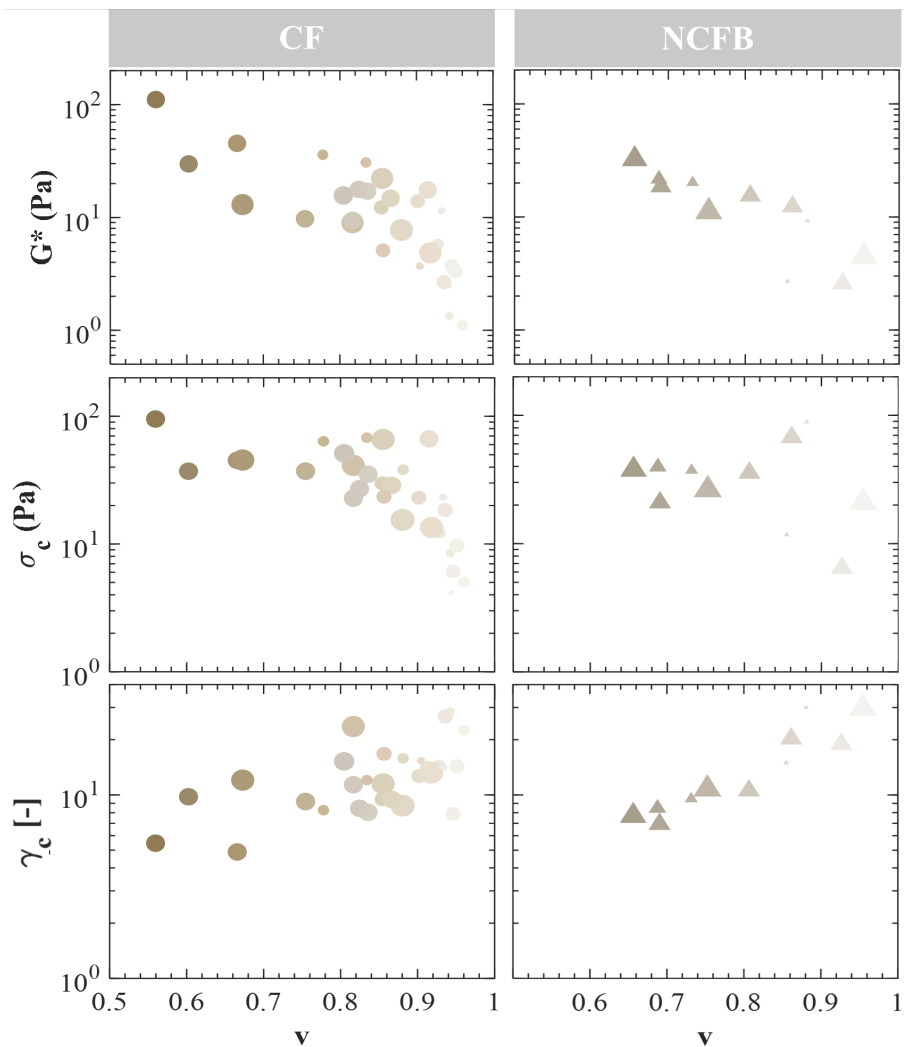


Figure 7.7: Correlations between rheology and purulence as a function of total bacterial colonies. The size of the markers refer to the total number of colonies counted per sample. No influence of the bacterial load was observed on rheology or purulence.

In Fig 7.7 we plot the evolution of the rheological values with purulence. The size of the markers represent the total number of colonies counted in the collected sputa which went up to  $2 \cdot 10^7$  CFU/ml. The plotted data shows how we do not find an increasing amount of bacterial colonies with increasing viscoelasticity or purulence. In both diseases we find large amount of bacteria in some semi-purulent samples and some purulent samples with few colonies. Thus, the total concentration of colonies is uncoupled from sputum's viscoelasticity and purulence.

Still, we hypothesised maybe the presence of different types of bacteria had different viscoelastic effects. Maybe samples with mucoid *P. aeruginosa* which have a tendency to form biofilms would have a greater viscoelasticity. Or maybe, as shown by Tomaiuolo et al. [22], the presence of *B. cepacia* and *S. maltophilia* lead to higher  $G^*$  than samples colonised by *P. aeruginosa* or *S. aureus*.

The bacterial colonies we found in the CF and NCFB expectorations are displayed in Fig 7.8. CF samples overall had *S. aureus* and *P. aeruginosa* (PA), in particular mucoid PA were highly abundant. In less amount, CF samples also had *H. influenzae*, *B. cepacia*, *A. xylosoxidans* and *Inquilinus limosus*. NCFB expectorations were as well mainly colonised by strains of *P. aeruginosa*. Besides, *H. influenzae*, *S. aureus*, *Streptococcus pneumoniae* and *Pasteurella multocida* were also found in less quantity.

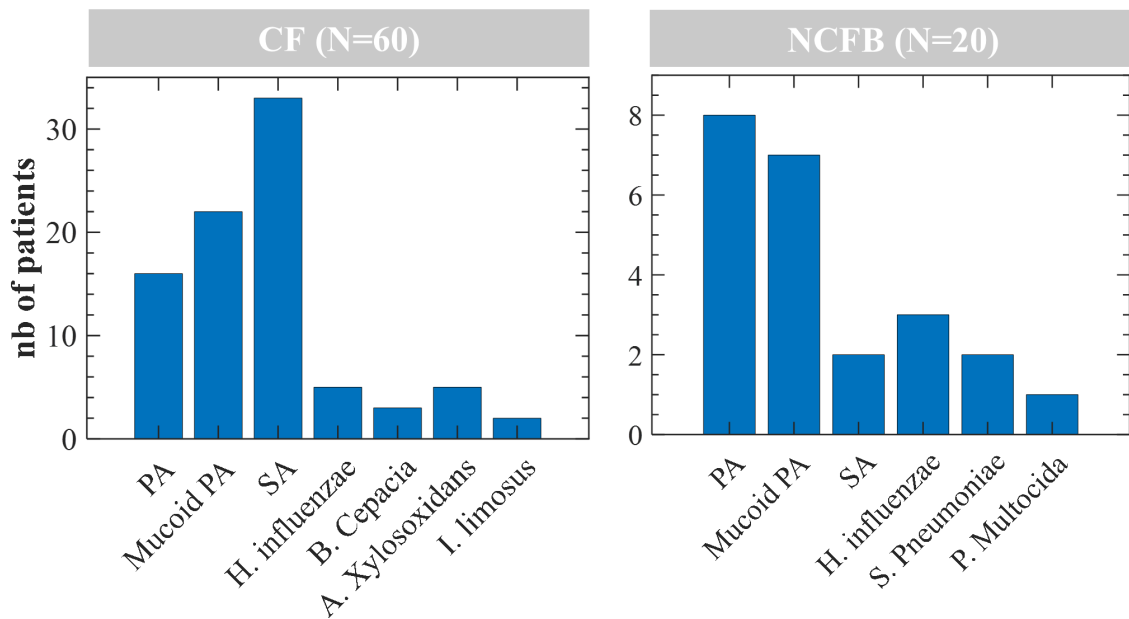


Figure 7.8: Bacterial colonies found in 60 CF and 20 NCFB sputum samples.

We first investigated the influence of the main bacteria retrieved in each expectoration on the patient's severity, evaluated by its  $FEV_1$  in 7.9. CF samples colonised by PA came from patients with mild severity with a median  $FEV_1$  of 72.5% while samples colonised by *S. aureus* showed a moderate pulmonary dysfunction with median  $FEV_1$  of 66%. NCFB samples had moderate severity when colonised by PA with median  $FEV_1$  of 61%. The most significant result was that patients from both CF and NCFB colonised by mucoid PA presented severe lung dysfunction with median  $FEV_1$  of around 40% in both diseases.

This result indicates that mucoid PA play an important role in the patient's state strongly worsening their expiratory capacity. It could be due to the viscoelastic

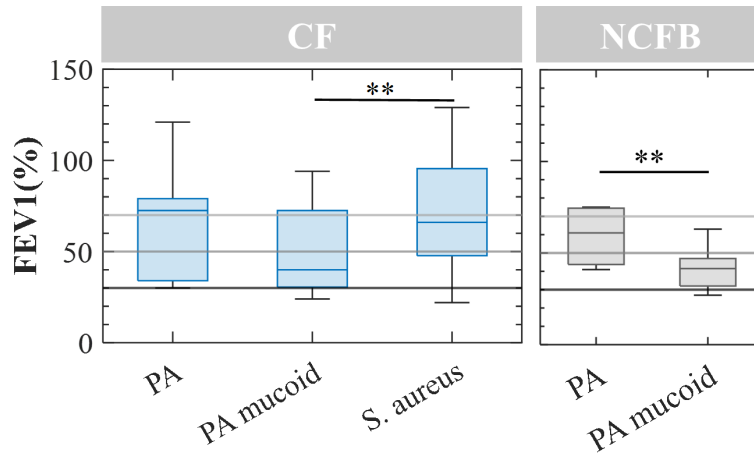


Figure 7.9: FEV1(%) as a function of the main bacteria found in each sample.

biofilms which mucoid PA form in the mucins network and if this was the case, we should be able to see a difference in rheology. To verify this theory we compared  $g^*$ ,  $s_c$  and  $d_c$  with the main bacteria found in each expectoration in Fig 7.10.

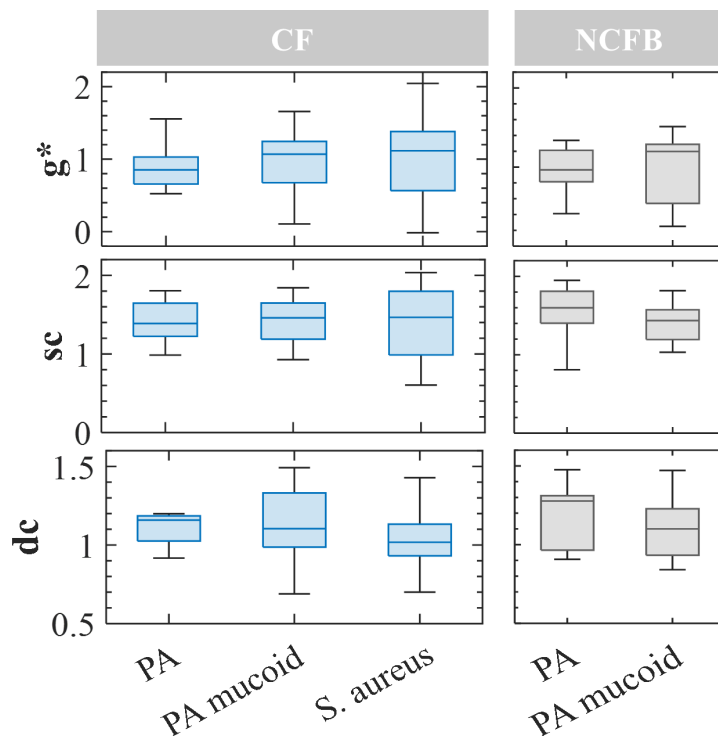


Figure 7.10: Rheological variables  $g^*$ ,  $s_c$  and  $d_c$  as a function of the main bacteria.

We observe samples mainly colonised by PA had a lower  $g^*$  and higher  $d_c$  than those colonised by their mucoid phenotype or *S. aureus*. Yet, the differences were not strong enough and are not statistically significant. Moreover, the effect of *S. aureus* on rheology was almost the same as mucoid PA. This result contrasts the differences on severity found previously in Fig 7.9 through the evaluation of the patient's  $FEV_1$ . We therefore decided to look at the data sample by sample to see if there was a certain tendency which stayed hidden when working with median values.

Fig 7.11 shows the correlations between sputum rheological variables. The colour

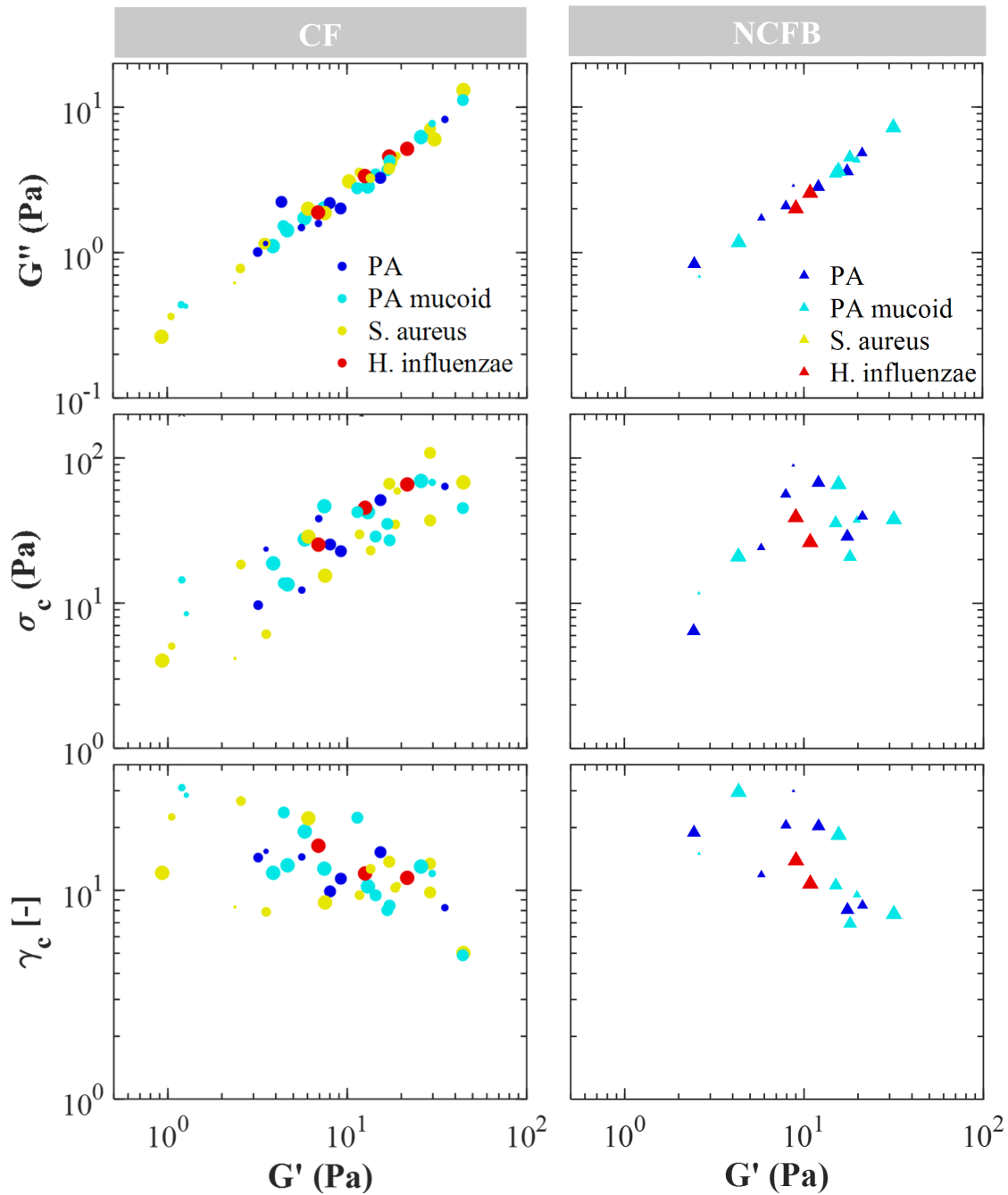


Figure 7.11: Correlations of  $G'$  with  $G''$ ,  $\sigma_c$  and  $\gamma_c$ . The main colony in each sample is represented by its colour and the amount of colonies by the size of the marker.

of the markers indicate the main bacterial strain and the size of the markers refers to the number of colonies. Contrarily to our hypothesis, we do not find any significant distinction on any of the variables due to PA, mucoid PA and *S. aureus*. Samples colonised by these strains are evenly spread along the whole distribution. However, we do observe that the few samples in which *H. influenzae* is dominant, present a relatively high viscoelastic and critical stress values with  $G' > 7$  Pa,  $G'' > 2$  Pa and  $\sigma_c > 25$  Pa.

In fact, previous studies indicate that colonisation with *H. influenzae* [2, 66] take place in acute patients. Therefore, in Fig 7.12 A and B, we compare patient's

severity with the logarithmic value  $s_c$  for CF and NCFB samples. We find that severe ( $FEV_1 < 50\%$ ) and very severe patients ( $FEV_1 < 30\%$ ) have  $s_c$  over 1.3 which in linear domain corresponds to  $\sigma_c = 20$  Pa. Interestingly,  $\sigma_c = 20$  Pa was the value at which we could observe a change in the slope of the sample's population in chapter 6. Chin et al. [66] found that *H. influenzae* strongly adhere to epithelial cells inducing a greater inflammatory response with increased neutrophil counts. Moreover, mucoid PA have also been related to higher inflammation in CF patients [67] through a raise in the cytokine concentration. This result is aligned with the size of mucoid PA colonies in Fig 7.11 where samples colonised by higher amount of colonies show higher  $G'$ ,  $G''$  and  $\sigma_c$ . Therefore, high critical stress might be associated with an important immune response and could be a biomarker for inflammation.

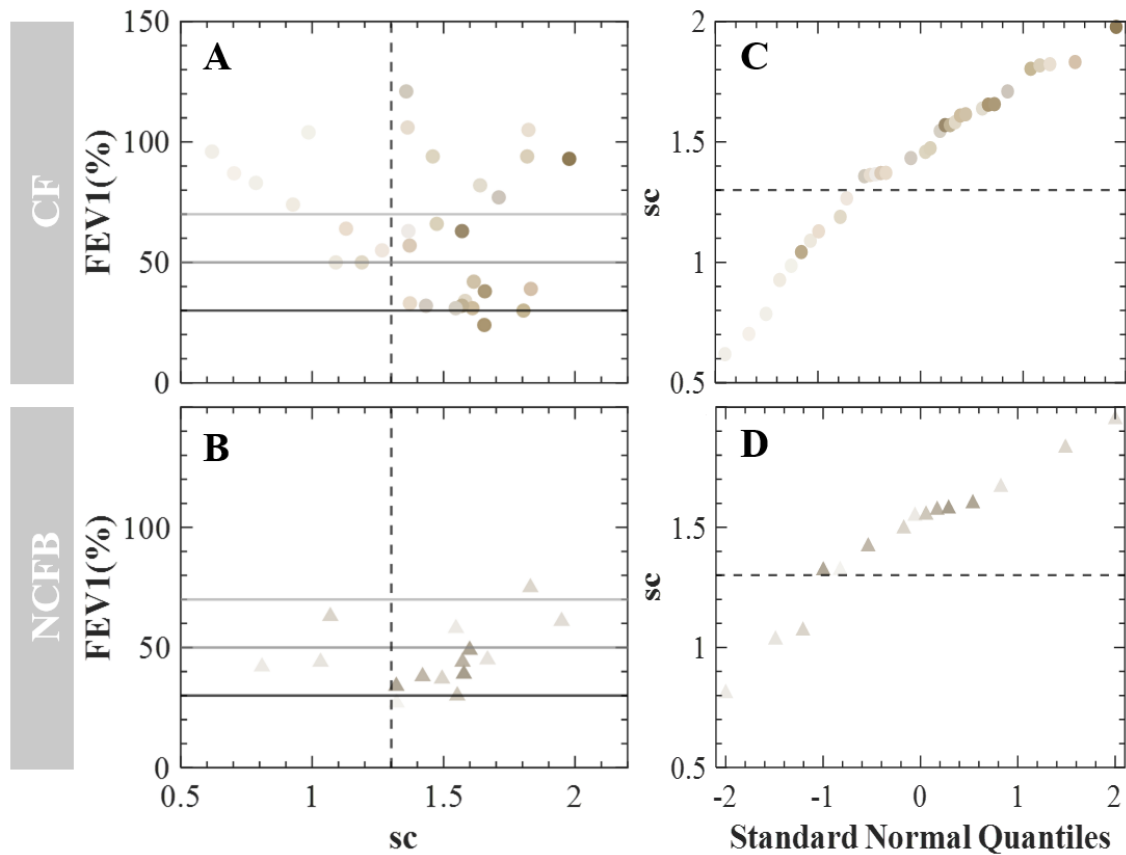


Figure 7.12: A and B: Severe and very severe CF and NCFB patients with low  $FEV_1$  show high critical stress values. C and D: The change of slope in CF and NCFB  $s_c$  population matches with the minimal  $s_c$  values for severe patients.

## 7.4 Neutrophils

The number of neutrophils is more important in purulent sputa as shown in Fig 7.13 where the counts are classified in three categories: absence, rare and some (see method's chapter 2 for details). In Fig A we can see how nearly all the samples under the established limit between semi-purulent and purulent samples ( $v = 0.85$ ) have the higher amount of neutrophils. Moreover, in Fig B we find purulence is increased with a median  $v = 0.84$  in the larger count while sputum with rare or

no neutrophils keep their mean values over 0.90. These differences are statistically significant with p-values of 0.009 and 0.05 for the absence of neutrophils and the rare counts compared to the larger count. These observations confirm previous studies which related sputum's colour with the concentration of myeloperoxidase reflecting the number of neutrophils [21].

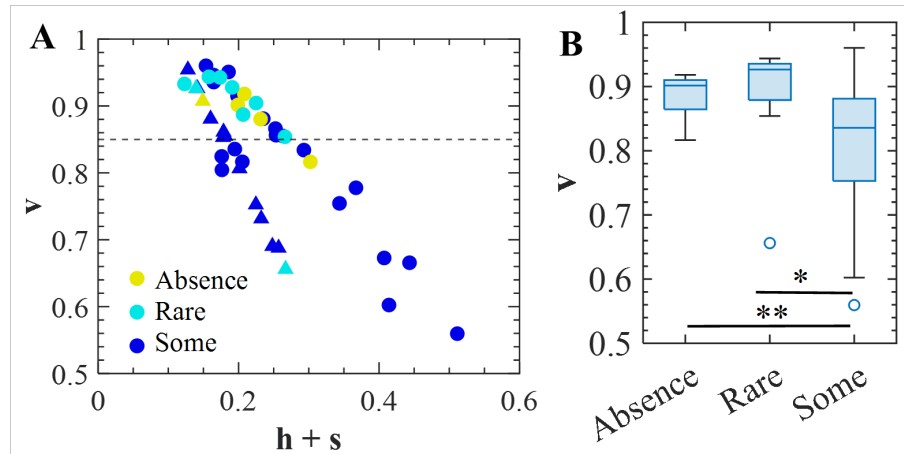


Figure 7.13: A: sputum's colour described by their  $v$  and  $s$  values compared to the neutrophil count. B: Statistical comparison between colour and the amount of neutrophils.

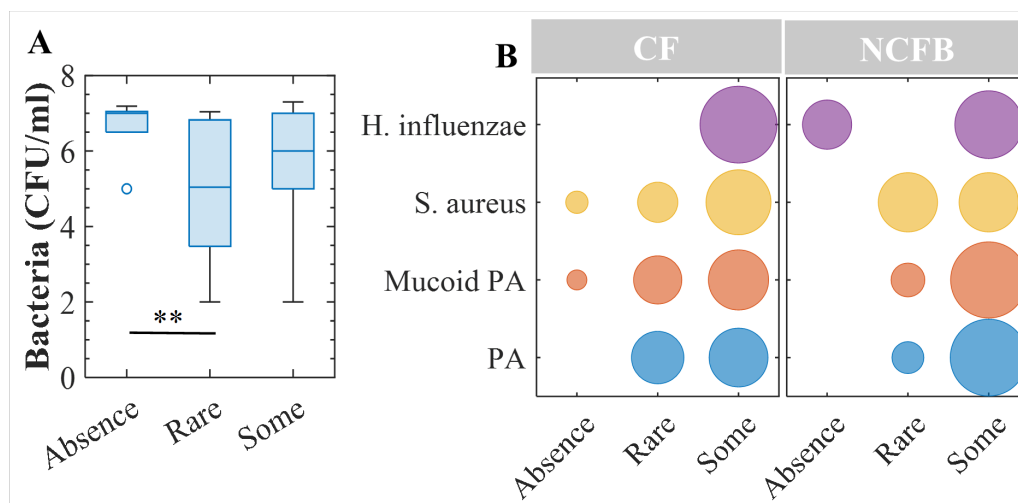


Figure 7.14: Relation between bacteria and neutrophil count. A: Total bacteria per sample. B: Proportion of each type of bacteria independent of the amount of colonies.

Therefore, when pathogens infect the pulmonary system the immune response is activated darkening the samples. Still we have observed that the neutrophil recruitment is not related that much to the total amount of bacteria but to specific colonies. In Fig 7.14 A we have compared the neutrophil count with the bacteria concentration and in Fig 7.14 B we see the proportion of patients which had colonies of certain bacteria no matter their size. From Fig 7.14 B we confirm that in both CF and NCFB sputum the inflammation is stronger in presence of *H. influenzae*. Moreover NCFB expectorations are strongly affected by PA and mucoïd PA.

In Fig 7.14 B, we observe that the samples with no neutrophils, are a small proportion but the ones which contain bacteria are colonised with a large amount of colonies (Fig 7.14 A). This could be because large amount of pathogens are found in patients at an early infection stage which are still not treated and their immune response has not still been activated. Indeed, looking into the clinical data of the patients showing no neutrophils and high bacterial content we discover that all the patients had a FEV<sub>1</sub> higher than 50% and semi-purulent samples with  $v$  values larger than 0.89. Therefore early bacterial colonisation can not be detected through FEV<sub>1</sub>, purulence or neutrophil count.

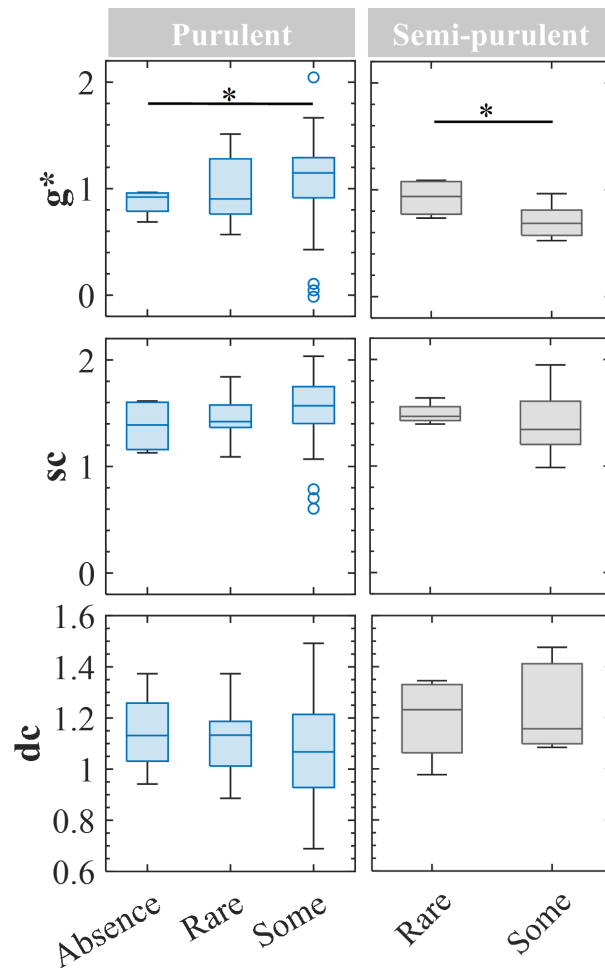


Figure 7.15: Relation between rheology and neutrophil count in purulent and semi-purulent expectorations. Data for semi-purulent samples with absence of neutrophils has not been plotted due to the lack of amount of data.

The issue now is to see if we are capable of detecting early infection through rheology. As the samples which had large amount of bacteria and no neutrophils were semi-purulent expectorations, we have looked at the effect of neutrophil count on rheology distinguishing samples by purulence in Fig 7.15. We do not plot a box in semi-purulent samples with no neutrophils because there were not enough data to have a significant representation. In this figure we notice a different behaviour of viscoelasticity when analysing purulent or semi-purulent sputum. While, purulent samples significantly increase  $g^*$  with increasing neutrophil count ( $p$ -value = 0.025),

semi-purulent samples see a drop in  $g^*$  (p-value = 0.039). The outcome of the purulent samples means that infected samples show higher viscoelastic modulus and a strong neutrophil recruitment. However, the outcome for the semi-purulent samples is contra-intuitive. Our interpretation of this results is that semi-purulent samples come from patients from either (1) early infection which sputum has thickened but not enough to recruit neutrophils or (2) post-infection with lighter sputum.

## 7.5 Conclusions

In this chapter we have seen how purulence is classically categorised by visual inspection following a colour chart. This classification leads to large variability as it is user-depended. Therefore we have developed a methodology based on image treatment to quantitatively classify sputum's purulence. Moreover through the application of this new method we can obtain estimations of the solid fraction in the sample and its viscoelastic modulus. The more purulent the sample, the more solid fraction it has and the higher its viscoelastic modulus.

Then, we have seen how purulence and  $\sigma_c$  are indicators of severe and very severe lung dysfunction. In particular, darker expectorations with  $\sigma_c > 20$  Pa show FEV1  $< 50\%$ .

Lastly, the darkening of highly viscoelastic sputum has always been said to come from the amount of neutrophils. Here we have showed how some light coloured semi-purulent samples can also have a large amount of neutrophils and still have low viscoelasticity. We therefore suggest purulence is a result of the cycle created between chronic bacterial infections and neutrophil count. For instance, the presence of large amount of mucoid *Pseudomonas aeruginosa* and *Haemophilus influenzae* recruits neutrophils and hardens sputum showing a  $\sigma_c > 20$  Pa. Still, the quantification of mucins and DNA would be key to address all the components present in mucus.

# Chapter 8

## Conclusions and perspectives

In the last decades sputum rheology has been measured leading to important insights of sputum physical and mechanical properties, which are critical for understanding its role in normal physiological processes and disease states. Although quantitative conclusions as increased viscoelasticity in sputum from patients with mucobstructive diseases have been found, there is often discordance between different studies. Thus, our initial focus was on establishing a robust sputum management protocol, which we successfully achieved and led to a publication in Scientifics Report Journal (DOI: 10.1038/s41598-023-34043-9). With this methodology in place, we proceeded to perform reliable rheological measurements on sputum samples from CF and NCFB patients, in order to identify rheological biomarkers that could serve as indicators of their clinical condition.

### 8.1 Sputum handling prior to rheometry

In the first part of this project, freezing at  $-80\text{ }^{\circ}\text{C}$  has been proven not to alter sputum rheology establishing a simple and reliable storing procedure, eluding the effect of samples' ageing which has been observed particularly important in purulent samples with reductions of  $G' \sim 50\%$  after 6 hours. The study also showed heat inactivation of potentially present pathogens such as COVID or *Mycobacterium tuberculosis* prior to rheology is inadvisable since sputum is highly sensitive to heat destroying its gel-structure. We therefore recommend to snap-freeze sputum samples as soon as possible after collection and store them while, for instance, waiting for a virology test or simply until the measurement can be performed. In addition, the use of the vortex to reduce sputum's heterogeneity reduces the variability within aliquots.

#### 8.1.1 Vortex effect on sputum

Although vortexing for 30 s was sufficient for most of the samples, some kept larger error bars. To improve mixing efficiency, we conducted experiments using a biphasic model fluid that simulated sputum by adding plugs to a matrix where  $G'_{\text{plug}} > G'_{\text{matrix}}$ . The experiment aimed to investigate if extending vortexing time improved mixing efficiency. We found that extending the vortexing time to 3 minutes resulted in a mixing efficiency of at least 95% for all the tested viscoelasticity contrasts.

However, it will be interesting to investigate if the mixing efficiency is also improved in sputum samples verifying not only macroscopically but also at a micro-

scopic scale. A microscopic study will also detect possible changes in the polymeric network due to vortexing. Preliminary data in Fig 8.1 shows the increase in mobility of  $0.5 \mu\text{m}$  fluorescent particles with longer vortexing times, suggesting the disruption of connections within the microstructure. In Fig 8.1 the histograms of the pixel intensities move towards higher values of  $\alpha$  indicating increased diffusion. Moreover, the histograms become tighter with increasing vortexing times confirming the sample is homogenising.

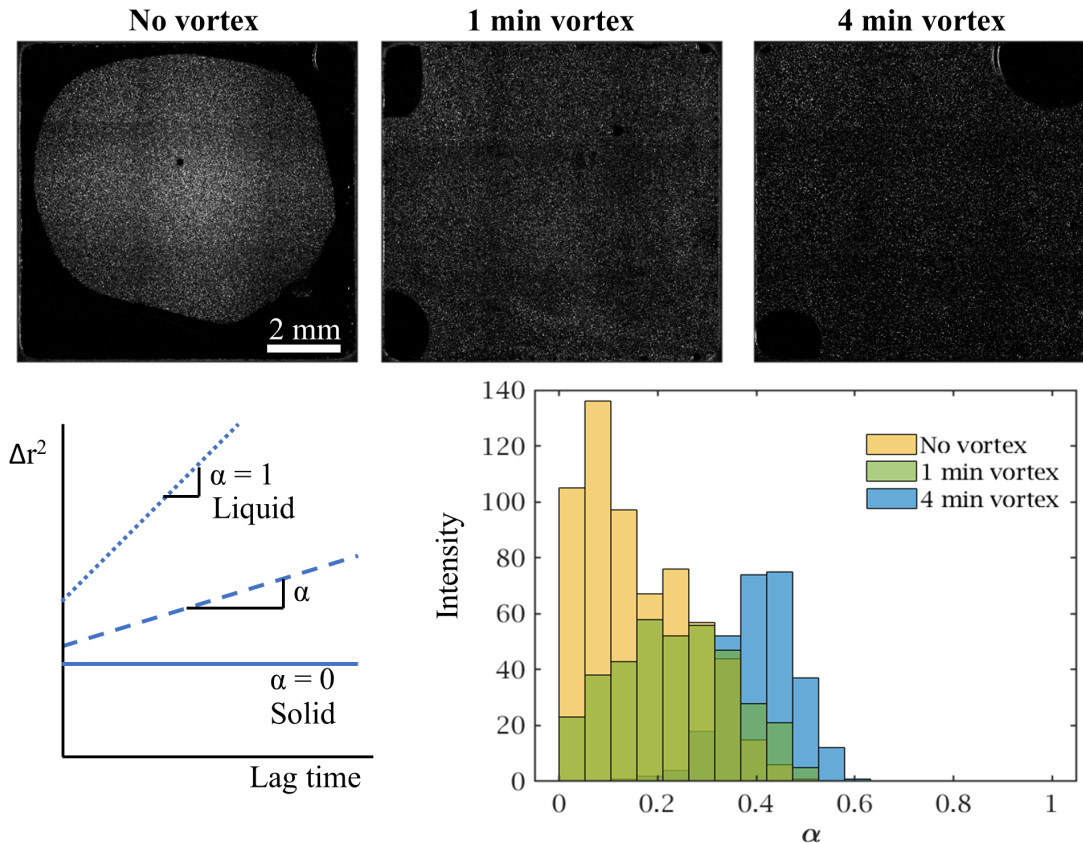


Figure 8.1: A: Flopaam 6035S plug with  $0.5 \mu\text{m}$  fluorescent particles in a transparent matrix without vortex and after vortexing for 1 and 4 minutes. B: evolution of the mean square displacement ( $\Delta r^2$ ) of the particles for solids ( $\alpha = 0$ ), liquids ( $\alpha = 1$ ) and intermediate solutions. C: Histogram of number of fluorescent particles moving at a certain  $\alpha$ .

## 8.2 Solid content of sputum

CF and NCFB sputum samples are heterogeneous fluids composed of water and  $\sim 5\%$  w/w of solid matter including salt ( $\sim 1\%$  w/w) and organic matter ( $\sim 4\%$ ). The sputum's network, formed by its organic components, including mucins, DNA, pathogens, and inflammatory cells, dictates its viscoelastic properties. As the solid content increases, the interactions between these components become more numerous, resulting in higher viscoelasticity. Specifically, our samples displayed power-law relationship between  $G^*$  and solid concentration with exponents higher than 1. In contrast, the viscoelasticity of diluted sputum samples shows less variation. This

result could be due to the fact that, at high concentration, the network has multiple contact points that increase  $G^*$ . On the other hand, in diluted samples, we primarily measure the response of the solvent as the solids are more isolated and dispersed.

However, it should be noted that although concentrated mucus from epithelial cells conforms to the power law with low dispersion [8], expectorations from CF and NCFB exhibit greater dispersion from the power law fit. We hypothesise that the dissimilarity in composition between these two types of samples could be the underlying reason for this contrast. While HBE mucus only contains mucins and globular proteins, CF and NCFB samples may also contain bacteria and inflammatory cells which can secrete polymeric content [65, 59, 19] increasing  $G^*$  and degrade protein networks due to protease activity [44, 58]. The dispersion in pathological sputum may therefore be a marker of disease. To further enhance this study, it would be beneficial to quantify DNA, MUC5AC, and MUC5B mucins separately to distinguish their individual effects from the impact of pathogens and inflammation.

Finding a proper methodology to quantify mucins is however, a point of discussion in literature. Their large size, extensive glycosilation and gel properties complicate their accurate detection and quantification [68]. The principal methods are [69]:

- solution assays as colourimetric assays in which a dye that binds specifically to mucins leads to a colour change that can be measured spectrophotometrically;
- membrane-based methods that separates mucin molecules based on their size. The eluted fractions can be analysed using techniques such as refractive index detection or light scattering to quantify the amount of mucin;
- identification of specific parts of the mucins through the use of antibodies as enzyme-linked immunoabsorbent assays (ELISA);
- and mass spectrometry which can be used to identify and quantify specific mucin proteins in sputum samples based on their mass-to-charge ratio.

Each of these techniques have their advantages and disadvantages. Solution methods typically require larger volumes, but they are less prone to selective loss of components. Membrane-based methods allow for lower volumes of sample as they will be diluted into larger volumes, however, they may result in the loss of components that do not adhere to the membrane. Methods using antibodies are susceptible to artefacts in highly concentrated samples [69]. Finally, although mass spectrometry has a high sensitivity and accuracy, sample's preparation and the interpretation of the results is very complex.

We have therefore developed a protocol combining membrane techniques, staining of glycoproteins, and the addition of specific antibodies. The first part of the protocol including the glycoproteins fixation on a nitrocellulose membrane and its staining are described in A. This protocol was done in collaboration with David Thornton from the University of Manchester but due to lack of time we have not been able to put it in place.

## 8.3 Purulence

Purulence is usually described as the colour of the sputum, with yellow or green indicating the presence of infection. The severity of the purulence can also be an indicator of the severity of the underlying condition.

### 8.3.1 Image treatment method

We have introduced a novel quantitative technique based on colourimetry through image treatment to assess sputum purulence. It is a simple technique to set up with the need of only a microscope and a colour camera. Moreover, this methodology gives a gradient of purulence and not a categorical classification as the one given through visual inspection and comparison to a colour chart classically used in hospitals. As purulence increases resulting in darker samples, the colour parameter  $v$ , which indicates its transparency, decreases.

Our method is therefore a measure of absorbance in the visible spectrum. This arises the question of which elements are absorbing the light and how does this evolve as a function of patient's severity and type of disease. Indeed, we have observed differences in the tonality of CF and NCFB, with NCFB sputum appearing more grey which we have not been able to justify. The use of optical spectrometry over a range of non-optical wavelengths may be a suitable technique to bring light into some particular characteristic.

However, to validate our methodology we compared the absorbance gradient with the hospital's classification. We observed that from a certain threshold of  $v = 0.85$  we could differentiate between mucoid and purulent samples following the colour chart classification. Samples with  $v$  values above this threshold are classified as mucoid, while those below it are classified as purulent. Using this technique, we were able to identify several notable differences between purulent and mucoid samples.

### 8.3.2 Purulence and organic concentration

For a start, we observed a positive correlation between sputum solid content and purulence, with lower solid content being associated with lower purulence. This means that sputum with higher purulence contains more solid matter, leading to a higher viscoelastic modulus and critical stress.

Moreover, purulent samples contained higher neutrophil counts than mucoid expectorations, coinciding with data in the literature [11]. Moreover, the presented results extend previous data which have shown relations between sputum inflammatory mediators and sputum rheology. Although the presence of neutrophils was consistently linked to bacterial colonisation and higher  $G^*$ , as well as disease severity in patients, the presence of bacteria did not always coincide with high neutrophil counts. Specifically, patients with mild disease severity and bacterial colonisation exhibited mucoid expectorations with low  $G^*$  and large neutrophil counts. Previous studies have also found correlations between the presence of neutrophils and bacteria in COPD [20] and NCFB, in particular under the colonisation of *Pseudomonas aeruginosa* [64, 19]. However, contrarily to Tomaiuolo et al. [22] we do not find any correlation between the presence of specific types of bacteria and viscoelasticity.

### 8.3.3 Purulence and patient's severity

The clinical severity of patients CF and NCFB was found to exhibit a significant correlation with the degree of purulence observed in their sputum samples. Specifically, all patients with severe or very severe respiratory impairment, indicated by a forced expiratory volume in one second ( $FEV_1$ ) below 50%, and with a critical stress value exceeding 20 Pa, presented purulent samples. Therefore, the quantification of the critical stress, in conjunction with  $FEV_1$  measurements, serves as a robust biomarker for identifying sputum samples that are infected and exhibit a dark purulent appearance. These purulent samples display high viscoelasticity and pose challenges in terms of their clearance from the respiratory tract due to their limited flowing capacity characterised by a high critical stress.

### 8.3.4 Purulence and mechanical behaviour of sputum

Lastly, we have observed distinct variations in behaviour dependent on the purulence level. When subjecting sputum to strong deformation and then releasing the strain, purulent samples experience losses of  $G^*$ , while mucoid samples actually increase their  $G^*$ . Purulent samples, which contain high solid concentrations and have many contact points within its network, see how after strong deformations, some bonds irreversibly break. In contrast, mucoid samples have lesser solids, forming less connections, we therefore suggest that through the oscillatory stressed applied with the rheometer, we are homogenising the sample and getting solid bundles in touch consequently increasing  $G^*$ . However this mechanism should be verified by investigating what is happening in the network at the microscopic level and by systematically performing consecutive strain sweeps to address sputum recovery. Moreover, these findings questions again the effect of vortex in sputum samples. The difference recovery behaviour due to purulence may explain the two distributions found for error bars of the vortex samples.

Furthermore, protease activity plays a critical role in various cellular and physiological functions, but abnormal proteolysis can lead to diseases. In chronic lung diseases, mucus is characterised by increased protease activity, which can result from the release of proteases by neutrophils and bacteria, among other factors [44]. We have demonstrated that purulent samples, which contain more neutrophils and generally more bacteria, underwent significant degradation, with a 50% reduction in their elastic modulus after 6 hours. In contrast, mucoid or semi-purulent samples did not exhibit any changes in their viscoelasticity within 24 hours.

# Bibliography

- [1] Richard C. Boucher. “Muco-obstructive lung diseases”. In: *New England Journal of Medicine* 380 (20 2019), pp. 1941–1953. ISSN: 15334406. DOI: 10.1056/NEJMra1813799.
- [2] Marlou C. Bierlaagh et al. “A new era for people with cystic fibrosis”. In: *European Journal of Pediatrics* 180 (9 Sept. 2021), pp. 2731–2739. ISSN: 14321076. DOI: 10.1007/s00431-021-04168-y.
- [3] Bruce K. Rubin. “Mucus structure and properties in cystic fibrosis”. In: *Paediatric Respiratory Reviews* 8 (1 Mar. 2007), pp. 4–7. ISSN: 15260542. DOI: 10.1016/j.prrv.2007.02.004. URL: <http://linkinghub.elsevier.com/retrieve/pii/S1526054207000048>.
- [4] Gregg A. Duncan et al. “Microstructural alterations of sputum in cystic fibrosis lung disease”. In: *JCI Insight* 1 (18 Nov. 2016). ISSN: 2379-3708. DOI: 10.1172/jci.insight.88198.
- [5] Sooim Sin et al. “Mortality risk and causes of death in patients with non-cystic fibrosis bronchiectasis”. In: *Respiratory Research* 20 (1 Dec. 2019). ISSN: 1465993X. DOI: 10.1186/s12931-019-1243-3.
- [6] Diego J. Maselli et al. “Suspecting non-cystic fibrosis bronchiectasis: What the busy primary care clinician needs to know”. In: *International Journal of Clinical Practice* 71 (2 Feb. 2017). ISSN: 17421241. DOI: 10.1111/ijcp.12924.
- [7] Sara Lonni et al. “Etiology of non-cystic fibrosis bronchiectasis in adults and its correlation to disease severity”. In: *Annals of the American Thoracic Society* 12 (12 Dec. 2015), pp. 1764–1770. ISSN: 23256621. DOI: 10.1513/AnnalsATS.201507-4720C.
- [8] David B. Hill et al. “PHYSIOLOGY AND PATHOPHYSIOLOGY OF HUMAN AIRWAYMUCUS”. In: *Physiological Reviews* 102 (4 Oct. 2022), pp. 1757–1836. ISSN: 15221210. DOI: 10.1152/physrev.00004.2021.
- [9] Deborah Fass and David J. Thornton. “Mucin networks: Dynamic structural assemblies controlling mucus function”. In: *Current Opinion in Structural Biology* 79 (Apr. 2023). ISSN: 1879033X. DOI: 10.1016/j.sbi.2022.102524.
- [10] Caroline Ridley and David J. Thornton. “Mucins: The frontline defence of the lung”. In: *Biochemical Society Transactions* 46 (5 Aug. 2018), pp. 1099–1106. ISSN: 14708752. DOI: 10.1042/BST20170402.

- [11] David J. Serisier et al. “Macrorheology of cystic fibrosis, chronic obstructive pulmonary disease and normal sputum”. In: *Respiratory Research* 10 (1 Dec. 2009), p. 63. ISSN: 1465-993X. DOI: 10.1186/1465-9921-10-63. URL: <http://respiratory-research.biomedcentral.com/articles/10.1186/1465-9921-10-63>.
- [12] Jérémy Patarin et al. “Rheological analysis of sputum from patients with chronic bronchial diseases”. In: *Scientific Reports* 10 (2020), p. 15685. DOI: 10.1038/s41598-020-72672-6.
- [13] Rosy Ghanem et al. “Apparent Yield Stress of Sputum as a Relevant Biomarker in Cystic Fibrosis”. In: *Cells* (2021), p. 11. URL: <https://doi.org/10.3390/cells10113107>.
- [14] Michelle Dawson, Denis Wirtz, and Justin Hanes. “Enhanced Viscoelasticity of Human Cystic Fibrotic Sputum Correlates with Increasing Microheterogeneity in Particle Transport”. In: *Journal of Biological Chemistry* 278 (50 2003), pp. 50393–50401. ISSN: 00219258. DOI: 10.1074/jbc.M309026200.
- [15] David B. Hill et al. “A biophysical basis for mucus solids concentration as a candidate biomarker for airways disease”. In: *PLoS ONE* 9 (2 2014). ISSN: 19326203. DOI: 10.1371/journal.pone.0087681.
- [16] Alex Horsley et al. “Reassessment of the importance of mucins in determining sputum properties in cystic fibrosis”. In: *Journal of Cystic Fibrosis* 13 (3 May 2014), pp. 260–266. ISSN: 15691993. DOI: 10.1016/j.jcf.2013.11.002. URL: <http://dx.doi.org/10.1016/j.jcf.2013.11.002> <http://linkinghub.elsevier.com/retrieve/pii/S1569199313001902>.
- [17] Wayne H. Anderson et al. “The relationship of mucus concentration (hydration) to mucus osmotic pressure and transport in chronic bronchitis”. In: *American Journal of Respiratory and Critical Care Medicine* 192 (2 July 2015), pp. 182–190. ISSN: 15354970. DOI: 10.1164/rccm.201412-22300C.
- [18] Ashley G. Henderson et al. “Cystic fibrosis airway secretions exhibit mucin hyperconcentration and increased osmotic pressure”. In: *Journal of Clinical Investigation* 124 (7 July 2014), pp. 3047–3060. ISSN: 0021-9738. DOI: 10.1172/JCI73469. URL: <http://www.jci.org/articles/view/73469>.
- [19] Luigi Allegra et al. “Sputum color as a marker of acute bacterial exacerbations of chronic obstructive pulmonary disease”. In: *Respiratory Medicine* 99 (6 June 2005), pp. 742–747. ISSN: 09546111. DOI: 10.1016/j.rmed.2004.10.020.
- [20] Ken Chen et al. “A Systematic Review and Meta-Analysis of Sputum Purulence to Predict Bacterial Infection in COPD Exacerbations”. In: *COPD: Journal of Chronic Obstructive Pulmonary Disease* 17 (3 May 2020), pp. 311–317. ISSN: 15412563. DOI: 10.1080/15412555.2020.1766433.
- [21] R. A. Stockley et al. “Assessment of airway neutrophils by sputum colour: Correlation with airways inflammation”. In: *Thorax* 56 (5 2001), pp. 366–372. ISSN: 00406376. DOI: 10.1136/thorax.56.5.366.

- [22] Giovanna Tomaiuolo et al. “A New Method to Improve the Clinical Evaluation of Cystic Fibrosis Patients by Mucus Viscoelastic Properties”. In: *PLoS ONE* 9 (1 Jan. 2014). Ed. by Deepak Shukla, e82297. ISSN: 1932-6203. DOI: 10.1371/journal.pone.0082297. URL: <https://dx.plos.org/10.1371/journal.pone.0082297>.
- [23] Mathilde Volpato et al. “Rheology predicts sputum eosinophilia in patients with muco-obstructive lung diseases”. In: *Biochemical and Biophysical Research Communications* 622 (Sept. 2022), pp. 64–71. ISSN: 10902104. DOI: 10.1016/j.bbrc.2022.07.025.
- [24] Gebhard Schramm. “A Practical Approach to Rheology and Rheometry”. In: *Rheology* (1994), p. 291.
- [25] Jung Gun Nam et al. “Prediction of normal stresses under large amplitude oscillatory shear flow”. In: *Journal of Non-Newtonian Fluid Mechanics* 150 (1 2008), pp. 1–10. ISSN: 03770257. DOI: 10.1016/j.jnnfm.2007.10.002.
- [26] Kyu Hyun and Manfred Wilhelm. “Establishing a new mechanical nonlinear coefficient  $Q$  from FT-rheology: First investigation of entangled linear and comb polymer model systems”. In: *Macromolecules* 42 (1 2009), pp. 411–422. ISSN: 00249297. DOI: 10.1021/ma8017266.
- [27] Randy H. Ewoldt, A. E. Hosoi, and Gareth H. McKinley. “New measures for characterizing nonlinear viscoelasticity in large amplitude oscillatory shear”. In: *Journal of Rheology* 52 (6 2008), pp. 1427–1458. ISSN: 0148-6055. DOI: 10.1122/1.2970095.
- [28] Jake Olivier, William D. Johnson, and Gailen D. Marshall. “The logarithmic transformation and the geometric mean in reporting experimental IgE results: what are they and when and why to use them?” In: *Annals of Allergy, Asthma & Immunology* 100.4 (2008), pp. 333–337. ISSN: 1081-1206. DOI: [https://doi.org/10.1016/S1081-1206\(10\)60595-9](https://doi.org/10.1016/S1081-1206(10)60595-9). URL: <https://www.sciencedirect.com/science/article/pii/S1081120610605959>.
- [29] Ayanendranath Basu et al. “A Robust Wald-type Test for Testing the Equality of Two Means from Log-Normal Samples”. In: (Apr. 2018). DOI: 10.1007/s11009-018-9639-y. URL: <http://arxiv.org/abs/1804.10950><http://dx.doi.org/10.1007/s11009-018-9639-y>.
- [30] Ali Akbar Jafari and Kamel Abdollahnezhad. “Testing the equality means of several log-normal distributions”. In: *Communications in Statistics: Simulation and Computation* 46 (3 Mar. 2017), pp. 2311–2320. ISSN: 15324141. DOI: 10.1080/03610918.2015.1041976.
- [31] Paula Agostini and Nicola Knowles. “Autogenic drainage: the technique, physiological basis and evidence”. In: *Physiotherapy* 93 (2 2007), pp. 157–163. ISSN: 00319406. DOI: 10.1016/j.physio.2006.07.005.
- [32] M. P. Murray et al. “Sputum colour: A useful clinical tool in non-cystic fibrosis bronchiectasis”. In: *European Respiratory Journal* 34 (2 2008), pp. 361–364. ISSN: 09031936. DOI: 10.1183/09031936.00163208.

- [33] Myriam Jory. “Approche biophysique de la fonction muco-ciliaire de l ’ épithélium bronchique : propriétés d ’ écoulement du mucus et coordination du battement ciliaire. HAL Id : tel-02485748 DE L ’ UNIVERSITÉ DE MONTPELLIER”. In: (2020).
- [34] Caroline G. Baxter et al. “Homogenisation of cystic fibrosis sputum by sonication - An essential step for Aspergillus PCR”. In: *Journal of Microbiological Methods* 85 (1 Apr. 2011), pp. 75–81. ISSN: 01677012. DOI: 10.1016/j.mimet.2011.01.024.
- [35] “Evaluation of the mixing performance of three passive micromixers”. In: *Chemical Engineering Journal* 150 (2 2009), pp. 492–501. ISSN: 1385-8947. DOI: <https://doi.org/10.1016/j.cej.2009.02.033>. URL: <http://www.sciencedirect.com/science/article/pii/S1385894709001508>.
- [36] Ali Hashmi and Jie Xu. “On the Quantification of Mixing in Microfluidics”. In: *Journal of Laboratory Automation* 19 (5 Oct. 2014), pp. 488–491. ISSN: 22110690. DOI: 10.1177/2211068214540156.
- [37] J. Ramsay et al. “Mixing performance of viscoelastic fluids in a Kenics KM in-line static mixer”. In: *Chemical Engineering Research and Design* 115 (Nov. 2016), pp. 310–324. ISSN: 02638762. DOI: 10.1016/j.cherd.2016.07.020.
- [38] Sinthuran Jegatheeswaran, Farhad Ein-Mozaffari, and Jiangning Wu. “Laminar mixing of non-Newtonian fluids in static mixers: Process intensification perspective”. In: *Reviews in Chemical Engineering* 36 (3 Apr. 2020), pp. 423–436. ISSN: 01678299. DOI: 10.1515/revce-2017-0104.
- [39] Paulo E. Arratia and Fernando J. Muzzio. “Planar laser-induced fluorescence method for analysis of mixing in laminar flows”. In: *Industrial and Engineering Chemistry Research* 43 (20 Sept. 2004), pp. 6557–6568. ISSN: 08885885. DOI: 10.1021/ie049838b.
- [40] Volker Hessel, Holger Löwe, and Friedhelm Schönfeld. “Micromixers - A review on passive and active mixing principles”. In: vol. 60. Apr. 2005, pp. 2479–2501. DOI: 10.1016/j.ces.2004.11.033.
- [41] Younggon Son. “Determination of shear viscosity and shear rate from pressure drop and flow rate relationship in a rectangular channel”. In: *Polymer* 48 (2 Jan. 2007), pp. 632–637. ISSN: 00323861. DOI: 10.1016/j.polymer.2006.11.048.
- [42] A. V. Bazilevsky, V. M. Entov, and A. N. Rozhkov. “Liquid filament micrometer and some of its applications”. In: (1990), pp. 41–42.
- [43] Jeremy Charriot et al. “Methods of Sputum and Mucus Assessment for Muco-Obstructive Lung Diseases in 2022: Time to “Unplug” from Our Daily Routine!” In: *Cells* 11 (5 Mar. 2022). ISSN: 20734409. DOI: 10.3390/cells11050812.
- [44] Michael C. McKelvey et al. “Proteases, mucus, and mucosal immunity in chronic lung disease”. In: *International Journal of Molecular Sciences* 22 (9 May 2021). ISSN: 14220067. DOI: 10.3390/ijms22095018.
- [45] Bertrand D.E. Raynal et al. “Calcium-dependent protein interactions in MUC5B provide reversible cross-links in salivary mucus”. In: *Journal of Biological Chemistry* 278 (31 Aug. 2003), pp. 28703–28710. ISSN: 00219258. DOI: 10.1074/jbc.M304632200.

- [46] Samuel K. Lai et al. “Altering mucus rheology to "solidify" human mucus at the nanoscale”. In: *PLoS ONE* 4 (1 Jan. 2009). ISSN: 19326203. DOI: 10.1371/journal.pone.0004294.
- [47] Michael Rubinstein et al. “Elastic Modulus and Equilibrium Swelling of Polyelectrolyte Gels”. In: *Macromolecules* 29 (1 1996), pp. 398–406. URL: <https://pubs.acs.org/sharingguidelines>.
- [48] Sergei P Obukhov, Michael Rubinstein, and Ralph H Colby. “Network Modulus and Superelasticity”. In: *Macromolecules* 27 (1994), pp. 3191–3198. URL: <https://pubs.acs.org/sharingguidelines>.
- [49] Ferenc Horkay and David C. Lin. “Mapping the local osmotic modulus of polymer gels”. In: *Langmuir* 25 (15 Aug. 2009), pp. 8735–8741. ISSN: 07437463. DOI: 10.1021/la900103j.
- [50] Pierre-Gilles De Gennes and Pierre-Gilles Gennes. *Scaling concepts in polymer physics*. Cornell university press, 1979.
- [51] Matthew R. Markovetz et al. “Mucus and mucus flake composition and abundance reflect inflammatory and infection status in cystic fibrosis”. In: *Journal of Cystic Fibrosis* 21 (6 Nov. 2022), pp. 959–966. ISSN: 18735010. DOI: 10.1016/j.jcf.2022.04.008.
- [52] Charles R Esther Jr et al. “Mucus accumulation in the lungs precedes structural changes and infection in children with cystic fibrosis”. In: *Sci. Transl. Med* 11 (2019), p. 3488. URL: <http://stm.sciencemag.org/>.
- [53] “A review of nonlinear oscillatory shear tests: Analysis and application of large amplitude oscillatory shear (LAOS)”. In: *Progress in Polymer Science* 36 (12 Dec. 2011), pp. 1697–1753. ISSN: 00796700. DOI: 10.1016/j.progpolymsci.2011.02.002. URL: <http://dx.doi.org/10.1016/j.progpolymsci.2011.02.002> <https://linkinghub.elsevier.com/retrieve/pii/S0079670011000281>.
- [54] Ozlem C. Duvarci, Gamze Yazar, and Jozef L. Kokini. “The comparison of LAOS behavior of structured food materials (suspensions, emulsions and elastic networks)”. In: *Trends in Food Science and Technology* 60 (Feb. 2017), pp. 2–11. ISSN: 09242244. DOI: 10.1016/j.tifs.2016.08.014.
- [55] Shuai Ren et al. “Influence of cough airflow characteristics on respiratory mucus clearance”. In: *Physics of Fluids* 34 (4 Apr. 2022). ISSN: 10897666. DOI: 10.1063/5.0088100.
- [56] Paul T. King et al. “Characterisation of the onset and presenting clinical features of adult bronchiectasis”. In: *Respiratory Medicine* 100 (12 Dec. 2006), pp. 2183–2189. ISSN: 09546111. DOI: 10.1016/j.rmed.2006.03.012.
- [57] Camille Ehre, Caroline Ridley, and David J. Thornton. “Cystic fibrosis: An inherited disease affecting mucin-producing organs”. In: *International Journal of Biochemistry and Cell Biology* 52 (2014), pp. 136–145. ISSN: 18785875. DOI: 10.1016/j.biocel.2014.03.011.
- [58] Markus O. Henke et al. “Serine proteases degrade airway mucins in cystic fibrosis”. In: *Infection and Immunity* 79 (8 Aug. 2011), pp. 3438–3444. ISSN: 00199567. DOI: 10.1128/IAI.01252-10.

- [59] Kaitlyn R. Rouillard et al. “Effects of Mucin and DNA Concentrations in Airway Mucus on *Pseudomonas aeruginosa* Biofilm Recalcitrance”. In: *mSphere* 7 (4 Aug. 2022). ISSN: 23795042. DOI: 10.1128/msphere.00291-22.
- [60] Rebecca M. Landry et al. “Mucin-*Pseudomonas aeruginosa* interactions promote biofilm formation and antibiotic resistance”. In: *Molecular Microbiology* 59 (1 Jan. 2006), pp. 142–151. ISSN: 0950382X. DOI: 10.1111/j.1365-2958.2005.04941.x.
- [61] R. Pellegrino et al. “Interpretative strategies for lung function tests”. In: *European Respiratory Journal* 26 (5 Nov. 2005), pp. 948–968. ISSN: 09031936. DOI: 10.1183/09031936.05.00035205.
- [62] Markus O. Henke et al. “MUC5AC and MUC5B mucins increase in cystic fibrosis airway secretions during pulmonary exacerbation”. In: *American Journal of Respiratory and Critical Care Medicine* 175 (8 Apr. 2007), pp. 816–821. ISSN: 1073449X. DOI: 10.1164/rccm.200607-10110C.
- [63] Rudra Pangei et al. “Airway mucus in pulmonary diseases: Muco-adhesive and muco-penetrating particles to overcome the airway mucus barriers”. In: *International Journal of Pharmaceutics* 634 (Mar. 2023). ISSN: 18733476. DOI: 10.1016/j.ijpharm.2023.122661.
- [64] Federico L. Dente et al. “Neutrophilic Bronchial Inflammation Correlates with Clinical and Functional Findings in Patients with Noncystic Fibrosis Bronchiectasis”. In: *Mediators of Inflammation* 2015 (2015). ISSN: 14661861. DOI: 10.1155/2015/642503.
- [65] F. Heath Damron and Joanna B. Goldberg. “Proteolytic regulation of alginate overproduction in *Pseudomonas aeruginosa*”. In: *Molecular Microbiology* 84 (4 May 2012), pp. 595–607. ISSN: 0950382X. DOI: 10.1111/j.1365-2958.2012.08049.x.
- [66] Cecilia L. Chin et al. “*Haemophilus influenzae* from patients with chronic obstructive pulmonary disease exacerbation induce more inflammation than colonizers”. In: *American Journal of Respiratory and Critical Care Medicine* 172 (1 July 2005), pp. 85–91. ISSN: 1073449X. DOI: 10.1164/rccm.200412-16870C.
- [67] Sankalp Malhotra, Don Hayes, and Daniel J. Wozniak. “Mucoïd *Pseudomonas aeruginosa* and regional inflammation in the cystic fibrosis lung”. In: *Journal of Cystic Fibrosis* 18 (6 Nov. 2019), pp. 796–803. ISSN: 18735010. DOI: 10.1016/j.jcf.2019.04.009.
- [68] Ceri A. Harrop, David J. Thornton, and Michael A. McGuckin. “Detecting, Visualising, and Quantifying Mucins”. In: *Mucins: Methods and Protocols*. Ed. by Michael A. McGuckin and David J. Thornton. Totowa, NJ: Humana Press, 2012, pp. 49–66. ISBN: 978-1-61779-513-8. DOI: 10.1007/978-1-61779-513-8\_3. URL: [https://doi.org/10.1007/978-1-61779-513-8\\_3](https://doi.org/10.1007/978-1-61779-513-8_3).
- [69] Anthony P Corfield, Julia R Davies, and Ingemar Carlstedt. *Methods in Molecular Biology TM HUMANA PRESS Glycoprotein Methods and Protocols Edited by The Mucins Methods in Molecular Biology TM HUMANA PRESS Edited by The Mucins Glycoprotein Methods and Protocols Isolation of Large Gel-Forming Mucins*. Vol. 125. 2018.

## Appendix A

# Mucins identification and quantification

## Dot Blot + PAS staining

### Materials:

- Nitrocellulose membrane
- 10  $\mu$ L sputum
- PBS
- Dot blot vacuum system
- 4M Guanidine
- Poly-L-lysine (100  $\mu$ g/mL) - No need with guanidine
- 1% (v/v) periodic acid in 3% (v/v) acetic acid
- 0,1% (w/v) sodium metabisulfite in 1 mM HCl (SM)
- Schiff's reagent

### Methods:

- Dilute sputum in 10 times volume 4M Guanidine (50  $\mu$ L sputum, 500  $\mu$ L 4M guanidine)
- Dissolve rotating (at 4°C better)
- Make dilutions in PBS ( $2^0 - 2^4$ ). 50  $\mu$ L PBS + 50  $\mu$ L PBS/Sputum + Guanidine
- Add poly-L-lysine to the membrane (increases protein retention)
- Add **2  $\mu$ L** drops on the nitrocellulose membrane
- Wash the wells in distilled water
- Wash the membrane in 3 changes of PBS
- Wash membrane in 3 changes of water (1 mL / cm<sup>2</sup>)
- Transfer to fresh solution of 1% (v/v) periodic acid in 3% (v/v) acetic acid (1 mL/cm<sup>2</sup>) – 30 min at RT
- Rinse x2 (2 min, 1 mL/cm<sup>2</sup>) in fresh 0,1% (w/v) sodium metabisulfite in 1 mM HCl (SM).
- Transfer to Schiff's reagent – 15 min (0,5 mL/cm<sup>2</sup>)
- Wash x3 for 2 min in SM
- Dry membrane in warm air steam